

**Large Displacement Analysis and Design of Stiffened Plates with Parallel Ribs in
Large Industrial Ducts**

ALI REZAIEFAR

A Thesis

In the Department of

Building, Civil and Environmental Engineering

Presented in Partial Fulfillment of the Requirements

For the Degree of

Doctor of Philosophy (Civil Engineering) at

Concordia University

Montréal, Québec, Canada

June 2021

© Ali Rezaiefar, 2021

CONCORDIA UNIVERSITY

School of Graduate Studies

This is to certify that the thesis prepared

By: Ali Rezaiefar

Entitled: Large Displacement Analysis and Design of Stiffened Plates with Parallel Ribs in Large Industrial Ducts

and submitted in partial fulfillment of the requirements for the degree of

Doctor of Philosophy (Civil Engineering)

complies with the regulations of the university and meets the accepted standards with respect to originality and quality.

Signed by the final examining committee:

Dr. Alex De Visscher Chair

Dr. Magdi Mohareb, University of Ottawa External Examiner

Dr. Rajamohan Ganesan, MIAE External to Program

Dr. Lucia Tirca, BCEE Examiner

Dr. Ashutosh Bagchi, BCEE Examiner

Dr. Khaled Galal, BCEE Thesis supervisor

Approved by _____
Dr. Michelle Nokken, Graduate Program Director
Department of Building, Civil and Environmental Engineering

Dr. Mourad Debbabi, Dean
Faculty of Engineering and Computer Science

Date of Defence: 2021-06-11

ABSTRACT

Large Displacement Analysis and Design of Stiffened Plates with Parallel Ribs in Large Industrial Ducts

Ali Rezaiefar, Ph.D.

Concordia University, 2021

The structural design of stiffened plates of the walls of rectangular-sectioned industrial ducts and similar structures is conventionally based on the linear beam theory assuming that the displacements are small and the membrane forces that generate in the panel plate are negligible. The design of such stiffened plates is divided into two main steps where the panel plate and the rib stiffener are designed sequentially. Depending on the nature of the loads applied to the industrial duct, a third step might involve determining the vibration frequency of the panel plates for resonance verifications.

In the first phase of this thesis, the conventional design method for the panel plate is studied in order to examine the effects of large displacements on the behaviour of the structure and ultimately present a new design approach accordingly. Two different sets of formulas are presented based on Finite Element analysis of rectangular plates with relatively long aspect ratios that estimate the maximum stress and deformation in the typical and edge panels of stiffened plates. These formulae are then applied to establish empirical design equations for the panel plates. The new design approach is capable of reducing the panel plate thickness significantly in comparison with the conventional method.

In the second phase of the thesis, the structural design of the rib stiffeners is evaluated through a comparison between the conventional design which is based on Modelling the stiffened plate using an Equivalent Beam Analogy (EBA) and calculating the geometrical cross-sectional properties of it in linear beam theory, and FE analysis of the stiffened plate using shell elements with and without the consideration of large displacement effects. It is shown that the EBA and linear beam theory, as well as the FE using small displacements, are not relevant for the analysis and design of stiffened plates. In this phase, it is shown that the load-displacement behaviour of

stiffened plates with parallel ribs could be different under positive and negative pressures as the membrane forces generated in the panel plate would affect the overall behaviour of the stiffened plate differently.

The third phase of the thesis provides means for obtaining the first three significant vibration modes for rectangular plates based on mass participation ratios. A non-dimensional frequency parameter is presented which results in the vibration frequency of rectangular plates at each of these three significant modes. Various aspect ratios and four combinations of boundary conditions at the plate edges are studied, and a correlation between the nonlinear load-deformation behaviour of the panel plate and its vibrational behaviour is also presented accordingly. It is demonstrated that the vibration frequency of the studied rectangular plates increases significantly upon increasing the applied lateral pressure if the large deformation effects are considered in the analysis. The easy-to-follow method of frequency calculation presented in this paper is useful for assessing the dynamic characteristics of rectangular plates with or without lateral pressure that are subject to vibration.

Dedication

To my wife, Mahsa, for her love, passion and friendship

...also, to my two kids, Nava and Neil, for if not because of them, this would have been finished a long time ago!

Acknowledgements

First and foremost, I would like to express my gratitude towards my supervisor, Professor Khaled Galal, for his support, help, and guidance throughout my time at Concordia University. His continuous encouragement has given me the confidence to focus and proceed. I also greatly appreciate the support I received from my mentor, Mr. Krzysztof Rosiak, for his patience, support and flexibility during my work/study time.

Also, I would like to acknowledge and appreciate the support I received from the industrial partners in this research, Fives Solios Inc. and Strudes Inc. The invaluable first-hand experience in engineering design provided to me by Mr. Henry Nowodworski of Strudes Inc. and Mr. Philippe Martineau of Fives Inc. gave me the insights required to relate my research with the needs of the industry in real life.

My duty is failed if I do not mention special thanks to my friends Dr. Hamid Arabzadeh and Dr. Morteza Aboutalebi for helping me with their humour and friendship along with their great knowledge support whenever I reached out to them.

I would like to acknowledge the financial support from the Natural Science and Engineering Research Council of Canada (NSERC) as well as the financial support from le Fonds de Recherche du Québec–Nature et Technologies (FRQNT) and Solios Environments Inc. in the form of the BMP Innovation award program number 180371.

Last but not least, I thank my parents for, without them, I would not be who I am today. Words are failing me to mention my gratitude towards my wife and best friend, Mahsa, who sacrificed her career goals for mine and provided me with love, passion and support for the better part of my life during the past 19 years. This thesis and anything I achieve in life are dedicated to her.

Co-Authorship

This thesis has been prepared in accordance with the regulations for a manuscript basis (sandwich) thesis format. This research presents numerical, analytical and empirical work carried out solely by Ali Rezaiefar. Advice and guidance provided for the whole thesis by the academic supervisor Professor Khaled Galal. This thesis consists of the following chapters:

- Chapter 3

Rezaiefar, A., and Galal, K., (2016). “Structural Design of Stiffened Plates of Industrial Duct Walls with Relatively Long Panels Undergoing Large Deformations,” Elsevier Journal of Thin-Walled Structures, 108, 406-415

- Chapter 4

Rezaiefar, A., and Galal, K., (2021). “Large Displacement Analysis of Stiffened Plates with Parallel Ribs under Lateral Pressure,” Submitted to Elsevier Journal of Engineering Structures.

- Chapter 5

Rezaiefar, A., and Galal, K., (2018). “Free Vibration of Thin Rectangular Steel Plates with Geometrically-Nonlinear Load-Displacement Behaviour,” Elsevier Journal of Thin-Walled Structures, 129, 381-390.

Table of Contents

List of Figures.....	xi
List of Tables	xv
CHAPTER 1 Introduction	1
1.1 Background and Problem Definition.....	1
1.2 Research Significance and Motivation.....	2
1.3 Objectives and Scope of Work.....	3
1.4 Thesis Layout	4
CHAPTER 2 Literature Review.....	6
2.1 Background.....	6
2.2 Large displacement analysis of thin rectangular plates.....	6
2.3 Analysis and design of stiffened plates	11
2.4 Modal analysis and free vibration of rectangular plates with large deformations	18
CHAPTER 3 Structural Design of Stiffened Plates of Industrial Duct Walls with Relatively Long Panels Undergoing Large Deformations.....	23
3.1 Abstract.....	23
3.2 Introduction	23
3.3 Analysis and Design of Long-Spanned Rectangular Plates	26
3.3.1 Linear analysis of long rectangular plates under uniform lateral pressure.....	26
3.3.2 Nonlinear Analysis of Plates Under Uniform Lateral Pressure with Large Deformations	28
3.4 Nonlinear Finite Element Analysis of Duct Walls	32
3.4.1 Validation of Modelling and boundary conditions.....	33
3.4.2 Multi-span plates with internal line supports	37
3.5 Design of Duct Wall Plates Based on Nonlinear Analysis.....	39
3.5.1 Stress criterion	39
3.5.2 Deflection criterion.....	41
3.5.3 Application of design equations	42

3.5.4	Displacement limits for the design of duct walls	45
3.6	Conclusions	46

CHAPTER 4 Large Displacement Analysis of Stiffened Plates with Parallel Ribs under Lateral Pressure		47
4.1	Abstract.....	47
4.2	Introduction	47
4.3	Stresses in Rectangular Plates in Theory.....	51
4.4	Equivalent Beam Analogy.....	51
4.5	Finite Element Modelling and Verification.....	55
4.5.1	Geometry, loading, and boundary conditions of the FE models	55
4.5.2	Verification of FE Modelling	57
4.5.3	FE analysis output	59
4.6	Load-Displacement Analysis.....	60
4.7	Stress Analysis.....	61
4.7.1	Membrane forces and bending moments in the panel plate	62
4.7.2	Global stresses in the panel plate.....	64
4.8	Limit States Design of Stiffened Plates with Parallel Ribs	68
4.8.1	Ultimate Limit State (ULS).....	68
4.8.2	Serviceability (displacement) Limit State (SLS).....	69
4.8.3	Limit states design based on LDA.....	69
4.9	Conclusions and Future Works	71

CHAPTER 5 Free Vibration of Thin Rectangular Steel Plates with Geometrically-Nonlinear Load-Displacement Behaviour		73
5.1	Abstract.....	73
5.2	Introduction	73
5.3	Theoretical Background, FE Modelling, and Verification.....	75
5.4	Free vibration of Rectangular Plates at Rest	80
5.4.1	Structurally significant modes	81
5.4.2	Vibration frequencies of significant modes for rectangular plates at rest	83

5.5	Free vibration of rectangular plates with uniform lateral pressure and large deformation effects	85
5.6	Analysis example.....	88
5.7	Concluding remarks.....	90

CHAPTER 6 SUMMARY, CONCLUSIONS, LIMITATIONS AND RECOMMENDATIONS FOR FUTURE WORKS 92

6.1	Summary.....	92
6.2	Concluding Remarks	93
6.3	Limitations.....	94
6.4	Recommendation for Future Works	95

References 96

List of Figures

Fig. 2.1: Load-displacement charts for square clamped (right) and simply-supported (left) plates by Levy (1941-a and 1941-b)	8
Fig. 2.2: Schematic section view of the testing apparatus for clamped plates (Ramberg et al., 1942)	8
Fig. 2.3: Load-displacement charts for square clamped plates by Ramberg et al. (1942).....	9
Fig. 2.4: Load-displacement charts for rectangular plates with aspect ratio of 1.5 (right), and 2.0 (left) by Wang (1948)	10
Fig. 2.5: Three-point Bezier approximation of the load-displacement chart by El-Aghoury and Galal (2014).....	11
Fig. 2.6: Examples of stiffened plates and shells applications (Bedair, 2009)	12
Fig. 2.7: Schematic display of the effective breadth in a typical stiffened plate (Paik, 2008)	13
Fig. 2.8: The geometry and loading in the FE models by Paik and Seo (2009-b).....	13
Fig. 2.9: Schematic display of the stiffened plate; (a) Stiffened plate subjected to applied in-plane shear stress (S_{xy}) and in-plane, linear varying compression or tension stress (S_x , S_y), and cross section of an eccentric, (b) flat bar and (c) T-stiffener. (Brubak and Hellesland, 2007-a, 2007-b, 2007-c, 2008).....	14
Fig. 2.10: Actual midship section of a double-hull oil tanker (Badran et al., 2013)	15
Fig. 2.11: The test setup and one of the specimens tested by Xu and Guedes Soares (2013)	16
Fig. 2.12: Test setup and deformed shape of the stiffened plate specimen (Kwon, 2014).....	17
Fig. 2.13: Test setup (up), and the sectional view of the test setup (down) by Shanmugam et al. (2014).....	18
Fig. 2.14: Experimental test setup of Amabili (2006)	20
Fig. 2.15: The experimental test setup (up), and the expected modal shapes for the duct segment (down) by David et al. (2018).....	21
Fig. 3.1: (a) Large industrial rectangular duct segments under construction (courtesy of fives-solios Inc.). (b) Schematic view of a typical rectangular duct segment.....	24
Fig. 3.2: Unit-width strip and beam analogy	26
Fig. 3.3: Rectangular simply supported plate under uniform lateral pressure. a) Plate dimensions and loading b) Contour display of plate deflection.....	29
Fig. 3.4: SHELL181 geometry and stress output (ANSYS, 2010-b)	33

Fig. 3.5: Boundary conditions for the single-span plate model (a): Typical panel (b): Edge panel	34
Fig. 3.6: Load-deformation curve of rectangular plate (typical panel).....	34
Fig. 3.7: Normalized tangential (membrane) and total stresses for single span rectangular plate with large deformations	35
Fig. 3.8: Loading and free body diagram for the equilibrium of continuous beams with large deformation.....	35
Fig. 3.9: Geometry and FE mesh of a sample 3D duct segment model.....	36
Fig. 3.10: Absolute deformation and rotation of the duct segment model under the applied internal pressure (rib elements removed from the view for clarity)	37
Fig. 3.11: General arrangement of duct wall plate models with internal and edge line supports resembling the restraints provided by the end panels, ribs and other walls of the duct when expansion joints exist at both ends of the segment.....	38
Fig. 3.12: Displacement contours in three global directions for 10-span plate model with internal line supports and span aspect ratio $S=5$	38
Fig. 3.13: Out of plane load-displacement charts for different panels of the plate with internal line supports in three aspect ratios $S=2$, $S=5$ and $S=10$	39
Fig. 3.14: Maximum von-Mises stress in typical and edge panels of multi-span plates with aspect ratios from 2 to 10.....	40
Fig. 3.15: Load-deformation charts for typical panel with aspect ratios $S=2$ to $S=10$	41
Fig. 3.16: Load-deformation charts for edge panel with aspect ratios $S=2$ to $S=10$	41
Fig. 3.17: Normalized plate length-to-thickness ratio for various lateral pressures on duct walls typical and edge panels	43
Fig. 4.1: A duct segment with stiffened plate walls being delivered in an industrial project [courtesy of Fives Inc.].....	48
Fig. 4.2: Stiffened plates with common types of stiffeners and their effective breadth forming the equivalent beam cross-section	52
Fig. 4.3: Effect of the ratio of stiffener area over plate area (A_s/APL) on the EB moment of inertia in stiffened plates with flat-bar ribs	53
Fig. 4.4: Effect of the ratio of stiffener area over plate area (A_s/APL) on the EB flexural strength in stiffened plates with various ribs profiles.....	54

Fig. 4.5: Geometry of the FE models.....	56
Fig. 4.6: Geometry and load setup for verification model; Left: Experimental specimen of Shanmugan et al. (2014); Right: FE mesh and loading in the current study	58
Fig. 4.7: Lateral load-displacement charts for three experimental tests of Shanmugan et al. (2014) and resulted from the FE analysis.....	58
Fig. 4.8: Displacement profile of stiffened plate at midspan (only half of the stiffened plate is shown for better display)	59
Fig. 4.9: (a) Bending moments and resulting stresses; (b) Membrane forces and resulting stresses	60
Fig. 4.10: Mid-span load-displacement charts for the clamped (left) and simply-supported (right) models.....	61
Fig. 4.11: Membrane force ratio NZ/N_{Yield} in the panel plate at $q^*=0.5$ for simply-supported models (stiffener is not shown).....	62
Fig. 4.12: Membrane force NX/N_{Yield} in the panel plate at $q^*=0.5$ for simply-supported models (stiffener is not shown)	62
Fig. 4.13: Bending moment MZ/M_{Yield} in the panel plate at $q^*=0.5$ for simply-supported models (stiffener is not shown)	63
Fig. 4.14: Bending moment MX/M_{Yield} in the panel plate at $q^*=0.5$ for simply-supported models (stiffener is not shown)	64
Fig. 4.15: Panel plate load-stress charts at Point 1 for SD-C, LD-C, SD-S, and LD-S	65
Fig. 4.16: Panel plate load-stress charts at Point 2 for SD-C, LD-C, SD-S, and LD-S	66
Fig. 4.17: Panel plate load-stress charts at Point 3 for SD-C, LD-C, SD-S, and LD-S	66
Fig. 4.18: Panel plate load-stress charts at Point 4 for SD-C, LD-C, SD-S, and LD-S	67
Fig. 4.19: Contour plots of the deformed shape and the von Mises stress distribution in the clamped model at four stages of loading (only half of the plate length is shown for better clarity) upper: positive pressure, lower: negative pressure	67
Fig. 4.20: Mid-span load-displacement chart for the C1-N model and the bilinear design points	70
Fig. 4.21: Ultimate load and displacement at Point-A obtained from the LDA in comparison with the conventional EBA methods for the clamped (left) and the simply-supported (right) models	71

Fig. 5.1: (a) General view of the nodes, surfaces, global and local coordinates of the shell element	
(b) Local degrees of freedom at a given joint.....	77
Fig. 5.2: First stage of the validation study: Comparison of the results of FE analysis (current work) with available literature for the nonlinear load-deformation of rectangular plates under lateral uniform pressure	79
Fig. 5.3: Second stage of the validation study: Comparison of the FE results (current work) with the natural frequencies of 15 modes of vibration of the plate tested by Amabili (2008) and their reported analytical results.....	79
Fig. 5.4: Third stage of the validation study: Non-dimensional frequency $[\omega L^2(\rho h/D)^{0.5}]$ of rectangular SC plates with uniaxial membrane force resulted from FE analysis (current work) against the analytical results of Wang et al. (2006) (a) Plate aspect ratio: 1.0 (b) Plate aspect ratio: 0.5	80
Fig. 5.5: Non-dimensional frequencies associated with the first 20 modes of vibration for simply-supported (SS) and clamped (CC) rectangular plates with aspect ratios $S=1.0$, $S=2.0$ and $S=4.0$	81
Fig. 5.6: Visual display of the first 20 modes of vibration for a rectangular plate with aspect ratio $S=2.0$ and SS boundary conditions	83
Fig. 5.7: Frequency parameter associated with the three significant modes for rectangular plates with various boundary conditions and aspect ratios	84
Fig. 5.8: Deformation of a CC rectangular plate under uniform lateral pressure	85
Fig. 5.9: Non-dimensional frequency parameter charts for plates with different boundary conditions and aspect ratios under various non-dimensional pressure (q^*) values	87
Fig. 5.10: Non-dimensional frequency parameter charts for plates with different boundary conditions and aspect ratios under various uniform lateral loads	88
Fig. 5.11. Application of the pressure-frequency charts in an example	90

List of Tables

Table 3.1. Stresses and deflections of long plates when using unit-width strip method and beam analogy	27
Table 3.2. Aspect ratio numerators to be used in Eq. 3.9	40
Table 3.3. Aspect ratio numerators to be used in Eq. 3.10	42
Table 3.4. Aspect ratio numerators to be used in Eq. 11	43
Table 3.5. Comparison between the length-to-thickness ratios resulted from the nonlinear and linear designs for edge and typical panels	44
Table 3.6. Ratio of maximum lateral pressure resulted from the nonlinear approach to linear method, $q(\text{nonlinear})/q(\text{linear})$	45
Table 4.1. Effective breadth of the plate in stiffened plates in the available literature.....	53
Table 4.2. First set of FE models	56
Table 4.3. Second set of FE models.....	57
Table 5.1. Various boundary conditions combinations for a panel of industrial duct walls....	78
Table 5.2. Modal mass participation ratios at the six DOFs for the rectangular plate with aspect ratio $S=2.0$ and SS boundary conditions.....	82
Table 5.3. Values of ω^* associated with the three significant modes for rectangular plates with various boundary conditions and aspect ratios	84
Table 5.4. Frequencies resulted from the method in this paper and case-specific FE analysis	90

CHAPTER 1

Introduction

1.1 Background and Problem Definition

Stiffened plates with parallel ribs account for a major part of thin-walled structures found typically in industrial facilities in the forms of rectangular ducts, dust collectors, boilers, hoppers, containers, and similar structures. Although the structural design of such structures is not directly addressed in the North-American codes, engineers usually refer to CSA-S16 in Canada and AISC Steel Construction Manual in the US. They often make several simplifications that lead to proper design procedures based on the nature of the loading and configurations of the stiffened plates. On the other hand, Eurocodes EN-1993: Design of Steel Structures addresses the steel plates and shells in parts 1-5, 1-6, and 1-7 and provides guidelines for designing such structures. However, in all those codes and standards, the panel plates in the stiffened plates with long spans (i.e., $L \geq 2B$) are often simplified and regarded as a unit-width beam for which the classical beam theory is deemed appropriate and acceptable.

The principal assumption associated with the structural design of stiffened plates in the conventional methods, based on the classical beam theory, is that the plate displacements are infinitesimally small compared to their dimensions. Thus, the principal internal stresses in the panel plate following this assumption are produced by the flexural behaviour. This assumption, however, does not result in the correct load-displacement behaviour of the panel plate if the displacements are not infinitesimally small. The definition of large displacement is often provided with respect to the plate thickness. The following are some examples for such definition in the literature, in all of which δ is the maximum deflection and t is the thickness of the plate:

- $\delta > 0.5t$ (Levy, 1941a),
- $\delta > 1.0t$ (Timoshenko and Woinowsky-Kreiger, 1959) and (Ugural, 1981), or,
- $\delta > 0.2t$ (Bakker et al., 2008).

In large displacement analysis, the contribution of the membrane (tangential) forces generated in the plate in combination with the flexural stresses are accounted for, as explained further in the upcoming chapters of this thesis.

1.2 Research Significance and Motivation

As the environmental challenges that face the planet call for an overall reduction of energy and resources in the construction industry, any improvement in the optimization of the usage of the materials would be of great significance. On the other hand, steel production has a 190% CO₂ emission rate, i.e., for each tonne of steel production, 1.9 tonne of CO₂ is released into the air bringing the steel industry accountable for 4-5% of the world's overall CO₂ emission according to the International Energy Agency annual data.

The ultimate goal of the research which led to this thesis is to demonstrate the effectiveness of the consideration of the membrane forces in the panel plate by utilizing the Large Displacement Analysis (LDA) as a replacement for the conventional design approach, which is based on the Small Displacement Analysis (SDA) that takes into account only the flexural behaviour of the panel plate. At the beginning of this research, an overall thickness reduction of 30% was set as a realistic goal. However, when the definitions of the limit states are explicitly set based on the nature of the structure in which the stiffened plates are utilized, a more significant reduction in the steel panel plate thickness is easily within reach, as shown in Chapter 3. Moreover, the LDA could also be implemented as a better replacement for the conventional approach for the rib stiffeners' design in which the stiffener and a portion of the panel plate are modelled as an equivalent beam cross-section and designed using the classical beam theory.

Another critical factor in the design of stiffened plates for industrial ducts is vibrational concerns. If the loading or flow-induced vibration resonates with the stiffened plate, the result would be excess structural vibration for natural modes with higher mass participation or excessive noise for natural modes with lower mass participation. A good design involves both of those aspects by calculating the natural frequencies of the stiffened plate. Although there are many analytical and empirical methods available in the literature to calculate the natural frequencies of rectangular plates, if the effects of membrane forces in the LDA are not considered, the calculated frequencies are not realistic. In this regard, there is a need for an easy-to-follow empirical method

that calculates the frequency of vibration in the structurally important modes of vibration for such plates under the applied lateral pressure in LDA.

1.3 Objectives and Scope of Work

In order to address the needs of the industry for a reliable and optimized design that is based on LDA, the objectives of this thesis are to (i) evaluate the applicability of the FE method for the LDA of rectangular plates and stiffened plates with parallel ribs, (ii) break down the structural design of industrial duct walls and stiffened plates in general from the perspective of LDA, (iii) review the limit stated design for stiffened plates and establish the applicable failure criteria, (iv) FE analysis of stiffened plates using the LDA and establish easy-to-follow empirical methods to estimate the load-displacement behaviour, the ultimate design load, and the vibrational frequencies of the rectangular plates accordingly. In order to achieve these objectives, the scope of the research in this thesis is as follows:

- Developing a reliable FE Modelling approach and appropriate elements and boundary conditions that best simulate the stiffened plates of the walls of rectangular ducts and similar industrial structures,
- Evaluating the FE results against the available experimental tests and analytical solutions in the literature,
- Performing LDA on various aspect ratios of rectangular plates and tabulate their load-displacement and load-stress behaviour,
- Establish a meaningful empirical design approach based on LDA for the rectangular panel plates of the walls of industrial ducts and similar structures,
- Performing LDA on stiffened plates with the most common form of rib stiffener and panel plate combinations in order to study the stress distributions in the panel plates as well as the load-displacement charts,
- Establish a meaningful approach for the estimation of the ultimate load for stiffened plates in limit states design,
- Evaluate the modes of vibration and mass participations in rectangular plates with various aspect ratios and loadings and determine the effect of LDA on their frequencies,

- Establish a meaningful and easy-to-follow approach to estimate the structural modes and their frequencies of vibration for rectangular plates with various aspect ratios under uniform lateral pressure.

1.4 Thesis Layout

The thesis is divided into six chapters and presented as followings:

- Chapter 1 consists of the introduction, research significance and motivation, and objectives and scope of work.
- Chapter 2 is the literature review that briefly addresses the available research on LDA topics of rectangular plates, stiffened plate analysis and design, and the vibration of rectangular plates.
- Chapter 3 consists of a numerical investigation of the LDA effects on the load-displacement and stress behaviour of rectangular panel plates of large industrial ducts. An evaluation of the existing design methodologies is presented, and the challenges in the FE Modelling of such structures are explained. Furthermore, the applicability of the existing LDA load-displacement estimations for the rectangular plates to the particular case of industrial duct walls is presented based on a thorough verification of the boundary conditions in such structures. A simple equation is presented at the end of this chapter for the limit states design of such panel plates based on the LDA and the applicable design standard.
- Chapter 4 focuses on the structural analysis and design of stiffened plates with parallel ribs from a general perspective. The conventional design based on the linear beam theory that simplifies the stiffened plate into a built-up cross-section is reviewed and discussed. The Equivalent Beam Analogy (EBA) relevance is discussed through comparisons of its results with the load-displacement behaviour of the stiffened plate and the stress distributions in the panel plate in the FE method with shell elements in LDA and SDA. Following this discussion, it is shown that the LDA is the correct analysis method for the stiffened plates as it captures the actual behaviour of such structural assemblies by taking into account the membrane forces in the analysis. A simple design methodology is presented at the end of this chapter which could be used

in future studies to generate empirical design equations for stiffened plates using the LDA.

- Chapter 5 is mainly focused on the dynamic behaviour of the panel plates in rectangular ducts. It involves estimating three structurally-significant modes of vibration for the rectangular panel plates based on their mass participation ratios. The panel plate FE models are analyzed under a uniform lateral pressure which is applied incrementally using LDA. At the end of each loading increment, the plate's natural frequencies are calculated for the three significant modes to study the effects of large displacements on the modal frequencies of the panel plate. At the end of this chapter, design charts are provided for various panel plate aspect ratios and loads based on which the vibration frequency of the three significant modes could be estimated for various applied pressures. A practical example of how to use the charts is also provided.
- Chapter 6 provides a summary of the research project, the main contributions and conclusions, and recommendations for future works.

CHAPTER 2

Literature Review

2.1 Background

There is a great wealth of literature about the structural analysis and design of stiffened plates with parallel ribs. This literature review is divided into three sections to distinguish the references used in various parts of this research study, as well as the FE methodology and the element utilized in the numerical studies of this thesis. Section 2.2 is mainly about the works on the large displacement analysis of thin rectangular plates. Section 2.3 focuses on the stiffened plates and the available analysis and design methods. Lastly, Section 2.4 consists of a selection of the available references on the topic of modal analysis and free vibration of rectangular plates.

2.2 Large displacement analysis of thin rectangular plates

Thin plates are defined based on their relatively small thickness compared to their planar dimensions. Although a clear distinguishing thickness-to-width ratio is not defined, many references, including Timoshenko and Weinomsky-Kreiger (1959) identify thin plates as those with $t < 0.1B$, where t and B are the plate thickness and width.

The Kirchhoff-Love plate theory is generally applied to thin rectangular plates with small displacements. The plate governing equation (Eq. 2.1) in this method involves the flexural behaviour in a single, linear differential equation.

$$\frac{\partial^4 w}{\partial x^4} + 2 \frac{\partial^4 w}{\partial x^2 \partial y^2} + \frac{\partial^4 w}{\partial y^4} = q/D \quad (\text{Eq. 2.1})$$

In this equation, w is the deformation at any point on the x,y plane of the plate, q is the applied lateral load, and $D=Et^3/12(1-\nu^2)$ is the flexural rigidity of the plate where E and ν are the plate material's modulus of elasticity and Poisson's ratio respectively.

There are several closed-form and numerical solutions to Eq. 2.1 in the literature for various rectangular plate dimensions and any combinations of loading and boundary conditions. However, if the plate deformations are relatively large, Eq. 2.1 is not relevant as it does not consider the

membrane (tangential) stresses. Different references have defined the large deformations in relation with the plate thickness including $\delta > 0.5t$ (Levy, 1941-a), $\delta > 1.0t$ (Timoshenko and Weinomsky-Kreiger, 1959) and (Ugural, 1981), and $\delta > 0.1t$ (Bakker et al., 2008). Regardless of the triggering deformation limit, large deformations introduce nonlinearities in the load-deformation behaviour of the plate and governed by the von-Kármán equations (Eq. 2.2 and 2.3).

$$\frac{\partial^4 F}{\partial x^4} + 2 \frac{\partial^4 F}{\partial x^2 \partial y^2} + \frac{\partial^4 F}{\partial y^4} = E \left[\left(\frac{\partial^2 w}{\partial x \partial y} \right)^2 - \frac{\partial^2 w}{\partial x^2} \frac{\partial^2 w}{\partial y^2} \right] \quad (\text{Eq. 2.2})$$

$$\frac{\partial^4 w}{\partial x^4} + 2 \frac{\partial^4 w}{\partial x^2 \partial y^2} + \frac{\partial^4 w}{\partial y^4} = \frac{t}{D} \left(q + \frac{\partial^2 F}{\partial y^2} \frac{\partial^2 w}{\partial x^2} + \frac{\partial^2 F}{\partial x^2} \frac{\partial^2 w}{\partial y^2} - 2 \frac{\partial^2 F}{\partial x \partial y} \frac{\partial^2 w}{\partial x \partial y} \right) \quad (\text{Eq. 2.3})$$

A solution to Eq. 2.2 for specific boundary conditions will result in the stress function (F) determining the membrane stresses in the middle surface of the plate. Once the stress function is determined, the displacements could also be calculated in Eq. 2.3. The membrane forces N_x , N_y , and N_{xy} are calculated based on the stress function and the plate thickness as:

$$\begin{cases} N_x = t \frac{\partial^2 F}{\partial y^2} \\ N_y = t \frac{\partial^2 F}{\partial x^2} \\ N_{xy} = -t \frac{\partial^2 F}{\partial x \partial y} \end{cases} \quad (\text{Eq. 2.4})$$

The existence of the stress function at the right side of the differential equation results in a nonlinear load-displacement and load-stress relation for the plate. This nonlinear behaviour is fundamentally different from the material nonlinearities induced by the plastic deformations.

The first general closed-form solution to the von-Kármán equations were presented by Levy (1941-a) for the case of rectangular simply-supported plate. The proposed solution was examined for the two geometries of square, and rectangular (1:3 ratio) plates in specific load cases of symmetrical normal pressure, uniform lateral pressure, and combined uniform lateral pressure and edge compression. Moreover, Levy (1941-b and 1942) provided another solution to the von-Kármán equations for the case of square plates with clamped edges under uniform lateral pressure. The load-displacement charts by Levy (1941-a and 1941-b) for square plates are shown in Fig. 2.1.

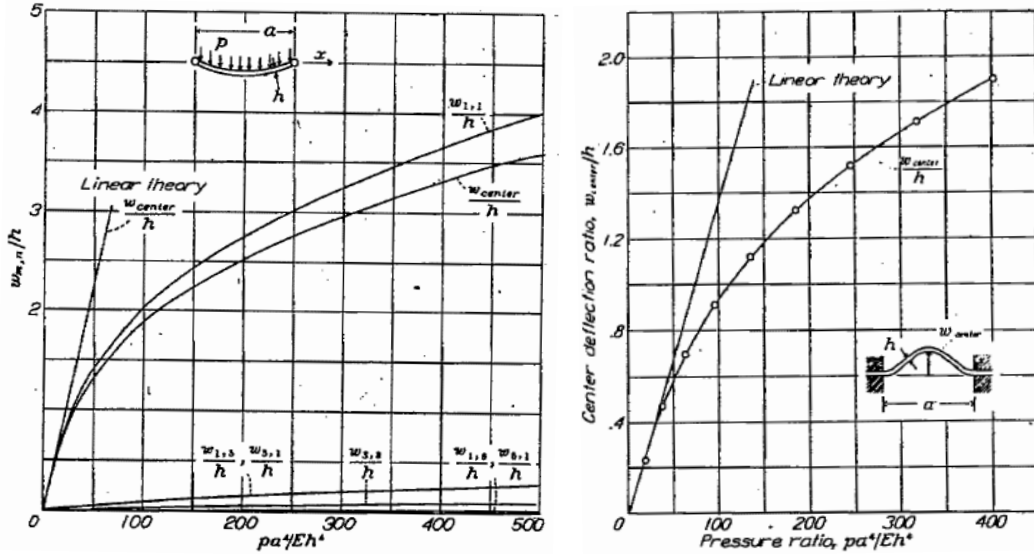


Fig. 2.1: Load-displacement charts for square clamped (right) and simply-supported (left) plates by Levy (1941-a and 1941-b)

Following the solutions by Levy, an experimental testing program on 56 rectangular plates with clamped edges, and 5 plates with freely-supported edges was conducted by Ramberg et al. (1942). The test setup was arranged as shown in the section view in Fig. 2.2.

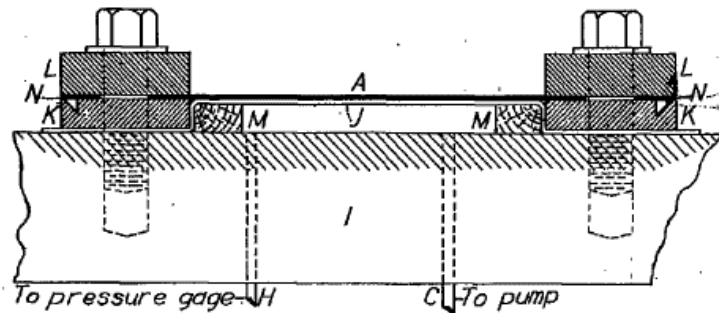
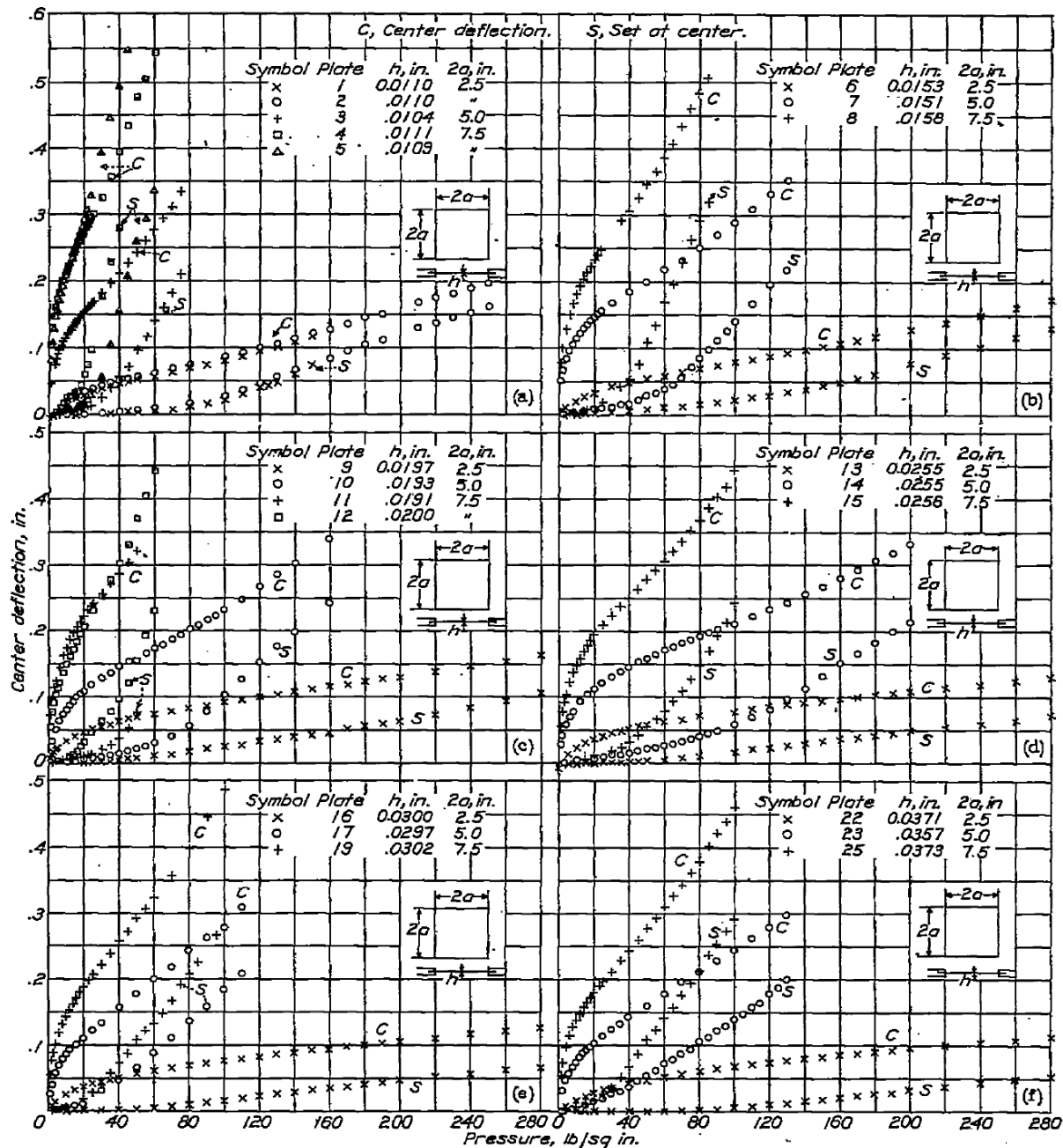


Fig. 2.2: Schematic section view of the testing apparatus for clamped plates (Ramberg et al., 1942)

The experimental tests of Ramberg et al. resulted in load-displacement and load-stress charts which were used as a reference for future research on the large-displacement analysis of rectangular plates. Some examples of these load-displacement charts are shown in Fig. 2.3.



(a) Plates 1,2,3,4, and 5. (b) Plates 6,7, and 8. (c) Plates 9,10,11, and 12.
 (d) Plates 13,14, and 15. (e) Plates 16,17, and 19. (f) Plates 22,23, and 25.

Fig. 2.3: Load-displacement charts for square clamped plates by Ramberg et al. (1942)

Given the importance of such advancements in the design of aeroplanes and warcrafts during the WW2 era, the Levy and Ramberg reports were kept classified for 50 years. Following these reports, some further solutions to the von Kármán equations for the cases of rectangular plates with planar aspect ratios of 1.5 and 2.0 were proposed by Wang (1948). The rectangular plates in

Wang's report had boundary conditions that resembled riveted edges and uniformly applied lateral pressure.

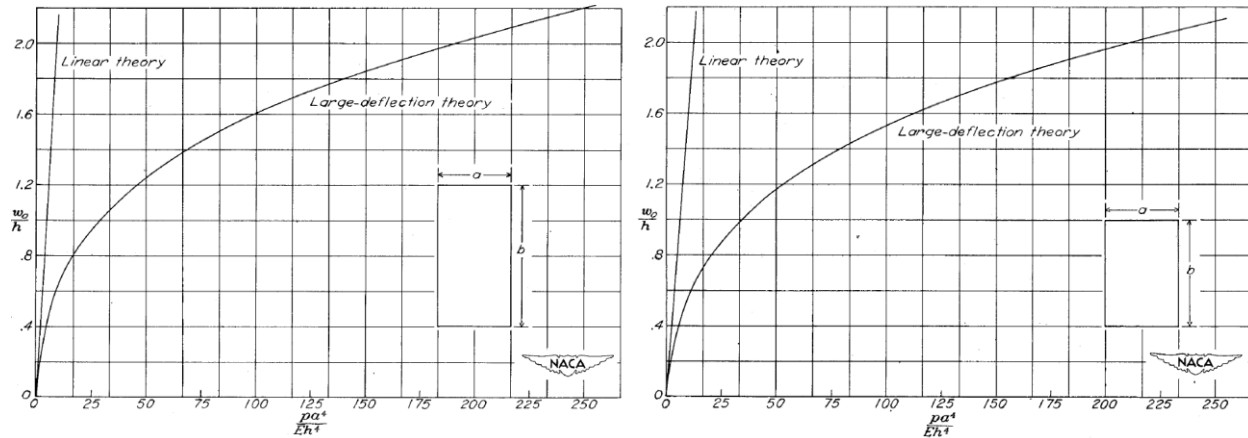


Fig. 2.4: Load-displacement charts for rectangular plates with aspect ratio of 1.5 (right), and 2.0 (left) by Wang (1948)

A series of equivalent equations were offered by Ciarlet (1980) for the von Kármán equations in which the nonlinear large deformation analysis of the plate was explained in the “method of asymptotic expansions”. This method which was claimed to be a simplified yet equivalent replacement to the von Kármán equations have never gained attention as it was stating the problem in a different set of equations with more terms and parameters, new assumptions, and different methodologies that those offered previously for the von Kármán equations. A series of numerical solutions to the von Kármán equations were offered by Katsikadelis and Nerantzaki (1994) in forms of an “analog equation method” in which two sets of linear bending problems were used as the stress and deflection functions.

In all references up to this point, the boundary conditions considered in the solutions were symmetrical, i.e., the plate had the same boundary conditions at opposite edges. A new method was offered by Little (1999) in which the large-displacement analysis of rectangular plates with special cases of boundary conditions combinations such as those supported at three edges and free at one edge became possible. Moreover, the solution by Little (1999) involved the consideration of potential initial imperfections on the plate surface, and out-of-plane equilibrium in forms of energy formulations.

Most recently, the large displacement analysis of rectangular plates gained more attention objectively by researchers trying to provide applicable analysis and design analogies in order to

implement it in the engineering design of thin-walled structures. Thanga et al. (2013) implemented this analogy to adopt a design method for the panels of the stiffened plates of duct walls. Their method was based on a FE Modelling on the ADINA platform in which three different stages of through-thickness yielding were defined as the limits for the ultimate load. Similarly, El-Aghoury and Galal (2014) provided an approximation of the nonlinear load-displacement behaviour of long rectangular plates using FE analysis and a 3-point approximation method as shown in Fig. 2.5.

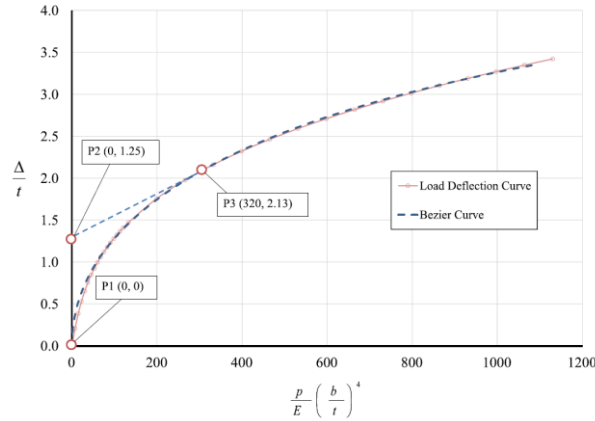


Fig. 2.5: Three-point Bezier approximation of the load-displacement chart by El-Aghoury and Galal (2014)

2.3 Analysis and design of stiffened plates

The dominant form for the walls of industrial structures, ship hulls, aircraft fuselage, and other similar structures is a combination of rectangular panel plates with rib stiffeners. The stiffened plate geometry and configuration make it very useful for warcraft and military applications. In this regard, there was a boost in the research on this topic in the 3rd and 4th decades of the previous century followed by some large time gaps afterwards due to the confidentialities imposed by the funding authorities at that era.

There are hundreds of published articles about the analysis and design of stiffened plates from the stand points of various applications, design methodology, and analysis. One of the most referenced works on the concept of stiffened plates is the book by Triotsky (1976) in which various topics surrounding the structural analysis and design of stiffened plates are addressed and discussed. A recent literature study by Bedair (2009) has provided a brief review over more than 400 such publications from the perspective of analytical techniques, closed-form and numerical solutions, and limit states design over the span of 1902 to 2008. According to Bedair’s literature

review, the earliest attempts on the analysis of stiffened plate were on the basis of simulations using the classical beam theory. As this thesis mainly focuses on the effects of large displacement on the behaviour of stiffened plates, most of the works in Bedair’s literature review are left out as irrelevant as their methodologies were based on the classical beam theory and small displacement analysis. However, it is worth mentioning that the simulation of stiffened plated as an *equivalent beam* (EB) has been the grounds for most of the literature on this topic.

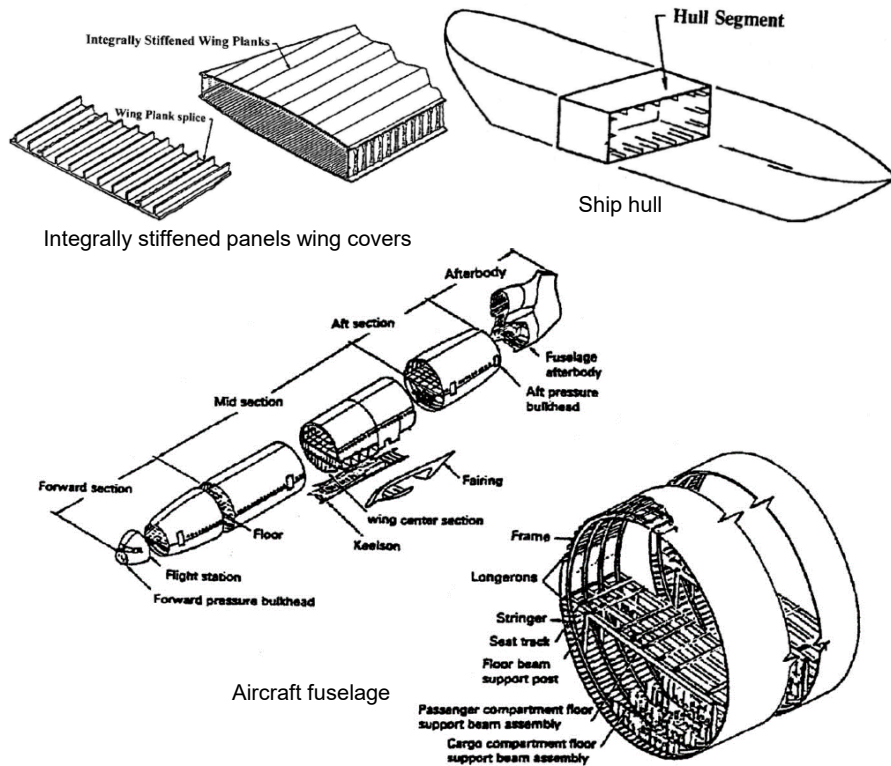


Fig. 2.6: Examples of stiffened plates and shells applications (Bedair, 2009)

When the stiffened plate is simplified into an EB, the rib stiffener and the panel plate take part in the overall resistance of the EB to flexural, shear, and axial stresses. An extensive literature review on the aspect of the effectiveness of the panel plate in the overall behaviour of the stiffened plate was published by Paik (2008) where some key terms such as effective breadth, effective width, and effective shear modulus were reviewed and discussed. The effective breadth was defined by Paik (2008) as a portion of the plate with contributions in the EB flexural resistance as shown in Fig. 2.7.

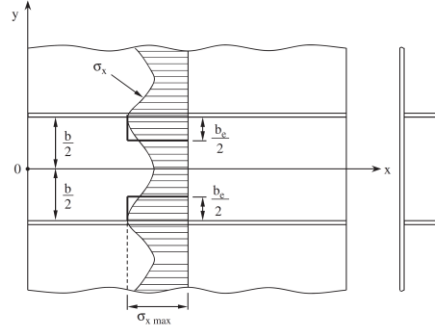


Fig. 2.7: Schematic display of the effective breadth in a typical stiffened plate (Paik, 2008)

Compared to the previously available values for the b_e in the literature such as, $b_e=32t$ (Blodgett, 1966), and $b_e=32t+t_s$ (ASCE, 1995), in which t and t_s are the plate and stiffener thicknesses respectively, Paik (2008) provided a more robust method for the calculation of b_e when the stiffened plate is under uniform lateral load as:

$$b_e = \frac{4L \sinh^2(\pi b/L)}{\pi(1+\nu)[(3-\nu)\sinh(2\pi b/L) - 2(1+\nu)(\pi b/L)]} \quad (\text{Eq. 2.5})$$

Where L is the length of the stiffened plate, b is the panel plate width, and ν is the plate material Poisson's ratio. An approximation of Eq. 2.5 was also presented by Paik (2008) as:

$$\frac{b_e}{b} = \begin{cases} 1.0 & \text{for } b/L \leq 0.18 \\ \frac{0.18}{(b/L)} & \text{for } b/L > 0.18 \end{cases} \quad (\text{Eq. 2.6})$$

Furthermore, Paik and Seo (2009-a) presented a FE analysis approach for steel stiffened plates under combined biaxial compression and lateral pressure aiming for providing grounds for the ultimate limit states (ULS) design of such structures mainly in ship hulls. They then applied their methodology and analysis approach to three stiffened plate models as shown in Fig. 2.8 (Paik and Seo, 2009-b).

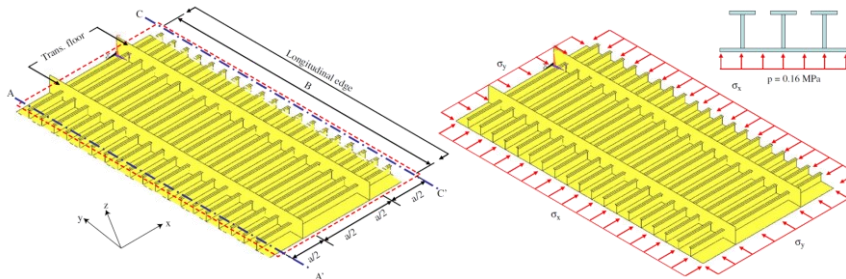


Fig. 2.8: The geometry and loading in the FE models by Paik and Seo (2009-b)

More recently, a study by Rahbar Ranji (2014) introduced an imaginary effective breadth/web concept for the evaluation and determination of the torsional buckling of the EB on the basis of the Euler stress for the coupled buckling mode.

Aside from the studies on the EB and the panel plate effectiveness, there are several attempts in the literature to formulate and simplify large displacement analysis of stiffened plates. In a series of papers, Brubak and Hellesland (2007-a, 2007-b, and 2007-c) studied the case of arbitrarily stiffened plates from the perspectives of buckling strength, local and global bending, and postbuckling by implementing a semi-analytical approach based on the von Mises yield criterion. The local and global equilibrium paths were traced in their work (2007-b) by using the large deflection theory combined with the Rayleigh-Ritz criterion on an incremental form. Furthermore, they evaluated various criteria to estimate the ultimate flexural strength of such structures using semi-analytical methods separately (Brubak and Hellesland, 2008). The general schematic view of the stiffened plate in all studies by Brubak and Hellesland is shown in Fig. 2.9. While the semi-analytical approach by Brubak and Hellesland was a great effort to obtain closed-form solutions to the large deflection analysis of stiffened plates, it often involved lengthy and sophisticated mathematical formulations with approximations and assumptions for case-specific boundary conditions. On the other hand, they also provided some verifications using FE analysis using ANSYS software to verify their method further.

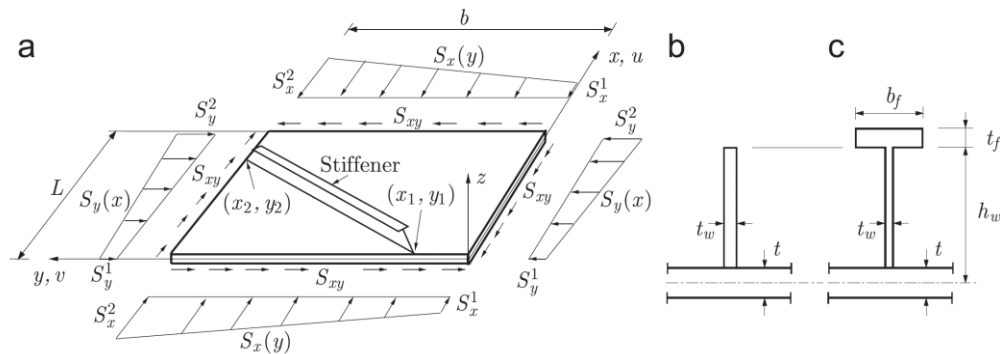


Fig. 2.9: Schematic display of the stiffened plate; (a) Stiffened plate subjected to applied in-plane shear stress (S_{xy}) and in-plane, linear varying compression or tension stress (S_x , S_y), and cross section of an eccentric, (b) flat bar and (c) T-stiffener. (Brubak and Hellesland, 2007-a, 2007-b, 2007-c, 2008)

Another approach for the large deflection FE analysis of stiffened plates was presented by Ojeda et al. (2007) in which the equilibrium equations were derived using the principle of virtual work.

A similar study by Leheta et al. (2015) focused on the application, analysis, and advantages of Y stiffeners as a replacement for other shapes and profiles of stiffeners typically used in the ship hull design and construction. Detailed comparisons of the geometrical characteristics of the newly-proposed rib stiffener shape with the typical ones were presented, and a FE analysis using ANSYS software on some stiffened plate panels from an existing ship hull design were followed.

While there is a great need for extensive experimental studies on stiffened plates, there are minimal such studies in the literature. The experimental program by Xu and Guedes Soares (2013) consisted five stiffened plate specimens under axial compression to obtain their load-deformation and collapse loads, as shown in Fig. 2.11. Following the experimental tests, an empirical design method was presented in which the effects of various parameters were included. Moreover, some general conclusions, including a suggested arrangement of the rib stiffeners to potentially avoid the collapse of the side bays, were presented at the end of the study.



Fig. 2.11: The test setup and one of the specimens tested by Xu and Guedes Soares (2013)

Another experimental study that could be related to the stiffened plates analysis and design was presented by Kwon (2014), in which the *direct strength method* that had been previously tested for cold-formed steel members was evaluated for welded steel members, including the stiffened plate geometry. A total of 14 specimens were tested under direct compression as shown in Fig. 2.12 by Kwon and the results were used for the evaluation of the direct strength method by the author. The experimental work ultimately resulted in an empirical equation for the calculation of the *limiting load*, which accounts for local and overall buckling of the stiffened plate under direct compression (Kwon, 2014).



Fig. 2.12: Test setup and deformed shape of the stiffened plate specimen (Kwon, 2014)

The experimental tests by Shanmugam et al. (2014) are unique because they are the only ones that include bending of stiffened plates and the combined bending and compression. A total of 12 stiffened plates were tested by Shanmugam et al. (2014) in two separate divisions: series A and series B with slenderness ratios (b/t) of 100 and 76. The test setup is shown in Fig. 2.13.

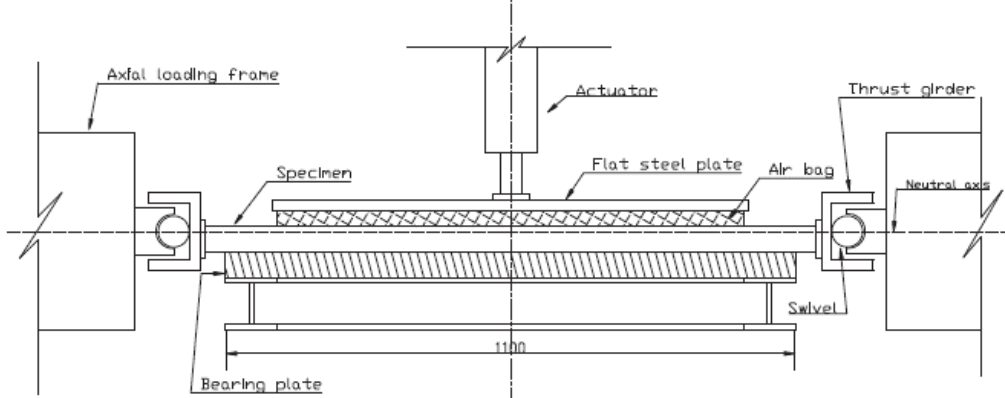


Fig. 2.13: Test setup (up), and the sectional view of the test setup (down) by Shanmugam et al. (2014)

Shanmugam et al. (2014) also included a FE modelling using ABAQUS software to establish an accurate modelling approach for such analysis. The tests results were presented in the form of comparisons between the deformed shapes observed from the tests and predicted by the FE analysis, lateral load-displacement charts, and interaction diagrams for axial load and lateral pressure.

2.4 Modal analysis and free vibration of rectangular plates with large deformations

The earliest attempts on the vibration analysis of rectangular plates in presence of in-plane (membrane and shear) forces were made by Dawe (1969) and followed by alternative solutions including numerical methods by Mei and Yang (1972), Dickinson (1973) and Bassily and

Dickinson, (1973). Chan and Foo (1979) were amongst the first to apply the *Finite Strip method* to solve the case of rectangular plate vibration with membrane forces.

The general equation of motion for a rectangular plate under lateral and in-plane loading is presented in Eq.2.7.

$$D \left[\frac{\partial^2 w}{\partial x^2} + \frac{\partial^2 w}{\partial y^2} \right]^2 + ch\dot{w} + \rho h\ddot{w} = f + q + N_x \frac{\partial^2 w}{\partial x^2} + N_y \frac{\partial^2 w}{\partial y^2} + 2N_{xy} \frac{\partial^2 w}{\partial x \partial y} \quad (\text{Eq.2.7})$$

In which D is the flexural rigidity of the plate, c is the viscous damping, ρ is the mass density per unit volume of plate material, h is the plate thickness and $w(x, y, t)$ is the dynamic displacement at any given point of plate surface at specific time (t). The first and second derivatives of w with respect to t (i.e. \dot{w} and \ddot{w}) represent the velocity and acceleration at a specific time. On the right side of Eq.2.7, f is the external excitation as a function of time, q is the lateral pressure applied at the plate surface while N_x, N_y are the membrane forces distributed along the edges of plate and N_{xy} is the in-plane shear force, respectively.

The simplest form of plate vibration analysis represents the free vibration of unloaded rectangular plates with negligible damping. In this case, the forcing terms at the right side and the viscous damping term at the left side of Eq. 2.7 are set to zero and it reduces to Eq. 2.8.

$$D \left[\frac{\partial^2 w}{\partial x^2} + \frac{\partial^2 w}{\partial y^2} \right]^2 + \rho h\ddot{w} = 0 \quad (\text{Eq. 2.8})$$

There is an infinite number of natural frequencies (and mode shapes) available from the closed-form or numerical solutions to Eq. 2.8 for various boundary conditions of rectangular plates (Amabili, 2008). As an example, the closed form solution to Eq. 2.8 for rectangular plates with all edges simply-supported could be presented as Eq. 2.9.

$$\omega_{m,n} = \pi^2 \left[\left(\frac{m}{L} \right)^2 + \left(\frac{n}{B} \right)^2 \right] \sqrt{D/\rho h} \quad (\text{Eq. 2.9})$$

In which m and n indicate the number of wave fronts along the length (L) and breadth (B) of the rectangular plate for any particular mode shape with natural frequency $\omega_{m,n}$. Amabili (2006) verified the natural frequencies of 15 modes of vibration resulted from Eq. 2.9 experimentally for the case of a rectangular aluminium plate as shown in Fig. 2.14.



Fig. 2.14: Experimental test setup of Amabili (2006)

In another case, the free vibration of rectangular plates with negligible damping in presence of membrane forces was studied by Singh and Dey (1990) using the energy method. They discretized the total energy of free vibration of the system by replacing the derivative terms with their Finite Difference equivalents and used a specific energy minimization technique to solve the resulting eigenvalue problem. One step further into the case of rectangular plate vibration with membrane forces, Leissa and Kang (2002) presented one of the first exact solutions for the case of vibration and buckling of rectangular plates with a particular boundary conditions in which two opposite edges of the plate were clamped and the two other edges were simply-supported. A linearly variable in-plane load was considered to act at the simply-supported edges (Leissa and Kang, 2002). A similar case was presented by Wang et al. (2006) that simplified Eq. 2.7 into the form presented in Eq. 2.10 for the case of free vibration of rectangular plates with membrane forces acting at opposite edges along x axis.

$$D \left[\frac{\partial^2 w}{\partial x^2} + \frac{\partial^2 w}{\partial y^2} \right]^2 + \rho h \ddot{w} = N_x \frac{\partial^2 w}{\partial x^2} \quad (\text{Eq. 2.10})$$

Wang et al. (2006) used the differential quadrature method to solve Eq. 2.10 and calculated the vibration frequency for six mode shapes of the rectangular ($m=1$ to 3 , $n=1$ and 2). They estimated the $w(x,y,t)$ function by $w(x,y)\sin(\omega t)$ and presented the in-plane force N_x with a linear function.

Aside from those references that address the plate vibration from a general point of view, there are some more detailed works that focus on some special aspects of the problems related to the

vibration of plates. Phillips and Jubb (1974) studied the effect of lateral distortion on the natural frequency of rectangular plates by performing experimental tests on a rectangular plate with approximately clamped edges and verified the findings with the existing theory.

Kaldas and Dickinson (1981-a) used the Finite Difference method and Rayleigh-Ritz analysis to estimate the vibration modes and frequencies of rectangular plates with complications such as weld lines or initial in-plane residual stresses. Furthermore, Kaldas and Dickinson (1981-b) studied the effects of weld runs and the residual stresses due to welding or flame cuts on the flexural vibrational characteristics of rectangular plates by applying Finite Difference analysis and the Rayleigh-Ritz method along with experimental tests on plates with beam characteristic functions. The case of forced vibration of rectangular plates with initial imperfections such as deflections or displaced supports was studied by Yamaki and Chiba (1983), and it was followed by the experimental tests by Yamaki et al. (1983) in order to address the nonlinear vibrations of a square plate with clamped edges in a more realistic way. Gorman (1982) applied the superposition method to obtain accurate solutions for the case of free vibration frequencies and mode shapes of rectangular plates resting on elastic supports at their edges. He generated an eight-by-eight matrix for the schematic presentation of the eigenvalues based on four-term expansions for building block solutions for different cases of supports flexibility.

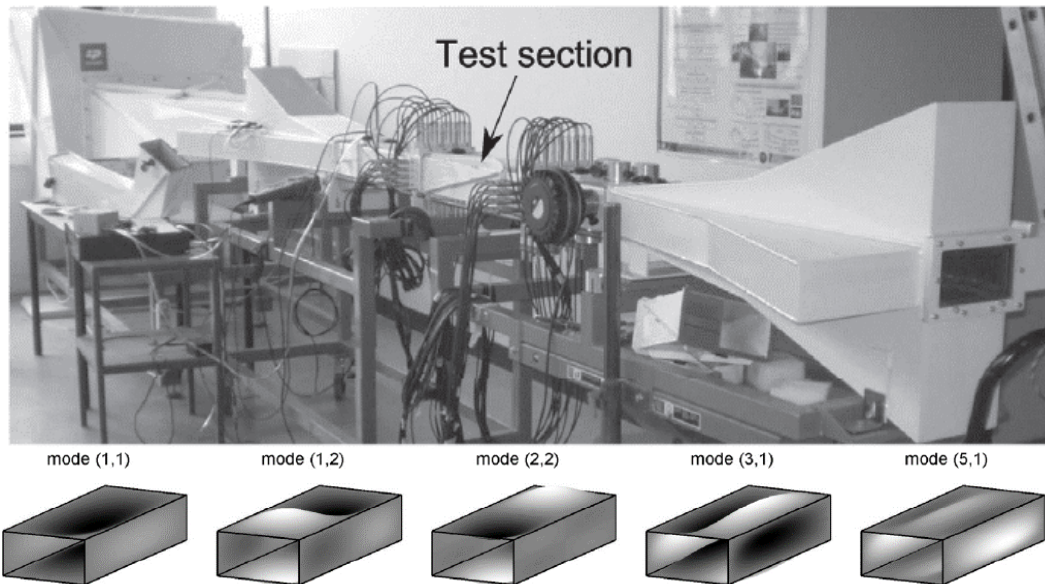


Fig. 2.15: The experimental test setup (up), and the expected modal shapes for the duct segment (down) by David et al. (2018)

The most recent work on the vibrational response of rectangular ducts was presented by David et al. (2018) in which the concept of flow-induced vibration in rectangular ducts was presented through experimental and analytical studies. A $0.2 \text{ m} \times 0.1 \text{ m}$ section of a steel duct with 0.5 m length was experimentally tested in the specifically-designed gas flow test table shown in Fig. 2.15 in order to obtain its vibration modes during various scenarios of turbulent flow with velocities of 20 m/s and 30 m/sec . The experimental results were then used to validate the results of the numerical analysis in which the acoustic and aerodynamic components of vibration were presented. They concluded that the prediction of the flow-induced vibrations is achievable by numerical analysis.

CHAPTER 3

Structural Design of Stiffened Plates of Industrial Duct Walls with Relatively Long Panels Undergoing Large Deformations

3.1 Abstract

Structural design of stiffened plates of the walls of rectangular-sectioned industrial ducts is currently based on the strip method that follows the linear flexural beam theory. The current design method assumes that the displacements generated in the plate are small and the membrane forces that generate in the plate are negligible. This paper addresses the current design method and discrepancies associated with it to present a new design approach that takes into account the effects of large displacements on the load-deformation and load-stress behaviour of stiffened plates. Two different sets of formulas are presented based on Finite Element analysis of rectangular plates with relatively long aspect ratios that estimate the maximum stress and deformation in the typical and edge panels of stiffened plates. These formulas are then used to establish design equations for stiffened plates. Based on the findings of this paper, a reduction of 30 to 40 percent in the plate thickness could be achieved if the new design approach is selected over the conventional design method.

3.2 Introduction

Many industries require transferring large amounts of air and flue gas between different points as part of their production or treatment procedures. Depending on the nature of flu gas and the volume of transfer, ducts with different shapes and sizes are used in various parts of a given industry. Most duct line assemblies consist of various segments connected to each other to form a conduit line that transfers large amounts of air or flue gas in industrial facilities. A segment of a duct line assembly forms a straight line or an elbow with circular, rectangular or transfer cross-sections. A typical rectangular duct segment consists of four plates sealed together to form the walls of a rectangular section resting on supporting frames at two ends. The wall plates are stiffened by rib elements at certain intervals throughout the length of the duct segment as shown

in Fig. 3.1 to form stiffened plates with relatively long rectangular panels. This paper studies the structural design of the stiffened plates of the walls of large rectangular sectioned industrial ducts.

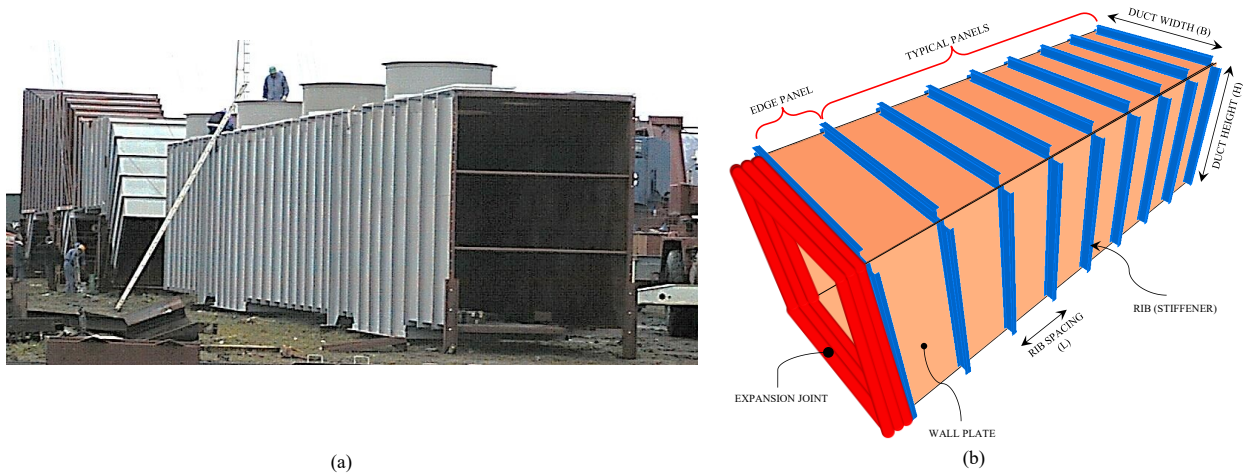


Fig. 3.1: (a) Large industrial rectangular duct segments under construction (courtesy of fives-solios Inc.). (b) Schematic view of a typical rectangular duct segment

ASCE (1995) defines various loads that apply to duct line assemblies considering the duct segment geometry, the method of application, environmental conditions, the indoor or outdoor location, the nature of flue gases transferred, the flow temperature and position of duct segment in the flow system. Although there are various external loads (dead, live, wind and earthquake loads) applicable to the duct segment, the main load acting on duct walls is the internal hydrostatic pressure that transfers the air or flu gas inside the ductline. The hydrostatic pressure inside the duct is positive if the fans that generate the flow are installed upstream but in most cases the pressure is negative (suction) since the fans are installed at the outlet of the flow (ASCE, 1995).

Structural design of duct walls consists of two stages namely, local and global design (ASCE, 1995). In the local stage, the plate thickness and stiffener arrangements are designed under the internal pressure whereas in the global stage the whole duct segment is designed for the external loads.

One of the major aspects in the analysis and design of industrial ducts and similar structures is the load-displacement behaviour of the stiffened plates. Although the effects of large deformations (i.e., geometrical nonlinearities) on the load-displacement behaviour of rectangular plates are well known, the design of plates in ductwork industries is mainly based on linear analysis without consideration of large deformations effects. ASCE (1995) briefly mentions the membrane forces

induced in the plate as a result of large deformations without giving any further technical guidance. Since then, the effects of large deformations on the failure criteria of long rectangular plates have been studied by several researchers. Young and Budynas (2002) presented nonlinear load-deformation curves of rectangular plates for various plate boundary conditions and aspect ratios considering large deformation effects. More recently, Thanga et al. (2011) studied the case of stiffened plates of duct walls while considering large displacements and allowing for partial yielding of the plate within an acceptable limit. They concluded that a design approach that is based on large deformation analysis would be more economic than the linear method stated in ASCE (1995) guideline. Following these findings, the load-displacement and load-stress relations for long rectangular plates were then formulated by El-Aghoury and Galal (2014) using Bezier equations. Similar findings were reported by Zhong (2014) for ducts with wall plate thicknesses ranging between 3/16" to 3/8". From the above, it can be noted that there is a need for developing design equations that take into account the effect of large deformations using boundary conditions that represent stiffened plates of duct walls.

The duct line segments are supported against the external loads by means of structural frames and footings or through connections with other segments. The term “structural design of duct walls” in this paper refers to the local design of duct wall plates. After the design of duct walls and segments, the duct line assembly shall be checked for thermal expansion. Thermal expansion might cause destructive axial force if restrained and should be released along the duct line by using expansion joints and elbows. It is practical in the design of duct lines to use expansion joints at one or both ends of straight segments (ASCE, 1995). An expansion joint may transfer shear, moment, torsion or a combination of all of them between two adjacent segments of the duct line but it generally provides full release of axial forces. Thus, the boundary conditions at the edge panel (see Fig. 3.1-b) at the location of the expansion joint are different from those of the typical panels of the wall plate. Therefore, this paper focuses on evaluating the linear and nonlinear behaviour of stiffened plates of duct walls considering the large deformation effects as well as the effects of expansion joints at the ends of the duct segment on the boundary conditions.

3.3 Analysis and Design of Long-Spanned Rectangular Plates

The current procedure of the design of long-spanned plates with aspect ratio greater than 2.0 is based on the application of flexural beam analogy by using a “unit-width strip” at the middle of the plate as shown in Fig. 3.2. The analysis of this unit-width beam element (design strip) could be linear or nonlinear depending on the nature of design.

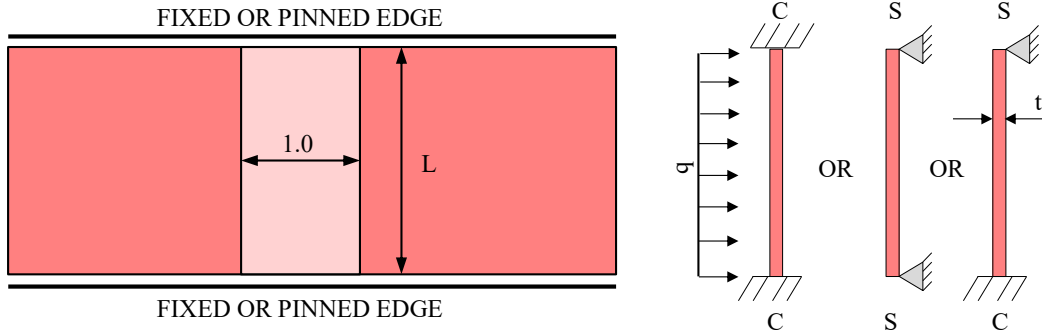


Fig. 3.2: Unit-width strip and beam analogy

3.3.1 Linear analysis of long rectangular plates under uniform lateral pressure

The principal assumption in the linear analysis of plates under uniform lateral pressure is that the deformations are small compared to the plate thickness, and strains are infinitesimal so the classic beam bending equations apply to the design strip of the plate as a beam element.

Using the unit-width beam analogy, the cross-sectional properties of the plate are calculated based on the plate thickness, t , as shown in Eq. 3.1.

$$\begin{cases} I = t^3/12 \\ S = t^2/6 \end{cases} \quad (\text{Eq. 3.1})$$

where S is the section modulus and I is the moment of inertia of the unit-width strip. Applying the beam bending analogy to the unit-width strip of the plate for the three boundary condition combinations shown in Fig. 3.2, results in the elastic stresses and deflections as shown in Table 3.1. In this table, q is the lateral uniformly distributed load, σ is *bending stress*, δ is the plate deflection and λ is the plate length-to-thickness ratio (L/t). The boundary conditions indicators “S” and “C” represent the simply-supported (hinged) and clamped (fixed) ends respectively. The

design stresses and deflections in Table 3.1 are calculated by applying the section modulus and moment of inertia in the classical bending moment equations, respectively.

Table 3.1. Stresses and deflections of long plates when using unit-width strip method and beam analogy

	Boundary Conditions		
	S-S	C-C	C-S
σ	$3qt^2x(L-x)$	$q(6xL-L^2-6x^2)/(2t^2)$	$0.75q(3xL-4x^2)/t^2$
σ^- (max)	0	$0.5q\lambda^2$ [at $x=0, x=L$]	$0.75q\lambda^2$ [at $x=0$]
σ^+ (max)	$0.75q\lambda^2$; [at $x=0.5L$]	$0.25q\lambda^2$ [at $x=0.5L$]	$0.422q\lambda^2$ [at $x=0.625L$]
δ/t	$q(xL^3-2Lx^3+x^4)/(2Et^4)$	$qx^2(L-x)^2/(2Et^4)$	$q(xL^3-3Lx^3+2x^4)/(4Et^4)$
δ/t (max)	$5q\lambda^4/(32E)$ [at $x=0.5L$]	$q\lambda^4/(32E)$ [at $x=0.5L$]	$12q\lambda^4/(185E)$ [at $x=0.5785L$]

The formulas presented in Table 3.1 are useful for the linear analysis of long (i.e. $S > 2.0$) rectangular plates based on the unit-width strip method. These equations could be interpreted in conventional design formulas in forms of Eq. 3.2 and Eq. 3.3 for the three applied boundary conditions combinations.

$$\left(\frac{q}{F_Y}\right)\lambda^2 = \begin{cases} 1.33(\sigma_{max}/F_Y); (S - S) \\ 2(\sigma_{max}/F_Y); (C - C) \\ 1.33(\sigma_{max}/F_Y); (C - S) \end{cases} \quad (\text{Eq.3.2})$$

$$\left(\frac{q}{E}\right)\lambda^4 = \begin{cases} 6.4(\delta/t); (S - S) \\ 32(\delta/t); (C - C) \\ 15.42(\delta/t); (C - S) \end{cases} \quad (\text{Eq.3.3})$$

In equations 3.2 and 3.3, the length-to-thickness ratio (i.e. λ) of plate is calculated for the given load (i.e. uniform pressure, q) by replacing the (σ_{max}/F_Y) and (δ/t) ratios with the maximum stress and deflection limits set by the design criteria (i.e. design codes adopted by the engineer). The final design results are the plate length and thickness that fit into the length-to-thickness ratio calculated from these design equations. Since the plate gauges are limited, it is practical to select the thickness of the plate from the available gauges then design the ribs spacing using equations 3.2 and 3.3. In cases where the presence of expansion joints dictates the boundary conditions of

the edge panel, a practical design calls for keeping the same plate thickness while reducing the rib spacing for the edge panel. In cases when the stress criterion is used, the rib spacing ratio for the edge panel would be calculated using Eq. 3.2 as:

$$\lambda_{\text{edge}}/\lambda_{\text{typical}}=(1.33/2.0)^{0.5} = 0.815$$

and similarly, for the deflection criterion using Eq. 3.3:

$$\lambda_{\text{edge}}/\lambda_{\text{typical}}=(15.42/32)^{0.25} = 0.833$$

Thus, as a general rule it is practical to design the rib spacing at the edge panels of duct segments within the range of 80% of the typical rib spacing when expansion joints are used.

3.3.2 Nonlinear Analysis of Plates Under Uniform Lateral Pressure with Large Deformations

Applying uniform lateral pressure to a rectangular plate results in deformations throughout the plate with the peak deflection at the centroid. A relationship between applied lateral pressure and the resulting deflections could be established if the types of stresses generated in the plate due to the applied pressure are known.

In general, plate stresses are categorized into three main types by the classic plates and shells theory namely the in-plane (tangential) stresses, the out-of-plane (shear) stresses and the bending (flexural) stresses (Love, 1888). One of the governing parameters in the classic plate theory is the thickness of the plate. In extremely thin plates, the effects of bending and shear stresses on the overall load-deformation behaviour are minimal and any out-of-plane deflection is significantly greater than the thickness of the plate. Plates with such behaviour are classified as membrane elements in most of the available references including Timoshenko and Woinowsky-Kreiger (1959). On the other hand in thicker plates, the effects of bending stresses on the overall plate behaviour increase with the thickness of plate while the tangential stresses and lateral displacements reduce significantly. In cases where the deflections are small compared to the thickness of the plate, the tangential stresses are negligible and the plate is considered as “pure bending plate” (Timoshenko, 1938).

In general, Kirschhoff-Love plate theory is applied to thin plates where the plate thickness is at least one degree smaller than its width (Timoshenko, 1938) as shown in Eq. 3.4.

$$\frac{\partial^4 w}{\partial x^4} + 2 \frac{\partial^4 w}{\partial x^2 \partial y^2} + \frac{\partial^4 w}{\partial y^4} = \frac{q}{D} \quad (\text{Eq. 3.4})$$

where w is the deformation at any point, x and y stand for the coordinates of the point where the deflection is desired, q is the applied uniform pressure and D is the flexural rigidity of the plate calculated as:

$$D = \frac{Et^3}{12(1-\nu^2)} \quad (\text{Eq. 3.5})$$

in which E and ν are the modulus of elasticity and Poisson's ratio of the plate material respectively. There are several available solutions for Eq. 3.4 when applying various boundary conditions in terms of closed-form and numerical approaches in the literature, including the solutions given by Timoshenko and Woinowsky-Kreiger (1959).

The contribution of shear stresses in the overall response of thick plates (e.g. thick concrete slabs) to the applied pressure must be considered in the plate governing equations. Such thick plates are often called the "Mindlin-Reissner plates" since their case was first presented and solved separately by Mindlin (1951) and Reissner (1945) as an extension to the Kirschhoff-Love plate theory. The case of thick plates with shear behaviour is out of scope of this paper.

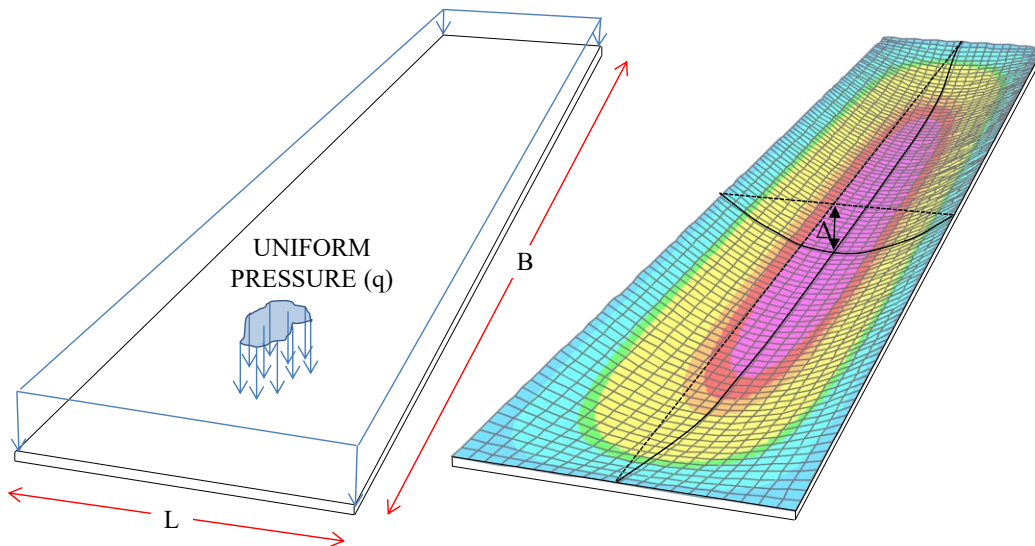


Fig. 3.3: Rectangular simply supported plate under uniform lateral pressure. a) Plate dimensions and loading b) Contour display of plate deflection

If the displacements of thin plates are relatively large, Eq. 3.4 does not result in accurate answers because it ignores the contribution of tangential stresses in the plate behaviour. The load-deformation behaviour of thin plates is governed by von-Kármán equations in the case of rectangular plates with large deformations. Different references defined large deformations based on portions of the thickness of the plate e.g. $\delta > 0.5t$ (Levy, 1941a), $\delta > 1.0t$ (Timoshenko and Woinowsky-Kreiger, 1959) (Ugural, 1981) and $\delta > 0.2t$ (Bakker et al., 2008) where δ is the maximum deflection normally at the center of plate as shown in Fig. 3.3. The von-Kármán equations are presented in Eq. 3.6 and Eq. 3.7 where F is a stress function of x and y (Timoshenko and Goodier, 1951).

$$\frac{\partial^4 F}{\partial x^4} + 2 \frac{\partial^4 F}{\partial x^2 \partial y^2} + \frac{\partial^4 F}{\partial y^4} = E \left[\left(\frac{\partial^2 w}{\partial x \partial y} \right)^2 - \frac{\partial^2 w}{\partial x^2} \frac{\partial^2 w}{\partial y^2} \right] \quad (\text{Eq. 3.6})$$

$$\frac{\partial^4 w}{\partial x^4} + 2 \frac{\partial^4 w}{\partial x^2 \partial y^2} + \frac{\partial^4 w}{\partial y^4} = \frac{t}{D} \left(\frac{q}{t} + \frac{\partial^2 F}{\partial y^2} \frac{\partial^2 w}{\partial x^2} + \frac{\partial^2 F}{\partial x^2} \frac{\partial^2 w}{\partial y^2} - 2 \frac{\partial^2 F}{\partial x \partial y} \frac{\partial^2 w}{\partial x \partial y} \right) \quad (\text{Eq. 3.7})$$

A solution to von-Kármán equations for specific boundary conditions results in *stress* and *deformation* functions. The stress function (F) determines the tangential stresses in the middle surface of the plate and the deformation function, (w) defines the deflected shape of the plate as:

$$\begin{cases} N_x = t \frac{\partial^2 F}{\partial y^2} \\ N_y = t \frac{\partial^2 F}{\partial x^2} \\ N_{xy} = -t \frac{\partial^2 F}{\partial x \partial y} \end{cases} \quad (\text{Eq. 3.8})$$

The bending and shear stresses could be then extracted from the classic plate theory considering small deformations. In other words, the distributed uniform load q could be resolved into two components q_1 and q_2 where q_1 is balanced in total by bending and shear stresses calculated using the equations of plates with small deformations and q_2 is balanced by the membrane (tangential) stresses calculated using Eq. 3.8 (Timoshenko and Woinowsky-Kreiger, 1959).

Although general closed form solutions to von-Kármán equations do not exist yet, several cases of plates with different geometry and boundary conditions are solved in the literature. First attempts were made by Levy in three separate reports for the National Committee for Aeronautics (Levy, 1941a, 1941b, 1942) to present a closed form solution to von-Kármán equations for specific

boundary conditions and geometries of rectangular and square plates. In order to support and verify the previously derived solutions by Levy, Ramberg et al. (1942) performed normal pressure experimental tests on 56 rectangular plates with clamped edges and 5 plates with freely supported edges. The results of those tests only qualitatively verified the results obtained from the theoretical solutions to the plate deformation equations, thus more improved solutions were required. Some improved solutions to von-Kármán equations for rectangular plates were obtained for the special cases of plates with aspect ratios of 1.5 and 2.0 under normal uniform pressure by Wang (1948). In similar attempts, other researchers (Little, 1999)(Wang and El-Sheikh, 2005)(Imrak and Gerdemeli, 2007) stated various closed form solutions for the same problem using different methods. Latest attempt to derive a closed form solution for the case of rectangular plate with large deformations was by Ibearugbulem et al. (2013) where the maximum deflection at the center of rectangular plates simply-supported at four edges (SSSS) was calculated. Rectangular plates with aspect ratios varying from 1.0 to 2.0 were solved by this method and the solutions were verified with the previous methods by Timoshenko and Krieger (Ibearugbulem et al. 2013).

Aside from the closed form types of solutions that lead to lengthy mathematical formulations which are not simple to follow by the design engineers, approximate and numerical methods were also suggested in most of the previously mentioned references. Bakker et al. (2008) used a shape function corresponding to the first buckling mode shape of the plate under in-plane compressive stresses in order to approximately determine the large deflection behaviour of rectangular simply-supported thin plates. In their approach, the large-deflection behaviour of the plate under transverse loading was estimated as a function of the ratio of the pre-buckling to post-buckling stiffness of the plate. Both pre- and post-buckling stiffnesses are available in the literature for rectangular plates.

As in most of the available references on plate analysis, in this paper long rectangular plates are those with aspect ratios of 2.0 and greater, which mainly refer to panels of stiffened plates used as the walls of thin-walled structures such as industrial ducts, bunkers and similar structures. There is very limited research work available in the literature addressing the behaviour of such plates under transverse pressure considering large deformations effects; this is in part due to the general definition of long plates as elements whose behaviour could be resembled as one-way plate action using beam theory as mentioned in the previous section. Thanga et al. (2011) used FE analysis in

order to study the effects of yielding of steel material on the behaviour of duct wall plates under lateral pressure considering the membrane forces induced by large deformation. They modeled a strip of plate with unit width and various lengths using shell elements. They established design equations for three different cases of through-thickness yielding namely 0%, 16.5% and 33% of the thickness of steel plate in order to increase the load carrying capacity. Same Modelling approach (unit width strip geometry) was used by El-Aghoury and Galal (2013) in a parametric study on the specific case of plates between two adjacent ribs of the walls of industrial ducts. The main result of their work was a very close approximation of the load-deformation of plates with large deformations under uniform pressure by applying the Bezier curves (Bezier, 1972) based on numerical Modelling. Both of last two references assumed that using a unit width strip model based on beam analogy give very accurate approximations of the case of long rectangular plates under lateral uniform pressure. Contrary to the traditional method of treating rectangular plates with aspect ratios higher than 2.0 as one-way plates, Wang and El-Sheikh (2005) showed that two-way plate action still applies to plates with aspect ratios from 1.5 to 10.0 and the application of one-way action will result in over-estimated deflections calculation for relatively long plates.

3.4 Nonlinear Finite Element Analysis of Duct Walls

The Finite Element Modelling and analysis in this paper are done using standard SHELL181 element from the element library of the general-purpose commercial software package ANSYS (ANSYS, 2013-a). SHELL181 is a 4-node shell element with six degrees of freedom (translation in and rotation about three dimensional axes) which is designed for the analysis of thin to moderately-thick shell structures (Dvorkin and Bathe, 1984). SHELL181 element covers three types of behaviour namely “plate-type” which covers only the bending-type using the classical Mindlin/Reissner theory, “membrane-type” which neglects any bending and considers pure membrane behaviour and “shell-type” that covers both bending and membrane behaviours by implementing the geometrical nonlinearities effects. The element is tested by ANSYS for the linear and nonlinear applications concerning large deformations, large rotations and large strains through benchmark verification examples (ANSYS, 2013-b). SHELL181 stress output covers the normal and shear stresses namely S_x , S_y and S_{xy} at top, bottom and middle of each shell layer. It also provides the equivalent von-Mises stresses as well as other types of common failure criteria. More importantly, it provides stress resultants corresponding to membrane forces (N_{11} , N_{22}), In plane

shear force (N_{12}), bending moments (M_{11} , M_{22}), in plane moment (M_{12}) and transverse shear forces (Q_{13} , Q_{23}) as shown in Fig. 3.4.

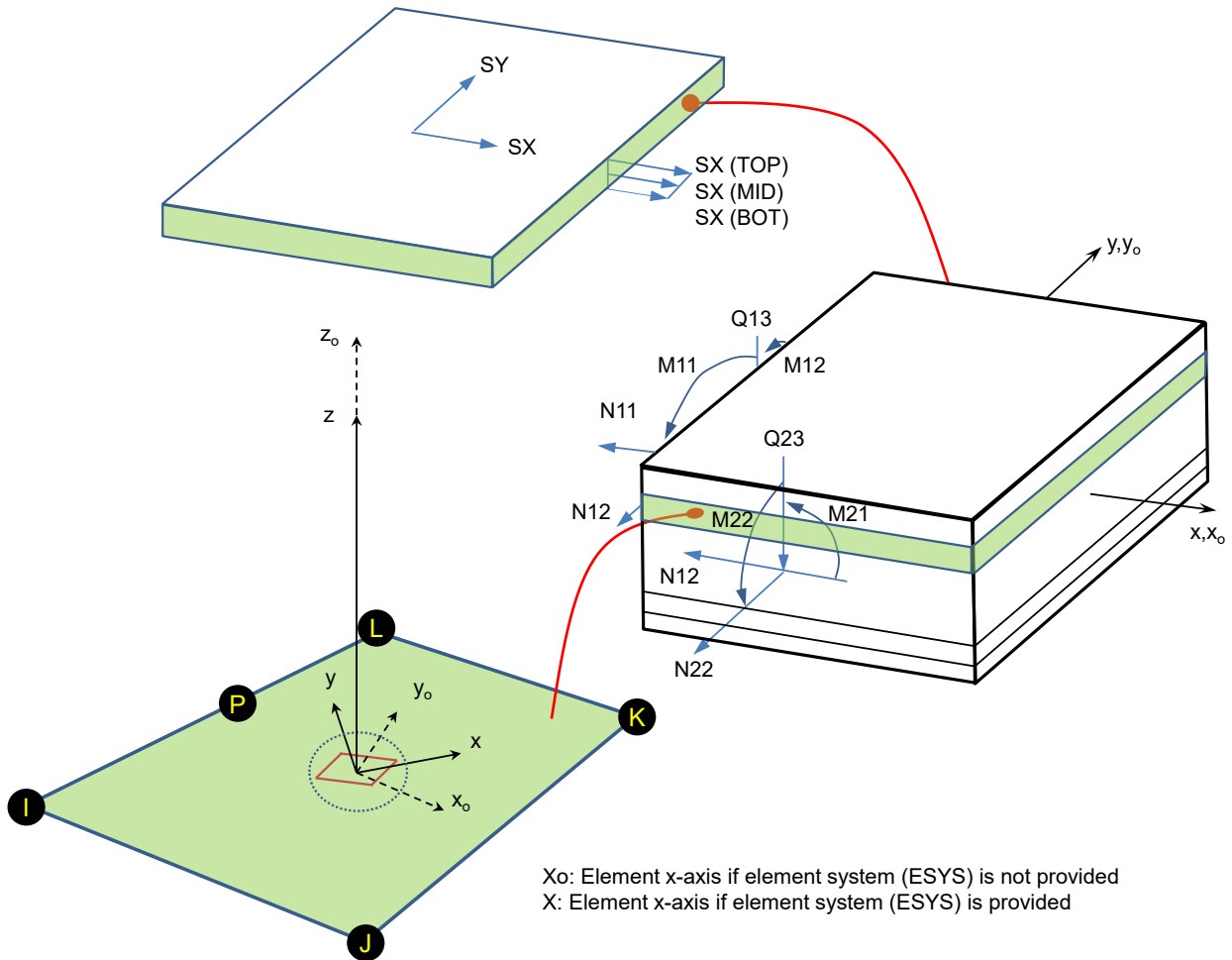


Fig. 3.4: SHELL181 geometry and stress output (ANSYS, 2010-b)

3.4.1 Validation of Modelling and boundary conditions

Most of the FE models and experimental tests available in the literature for rectangular plates under lateral pressure consist of a unit-width strip or a single panel plate model with clamped, hinged or free boundary conditions assigned to each of the four edges. This approach results in geometry and boundary conditions for the edge and typical panels of duct walls as shown in Fig. 3.5.

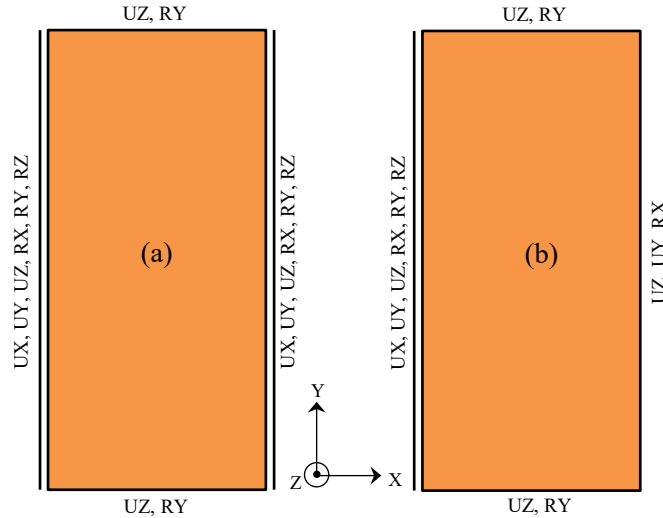


Fig. 3.5: Boundary conditions for the single-span plate model (a): Typical panel (b): Edge panel

The wall plate panel with boundary conditions shown in Fig. 3.5(a) is modeled here to verify the element and analysis method. The unitless load displacement curve is shown in Fig. 3.6 in comparison to the results of El-Aghoury and Galal (2013) and Young et al. (2002). Similarly in Fig. 3.7, the load-stress curves resulted from the FE analysis are presented against the available results in the literature.

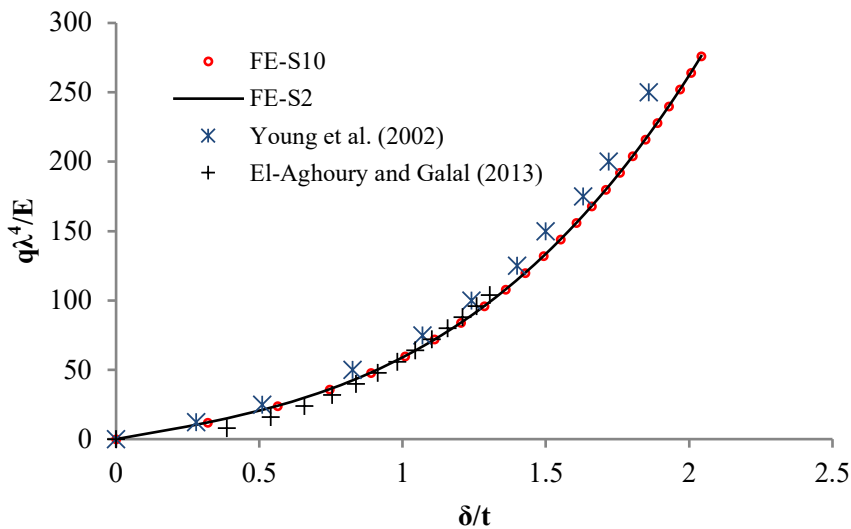


Fig. 3.6: Load-deformation curve of rectangular plate (typical panel)

Comparing the results of current study for the single panel plate with those available in the literature, it is seen that for the analysis of typical panel plates of duct walls independently (without considering the effects of expansion joints), the available equations in the literature are adequate in predicting the behaviour of duct wall plates. In other words, the plate model has no significant

advantage over the existing unit-width strip method that applies the large displacement beam theory to plates.

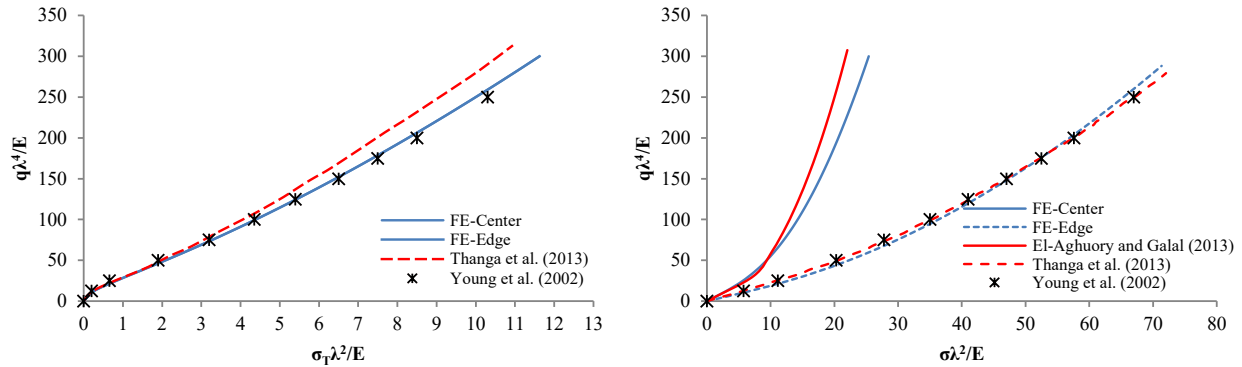


Fig. 3.7: Normalized tangential (membrane) stress (left); and total stresses (right) for a single span rectangular plate with large deformations

Expansion joints at one or both ends of a duct segment release the axial force and bending moment by providing discontinuity along the length of the stiffened plate. The equilibrium of forces and deformations changes with the release of axial force as shown in Fig. 3.8 for a sample three span beam (or plate strip) that is subjected to uniform load with consideration of large deformations. In case (a) the large deformations resulting from the distributed load produce the axial force N (membrane action) in each span and the reactions at the two ends of the beam as shown in the free body diagram in Fig. 3.8(a). If the axial restraint is removed at one end (or both ends), the axial force N could not generate due to the equilibrium of forces, hence the deflections will be larger and the large deflections result in cumulative in-plane displacements of the beam as shown in Fig. 3.8(b).

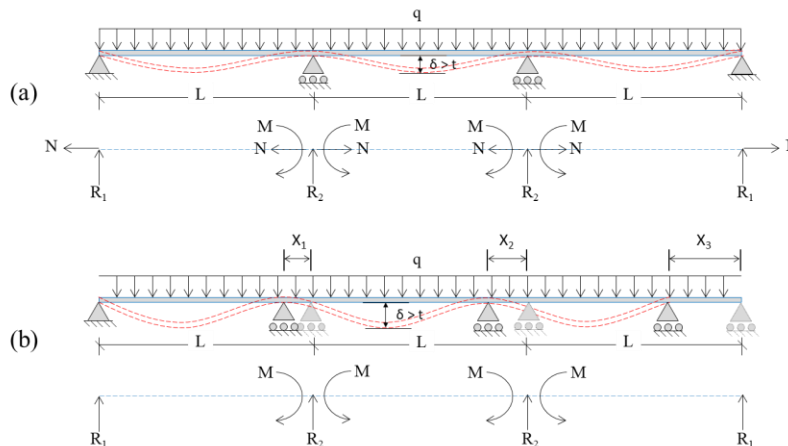


Fig. 3.8: Loading and free body diagram for the equilibrium of continuous beams with large deformation

Thus, neither the strip method used in the previous works nor the single span plate Modelling apply to the case of duct walls (typical and edge panels) if expansion joints are present in the duct assembly. In other words, a realistic model that represents the stiffened plates of duct walls must cover the geometry of the wall plates in a way that the assumed boundary conditions correspond to the existence of expansion joint at the edge of the duct segment. Such a plate model obviously cannot consist of only a single panel of the stiffened plate, thus in this paper multi-span plates are used.

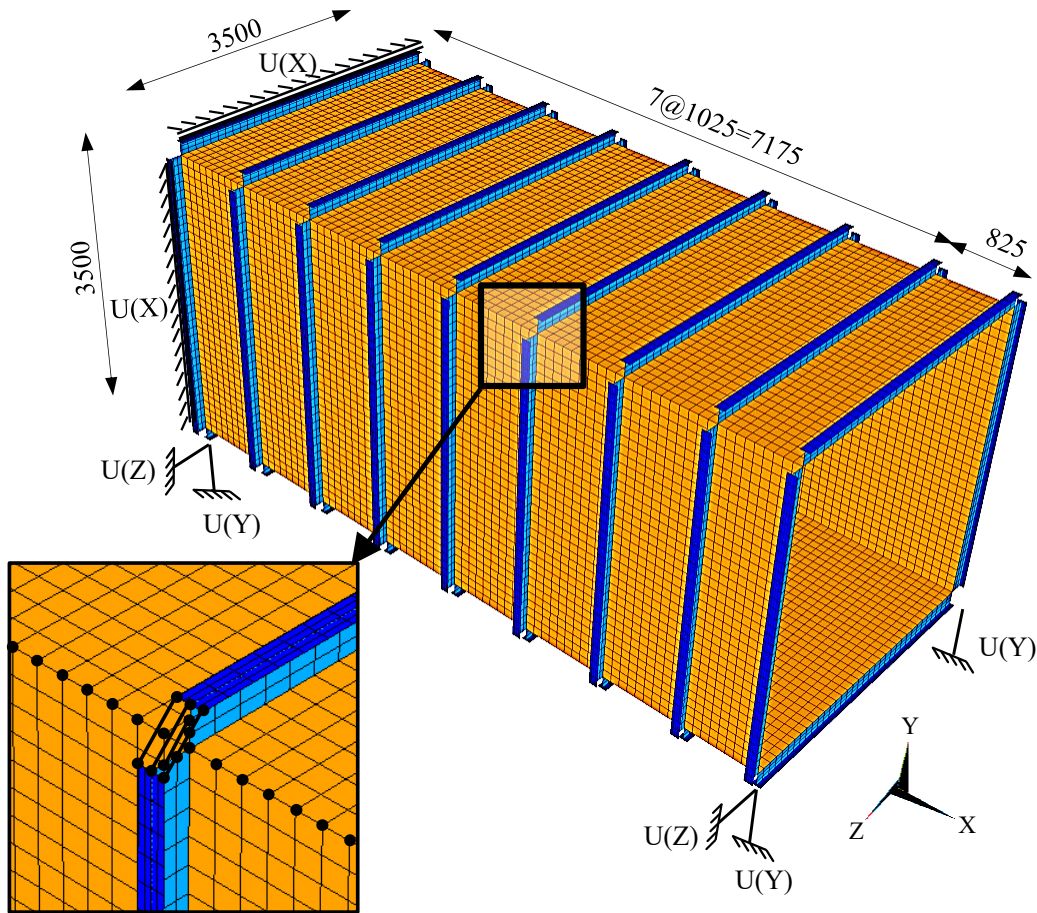


Fig. 3.9: Geometry and FE mesh of a sample 3D duct segment model

Fig. 3.9 shows the geometry, FE mesh and the boundary conditions of the 3D model of a duct segment that is designed based on the linear design method. In this model, the DOFs of plate elements at the corners of the duct segment are fully integrated to resemble the fully welded situation in reality. The rib stiffeners are also fully connected at the duct corners based on the

assumption of moment connection at the ends of the ribs. Geometric nonlinearities (large deformation effects) are included in the analysis to verify the behaviour of the duct segment.

Fig. 3.10 shows the absolute deformed shape of the duct segment model under internal uniform pressure in terms of displacements and rotations. The overall deformation of the wall plates is the sum of panel plates and rib stiffeners deformations. Since the rib elements are out of the scope of this paper, they are removed from the view in the figure. It is seen in Fig. 3.10 that the deformed shapes of the duct wall plates are similar for all the panels except for the edge panel where the expansion joint exists. It is observed from the absolute displacement contours that the edge panel displacements are smaller than those of the typical panels considering the smaller length used for the edge panels. It is also observed that the free edge of the edge panel shows the maximum rotation at the middle due to the connectivity of wall plates at the duct corners that prevent the rotations. Considering the symmetry of the deformations and rotations, it is concluded that a multi-span wall plate model will well represent the full duct segment model for the analysis of the wall plate.

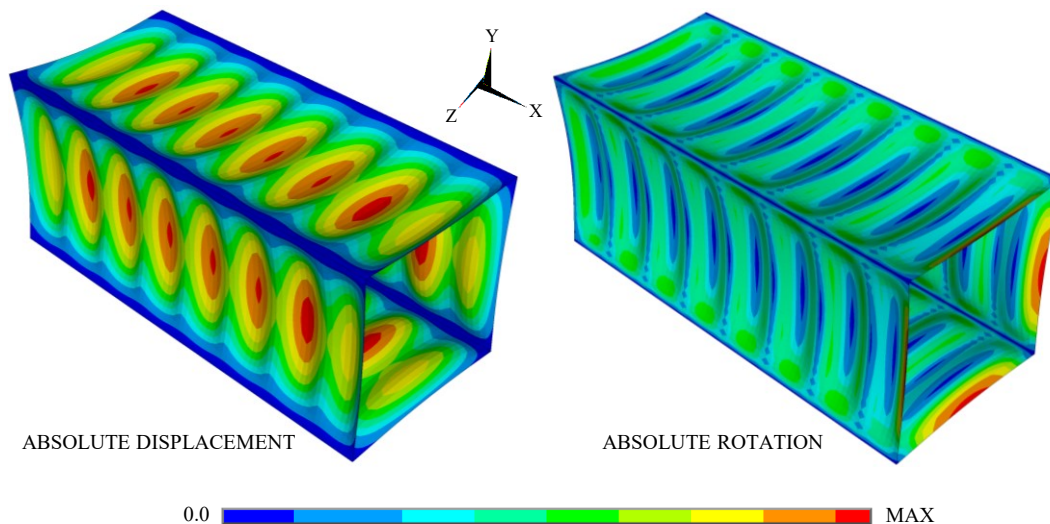


Fig. 3.10: Absolute deformation and rotation of the duct segment model under the applied internal pressure (rib elements removed from the view for clarity)

3.4.2 Multi-span plates with internal line supports

The total displacement of a duct wall plate consists of the rib displacements and the plate displacement (see Fig. 3.10). In order to study the wall plate behaviour, the plate load-displacement needs to be distinguished from that of the ribs. Thus, in the numerical models of this paper, multi-

span plates with internal line supports are used. Plates with internal line supports are an imaginary type of stiffened plates where the rib elements are assumed to be infinitely rigid so they could be replaced with appropriate boundary conditions. Fig. 3.11 shows the sketch of a 10-span segment of a duct wall plate with panel aspect ratio $S=5.0$ and internal line supports. The boundary conditions used in this model represent expansion joints at both ends of the segment. Equal rib spacing was used for all the panels in order to distinguish between the load-displacement behaviours of different panels.

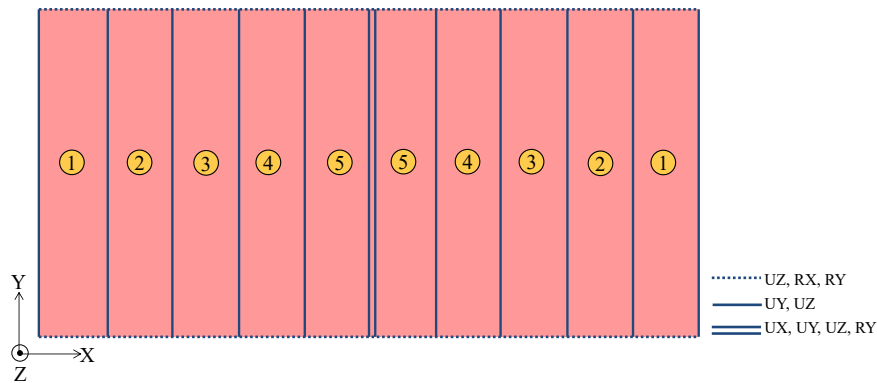


Fig. 3.11: General arrangement of duct wall plate models with internal and edge line supports resembling the restraints provided by the end panels, ribs and other walls of the duct when expansion joints exist at both ends of the segment

As seen in Fig. 3.12, the plate undergoes in-plane as well as out-of-plane deformations under the applied uniform pressure when the large displacements (geometrical nonlinearities) are included in the analysis. It is also seen in the $D(Z)$ contours in Fig. 3.12 that various panels of the stiffened plate tend to follow different load-displacement patterns.

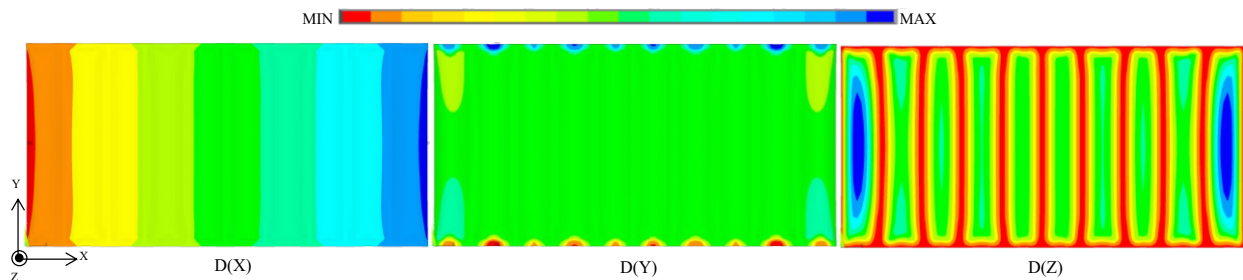


Fig. 3.12: Displacement contours in three global directions for 10-span plate model with internal line supports and span aspect ratio $S=5$

Fig. 3.13 shows the load-displacement curves of different panels of stiffened plates with three aspect ratios $S=2$, $S=5$ and $S=10$. As seen in Fig. 3.13 for plates with equal spans, the edge panel

has the weakest load-displacement behaviour i.e. under the same pressure it undergoes highest deformations. Similar observation exists for the case of linear analysis due to the boundary conditions provided by the expansion joint. On the other hand, the 2nd panel tends to have the lowest displacements under the same pressure in general comparing to the typical panels. The reason for this behaviour is that due to the free rotational degree-of-freedom at the free edge of the edge panel and the continuity of the plate between the edge and 2nd panel, the rotation at one edge of the 2nd panel has a non-zero value. Thus, the load-displacement curve of the 2nd panel shows slightly stiffer behaviour (i.e., lower displacement under the same pressure) compared to the typical panels where the rotation at the edges are zero.

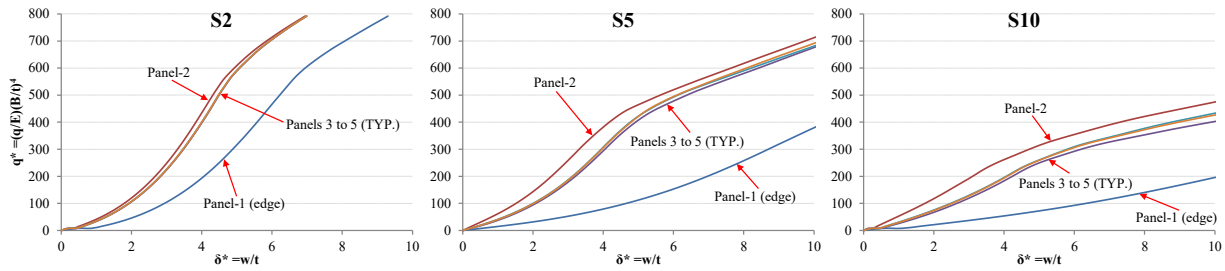


Fig. 3.13: Out of plane load-displacement charts for different panels of the plate with internal line supports in three aspect ratios S=2, S=5 and S=10

3.5 Design of Duct Wall Plates Based on Nonlinear Analysis

Based on the load-displacement charts in Fig. 3.13, two main categories for the panels of stiffened plates in this paper are the “edge” and “typical” while the design of typical panels could be conservatively applied to the 2nd panel accordingly. Similar to the conventional design, there are two criteria to be used in the nonlinear design of plates namely stress and deflection. In this section nonlinear equations will be driven from the FE analysis of 10 span plates with panel aspect ratios from 2 to 10 for stress and deflections criteria.

3.5.1 Stress criterion

The load-stress charts for the edge and typical panels of multi-span plates with various aspect ratios (S) from 2 to 10 are shown in Fig. 3.14. The stress in these charts is the maximum absolute von-Mises stress normalized with plate’s yield stress.

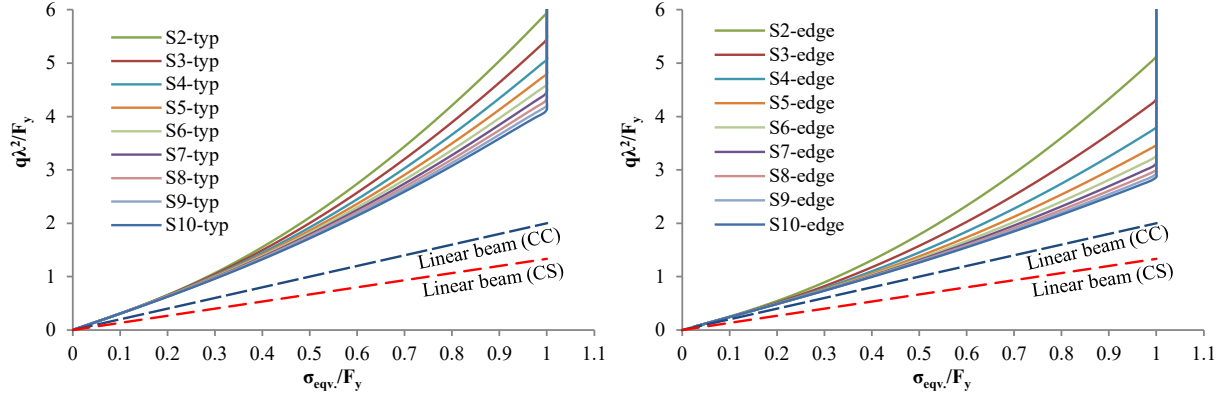


Fig. 3.14: Maximum von-Mises stress in typical and edge panels of multi-span plates with aspect ratios from 2 to 10

The charts in Fig. 3.14 are estimated using a trend line with second order equation as shown in Eq. 3.9.

$$q\lambda^2/F_y = a\left(\sigma/F_y\right)^2 + b\left(\sigma/F_y\right) \quad (\text{Eq. 3.9})$$

The values of “*a*” and “*b*” constants depend on the plate aspect ratio for the edge and typical panels and could be found in Table 3.2. Eq. 3.9 is applicable in both ultimate limit states and allowable stress design methods to calculate the length-to-thickness ratio for the given load when appropriate stress limits are used for σ/F_y .

Table 3.2. Aspect ratio numerators to be used in Eq. 3.9

S	TYPICAL PANEL		EDGE PANEL	
	a	b	a	b
2	3.42	2.52	3.07	2.05
3	2.82	2.61	2.27	2.03
4	2.41	2.65	1.72	2.06
5	2.1	2.69	1.35	2.1
6	1.87	2.72	1.09	2.14
7	1.69	2.75	0.91	2.18
8	1.55	2.76	0.76	2.21
9	1.43	2.77	0.66	2.23
10	1.33	2.78	0.57	2.25

3.5.2 Deflection criterion

The load-deformation charts of the typical and edge panels of the multi-span plates under uniform lateral pressure are shown in figures 3.15 and 3.16. These charts reflect the nonlinear load-deformation behaviour when the geometric nonlinearities are considered in the analysis.

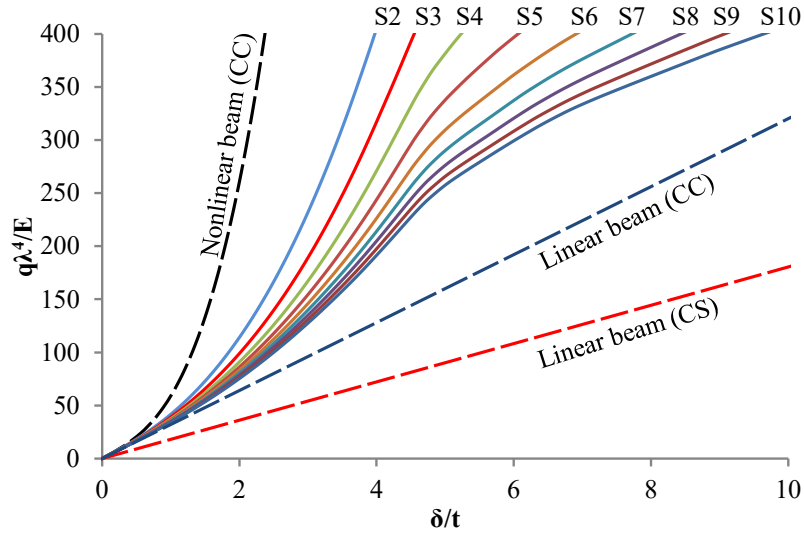


Fig. 3.15: Load-deformation charts for typical panel with aspect ratios S2 to S10

Fig. 3.15 shows that for typical plates the nonlinear behaviour has two trends. The first trend starts from the beginning of loading and follows a cubic function up to the point where the material yielding occurs.

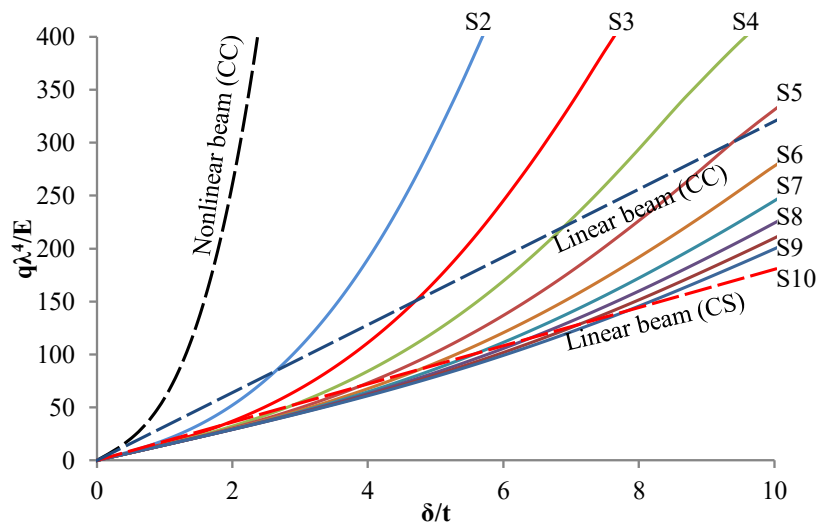


Fig. 3.16: Load-deformation charts for edge panel with aspect ratios S2 to S10

The second trend results from the addition of material nonlinearities after yielding in combination with stress redistributions to the original nonlinear load-displacement. The plastic behaviour of plate after yielding is out of scope of design for the plates being used for the walls of industrial ducts. Thus, if yielding of material is set as the limit state i.e., the first trend of the charts in figures 3.15 and 3.16 are used for the design, the load-displacement behaviour for the typical and edge panels could be estimated by a trend line with cubic equation as shown in Eq. 3.10.

$$q\lambda^4/E = a'(\delta/t)^3 + b'(\delta/t)^2 + c'(\delta/t) \quad (\text{Eq. 3.10})$$

where a' , b' and c' account for the plate aspect ratio (S) effects listed in Table 3.3.

Table 3.3. Aspect ratio numerators to be used in Eq. 3.10

S	Typical panels			Edge panel		
	a'	b'	c'	a'	b'	c'
2	2.51	7.82	31.34	1.28	3.97	14.1
3	1.52	5.93	31.51	0.58	1.49	13.72
4	1.01	5.15	31.18	0.31	0.8	13.62
5	0.67	4.95	30.55	0.17	0.69	13.47
6	0.47	4.69	30.35	0.11	0.5	13.5
7	0.35	4.46	30.09	0.08	0.42	13.55
8	0.27	4.27	29.79	0.06	0.36	13.64
9	0.26	3.82	29.87	0.05	0.31	13.73
10	0.23	3.58	29.74	0.04	0.26	13.83

3.5.3 Application of design equations

Design of duct wall plates consists of determination of plate thickness and length based on the stress limits defined by the adopted design code and verification of the deflections of the designed wall plate with the deflection limits set by the authorities. The calculation of plate maximum stress and deflection was covered in the previous section by means of equations 3.9 and 3.10 for the typical and edge panels respectively. In this section, those equations are used to provide a more meaningful design approach by adopting the ultimate limit states for stress set by the two main North American steel design codes for plates. The ultimate stress for plate elements under bending and tension is $\sigma_u=0.9F_y$ (CISC-S16.09), (AISC, 2003). Thus, for $\sigma_u/F_y=0.9$ in Eq. 3.9, $q\lambda^2/F_y=a(0.9)^2+b(0.9)$. Replacing a and b numerators in this equation with their values from Table

3.2 for various panel aspect ratios will result in a power function that calculates the normalized plate length-to-thickness ratio ($\lambda/\sqrt{F_y}$) for the given lateral pressure:

$$\lambda_u / \sqrt{F_y} = \eta q^{-1/2} \quad (\text{Eq. 3.11})$$

where λ_u is the ultimate plate length-to-thickness ratio based on the ultimate stress limit ($0.9F_y$), and η is the plate aspect ratio factor ($\eta=0.81a+0.9b$). The values of η for various panel aspect ratios are presented in Table 3.4 for the edge and typical panels. The last row in Table 3.4 shows the value of η for linear design by replacing the ultimate limit state stress in Eq. 3.2 for the edge (C-S) and typical (C-C) panels.

Table 3.4. Aspect ratio numerators to be used in Eq. 11

S	Typical panels	Edge panel
	η	η
2	2.24	2.08
3	2.15	1.91
4	2.08	1.80
5	2.03	1.73
6	1.99	1.68
7	1.96	1.64
8	1.93	1.61
9	1.91	1.59
10	1.89	1.58
Linear	1.34	1.09

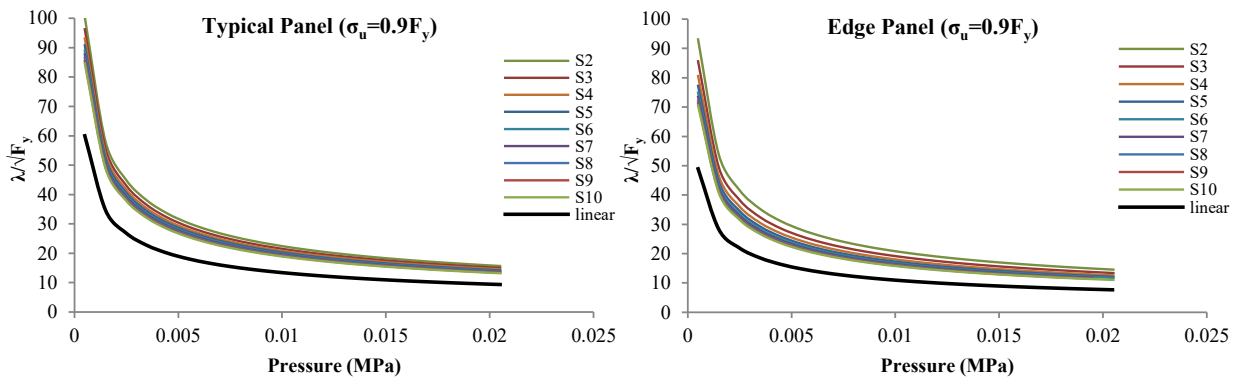


Fig. 3.17: Normalized plate length-to-thickness ratio for various lateral pressures on duct walls typical and edge panels

The normalized plate length-to-thickness ratio calculated from Eq. 3.11 is plotted against a regular range of lateral pressures set by ASCE (1995) in Fig. 3.17 for edge and typical panel plates.

The value of η in Table 3.4 indicates the effect of plate aspect ratio in the nonlinear design. In order to evaluate the effectiveness of nonlinear design in comparison with the conventional linear design, the length-to-thickness ratios resulted from Eq. 3.11 for typical and edge panels from nonlinear and linear designs are compared in Table 3.5. As seen in Table 3.5, the plate length for edge panel is 83 to 93 percent of the typical panel length if nonlinear design is used showing that for shorter aspect ratios the edge panel design gets closer to that of the typical panel. It is also seen in the table that for the typical panels the nonlinear design results in 41 to 67 percent higher length-to-thickness ratios accordingly depending on the aspect ratio. In other words, for the same plate length, the plate thickness resulted from the nonlinear design is 30 to 40 percent lower than what would result from the conventional linear design.

Table 3.5. Comparison between the length-to-thickness ratios resulted from the nonlinear and linear designs for edge and typical panels

S	$\lambda_u(\text{edge})/\lambda_u(\text{typical})$	$\lambda_u(\text{typical})/\lambda_u(\text{typical-linear})$	$\lambda_u(\text{edge})/\lambda_u(\text{edge-linear})$
2	0.929	1.67	1.91
3	0.888	1.60	1.75
4	0.865	1.55	1.65
5	0.852	1.51	1.59
6	0.844	1.49	1.54
7	0.837	1.46	1.50
8	0.834	1.44	1.48
9	0.832	1.43	1.46
10	0.83	1.41	1.41
Linear	0.815	1.00	1.00

It is worth to mention that although separate equations are presented for the design of edge and typical panels, it is practical not to use different plate thicknesses for the edge and typical panels. In other words, the design could be done by only calculating the length-to-thickness ratio for the typical panels using Eq. 3.9 and multiplying the length of the typical panel by the $\lambda_u(\text{edge})/\lambda_u(\text{typical})$ factor from Table 3.5 to get the length of the edge panel.

3.5.4 Displacement limits for the design of duct walls

Contrary to the ultimate limit states design or other approaches where the stress limitations are set by the codes, in the field of industrial structures design serviceability limit states (i.e., the displacement limits) are often set by the local authorities, mechanical engineers or the owner of the industrial facilities where the duct system is built in a way to keep the duct functional. A general rule of thumb followed by most of the design engineers for the displacement limits is a portion of the plate length (e.g., $L/50$, $L/75$, $L/100$ etc.). However, this type of displacement limits tends to meet the serviceability demands of building structures, it might result in unnecessary plate thicknesses without addressing the true nature of wall behaviour in thin-walled structures such as industrial duct assemblies. On the other hand, the authors were unable to find any tabulated displacement limits set for the duct wall plates (or similar structures) or any explanation on the basis of such limits as $L/50$ or $L/100$ in the literature.

Table 3.6. Ratio of maximum lateral pressure resulted from the nonlinear approach to linear method, $q(\text{nonlinear})/q(\text{linear})$

$(\delta/t)_{\max}$	S2	S3	S4	S5	S6	S7	S8	S9	S10
1.0	1.30	1.22	1.17	1.13	1.11	1.09	1.07	1.06	1.05
2.0	1.78	1.55	1.42	1.35	1.30	1.26	1.23	1.20	1.18
3.0	2.42	1.97	1.74	1.61	1.52	1.46	1.41	1.36	1.33
4.0	3.21	2.49	2.12	1.91	1.77	1.67	1.60	1.54	1.49
5.0	4.16	3.10	2.57	2.25	2.05	1.91	1.81	1.73	1.67
6.0	5.27	3.81	3.08	2.64	2.36	2.17	2.04	1.94	1.86
7.0	6.53	4.61	3.65	3.06	2.69	2.45	2.28	2.17	2.06
8.0	7.95	5.51	4.28	3.53	3.06	2.76	2.54	2.41	2.28
9.0	9.53	6.50	4.98	4.04	3.46	3.08	2.82	2.67	2.52
10.0	11.27	7.59	5.74	4.60	3.88	3.43	3.11	2.94	2.77

In order to be able to compare the nonlinear design approach to the conventional linear design method this paper uses a different way to set the displacement limits that tends to be more practical for the plate elements such as duct walls. The displacements in this method are compared to the plate thickness. By using this method, replacing the δ/t with the desired displacement limit in Eq. 3.10 will result in plate length to thickness ratio for the applied pressure. Since the displacement limits are different from case to case, it is not possible to formulate the design as in the ultimate limit states in which a certain stress limit is set by the code. The ratio of maximum lateral pressure calculated from Eq. 3.10 to the pressure resulted from Eq. 3.3 are shown in Table 3.6 for various plate panel aspect ratios and displacement limitations $(\delta/t)_{\max}$ from 1.0 to 10.0 respectively. As

seen in Table 3.6, the effectiveness of the presented nonlinear design approach in displacement criterion depends highly on the applied displacement limit and plate panel aspect ratio.

3.6 Conclusions

Two sets of design equations have been set using verified numerical analysis of multi-span plates with internal line supports under uniform lateral pressure that take into account the effects of large deformations nonlinearities. These equations stand for the design of plate length and thickness by applying stress and displacement criteria to the plate structure. If used appropriately in conjunction with well-defined stress and deflection limits, a duct wall plate designed by these equations will be up to 40% more economical compared to the conventionally designed plates that use the linear beam theory.

CHAPTER 4

Large Displacement Analysis of Stiffened Plates with Parallel Ribs under Lateral Pressure

4.1 Abstract

The conventional approach for the structural analysis and design of stiffened plates with parallel ribs involves assuming that the stiffened plate could be modeled as a beam with the geometrical properties of an equivalent built-up cross-section consisting the rib stiffener, and a portion of the plate. The load-displacement and the internal forces of this equivalent beam are then calculated based on the conventional beam theory in order to design it according to the adopted design criteria. This study numerically analyzes the stress distributions in such plates in order to assess the equivalent beam analogy while pointing out the significance of considering the large displacement effects. The numerical investigation indicated that the linear beam theory does not correctly presume the true behaviour of the stiffened plate, and the corresponding load-displacement estimation does not align with its actual behaviour. It also shows that the internal forces and stresses in the panel plate are calculated correctly, only if the large displacement effects are considered in the analysis. A method for the estimation of the ultimate load capacity of stiffened plates based on the large displacement FE analysis is provided at the end of this study which could be used in future to establish empirical design equations.

4.2 Introduction

Stiffened plates with parallel ribs are widely used in industrial structures, ship hulls, and marine applications. An example of such assemblies in industrial structures is the large industrial ducts with rectangular cross-sections (Fig. 4.1) for heavy industries such as cement plants, aluminum smelter facilities, steel manufacturing, etc., where significant amounts of air or flue gases are transferred.



Fig. 4.1: A duct segment with stiffened plate walls being delivered in an industrial project [courtesy of fives Inc.]

The structural design of stiffened plates has not been directly-addressed to official code provisions, standards, or guidelines that establish grounds such as limit states for basic estimations and procedures. However, there has been an extensive number of studies in the literature addressing the behaviour of longitudinally and transverse stiffened plates experimentally and analytically from various perspectives. Bedair (2009) has gathered the research conducted in the analysis and design of stiffened plates up to 2009, where the developments of the analysis methods, experimental works, and design fundamentals over the 20th century are presented by referring to more than 400 scientific publications. According to Bedair (2009), the earliest attempts on the formulization of load-deformation of the stiffened plates dates back to 1902, where the stiffened plate case was simulated as a simple beam resting on an elastic foundation. That approach was then used in the early 20th century by researchers to study the initial buckling of plates stiffened with transverse and longitudinal stiffeners and developed over the years based on the advances in the numerical methods and experimental capabilities. Another extensive literature review report was published by Paik (2008), which is mainly focused on the recent developments and advances in the field of stiffened plates under various types of loading regarding the effectiveness of plate elements when stiffened by a rib element. In that study, the concepts of effective breadth, effective width, and effective shear modulus were explained and categorized based on the details from the available literature. Those concepts are based on the main assumption that the stiffened plate assembly could be theoretically modeled by an equivalent beam (EB) for which the cross-sectional properties such as the moment of inertia and section modulus are calculated for the design. The displacements in that method are calculated with respect to the applied loads following the principles of the classical beam theory.

Recent research on stiffened plates was mainly focused on the ultimate limit states design and the nonlinear analysis of the EB for various types of stiffeners. The nonlinear analysis of stiffened plates considers the geometrical and material nonlinearities in the Finite Element method. An approach was introduced by Ojeda et al. (2007) for the large deflection analysis of isotropic and composite arbitrary orientated stiffened plates based on the principle of virtual works. The stiffeners modeled in that work were in the forms of Flat-bars with and without eccentricity from the centerline of the plate. In a similar work, Brubak and Hellesland (2008) applied various strength criteria in semi-analytical methods for the ultimate strength evaluation of arbitrarily stiffened plates. Two types of Flat-bar and Tee-bar profiles were studied for the stiffeners, considering the eccentricity of the ribs from the centerline of the plate.

One of the common places where the stiffened plates are most often used is the ship hull structures. Various types of stiffened plates with different combinations of panel plates and stiffeners are used widely in that industry worldwide. The ultimate strength analysis of stiffened plates used in the large ship hulls industry was presented by Paik and Seo (2009). The nonlinear analysis was performed using the Finite Element package ANSYS together with some semi-analytical methods. Three types of stiffeners were studied, namely Flat-bars, L-angles, and Tee-bars. However, that study lacks a profound parametric study to reveal the nature of stresses in the plate and stiffener. Sapountzakis and Dikaros (2012) proposed a general type of solution for the geometrically nonlinear analysis of stiffened plates with a parallel arrangement of stiffeners. They considered general arbitrary mono-symmetric cross-sections for stiffeners with a deformable connection subjected to arbitrary loading. The analytical solution was then compared to the findings of the FE analysis regarding the load-displacement curves. Two mostly-used types of rib stiffeners in ship hulls, namely T and Y shapes were studied by Badran et al. (2013). The main parameter studied was the initial imperfections and the impact on the load-deformation behaviour of such stiffened plates under combined uniaxial and lateral loading. They studied 200 different cases using nonlinear FE analysis and discussed the benefits and disadvantages of each type of stiffener. More recently, Brubak et al. (2013) studied the effects of various types of boundary conditions on the load-deformation behaviour of arbitrarily stiffened plates with T ribs. The buckling and post-buckling behaviour of plates with and without stiffeners under uniaxial thrust was presented by Sadamoto et al. (2013) where they implemented a mesh-free approach to perform

the nonlinear analysis of such plates and discussed the influence of various parameters on the analysis.

An experimental program in which four multi-span stiffened plates with narrow panels were tested under axial compression was conducted by Xu and Guedes Soares (2011-a) along with FE Modelling of the same specimens (Xu and Guedes Soares, 2011-b) in order to study the deflection shape, mode of failure, ultimate load and the load-displacement behaviour of such stiffened plates as well as verifying the FE Modelling. Furthermore, Xu and Guedes Soares (2013) extended their experimental studies by five new specimens with wide stiffened panels to measure their collapse strength under axial compression in comparison with the existing data from their previous tests and FE analysis. The deflection shape, load-displacement behaviour, and collapse mechanisms were identified for those specimens and utilized to better establish their future FE Modelling.

More recently, a total of twelve stiffened plates were experimentally tested to failure under combined in-plane and lateral pressure by Shanmugam et al. (2014) to measure their ultimate load-displacement behaviour and capacity. The correlations between the ultimate load-carrying capacity of stiffened plates with the axial load to lateral pressure ratio were discussed. Moreover, the plate slenderness was described as a key parameter with a major influence on the ultimate load capacity and the load-displacement behaviour. The experimental results were then compared to the FE analysis results and concluded that a well-established numerical Modelling would capture the true behaviour of the stiffened plates with acceptable margins.

Various buckling modes for plates stiffened with Flat-bar type of ribs were studied by Rahbar-Ranji (2014) in order to distinguish between the effectiveness of each failure mode and interactions between them. An equivalent cross-section for the case of Flat-bar stiffened plates was analyzed by introducing an “effective breadth/web concept” that tended to simplify the analysis of such stiffened plates. A more in-depth study on the ultimate strength of welded stiffened plates was presented by Tekgoz et al. (2015), in which various parameters involved in the welded interface of Flat-bar stiffeners to the plate were discussed in micro-scaled FE analysis. The work mainly focused on residual stresses and welding-induced issues in the design of stiffened plates with Flat-bar stiffeners. In a similar study, the case of residual stresses and welding of stiffened plates with Hat-type stiffeners was studied by Yetman et al. (2015) using micro-scaled nonlinear FE analysis.

4.3 Stresses in Rectangular Plates in Theory

The response of a rectangular plate to external forces is categorized into three main domains of membrane (in-plane) forces, shear (in-plane and out-of-plane) forces, and bending moments (flexural and twisting). These responses are mainly controlled by the following parameters:

- Boundary conditions,
- Plate aspect ratios,
- Plate thickness, and
- External loads nature.

There are several solutions to the plate's governing equation in the forms of analytical closed-form and numerical analysis in the literature, which include a vast array of combinations of the above-mentioned parameters. Those solutions often present simplified approaches that establish a meaningful relationship between the applied loads and the plate deformation. Among those solutions, there are several attempts for the case of thin plates that undergo large displacements. The definition of large displacements is often given in relation to the plate thickness. While displacements greater than the plate thickness are mostly considered as “large”, a recent study by Bakker et al. (2008) showed that even when the maximum displacement of the plate reaches 20% of the plate thickness, it should be calculated using the large displacement analysis (LDA) rather than the small displacement analysis (SDA). When a uniformly-distributed lateral pressure is applied to such thin plates, the in-plane bending moments and shear forces as well as the out-of-plane shear forces are negligible (Timoshenko and Woinomsky-Kreiger, 1959). In such plates, the membrane forces, the bending moments, and the deformations are calculated by solving the von Kármán equations in combination with the classical plate theory (Timoshenko and Woinomsky-Kreiger, 1959).

4.4 Equivalent Beam Analogy

Generally, the analysis and design of stiffened plates is a two-step procedure, with the first step involving the design of panel plates between adjacent ribs as a rectangular plate, and the second step consisting of the design of stiffeners. The outcomes of these two steps are the plate thickness, the ribs spacing, and the sizing of the ribs. The rib stiffener profile could be selected from the

library of the design standard on a case-by-case basis. Common types of stiffeners used in industrial applications are shown in Fig. 4.2.

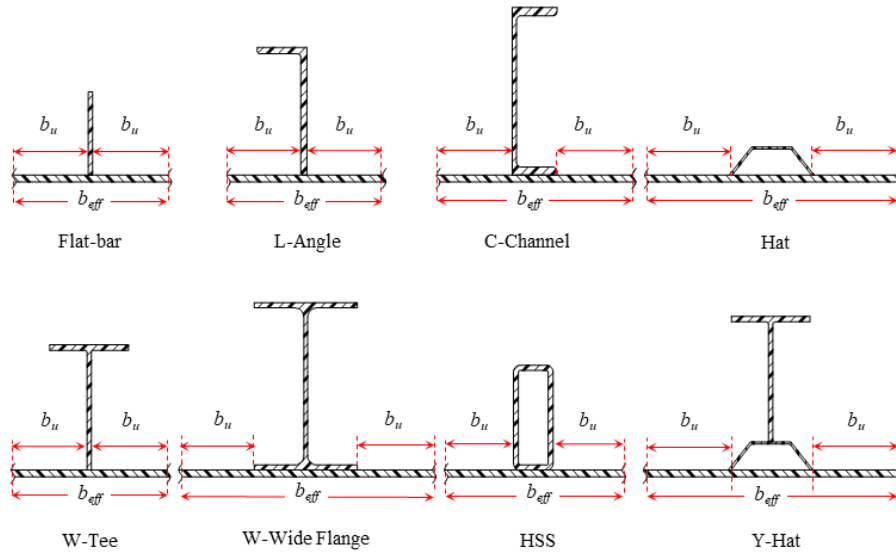


Fig. 4.2: Stiffened plates with common types of stiffeners and their effective breadth forming the equivalent beam cross-section

In the Equivalent Beam Analogy (EBA), the stiffener and the panel plate form a built-up cross-section with combined geometrical properties. The axial, bending, and shear stresses and deformations are therefore calculated for the built-up section as an individual structural shape called the *equivalent beam* (EB). The conventional design suggests that only a certain portion of the panel plate be taken into account in the EB cross-section. This portion of the panel plate is often called the “*effective breadth*” if the stiffened plate is mainly under bending stresses, i.e., the stresses induced in the plate are mainly influenced by the shear lag effects from flexure. On the other hand, the term “*effective width*” is often applied to this portion of the panel plate if the main stresses induced in it are due to axial compression (Paik, 2008).

Plate effectiveness in stiffened plate structures was first mentioned by von Karman et al. (1932) as an imaginary width of the continuous thin plate under compression that follows the Euler-buckling criterion while the remainder of the plate (i.e., the edges of this imaginary width) remain straight and follow the stress-strain criterion. The effective width concept was then expanded in various fields of steel structures design and became “the concept on which the categorization of steel structural profiles by the codes was established in order to classify the modes of failure for steel thin-walled profiles” (Rahbar Ranji, 2014).

As shown in Fig. 4.2, the effective breadth is the sum of the unstiffened breadth (b_u) at each side of the stiffener plus the portion of the breadth covered by the stiffener. Various sources defined b_u or b_{eff} based on the thickness, breadth, and yield stress of the plate, as summarized in Table 4.1.

Table 4.1. Effective breadth of the plate in stiffened plates in the available literature

Reference	b_u	b_{eff}
Blodgett (1966)	-	32t
ASCE (1995)	16t	-
Paik (2008)	-	0.18b/(b/L)
CSA S16 (2014)	$670t/(F_y)^{1/2}$	-

Aside from the values in Table 4.1, there are more specific methods available in the literature which take into account more parameters in order to address the effective breadth. An example of that is the set of three empirical equations presented by Rahbar-Ranji (2014) to calculate the effective breadth of stiffened plates with Flat-bar stiffeners based on the stiffener to plate cross-sectional area ratio. The *effectiveness* of the panel plate in the EBA was first discussed by Paik (2008), which ultimately resulted in his specific formula for the effective breadth (See Table 4.1).

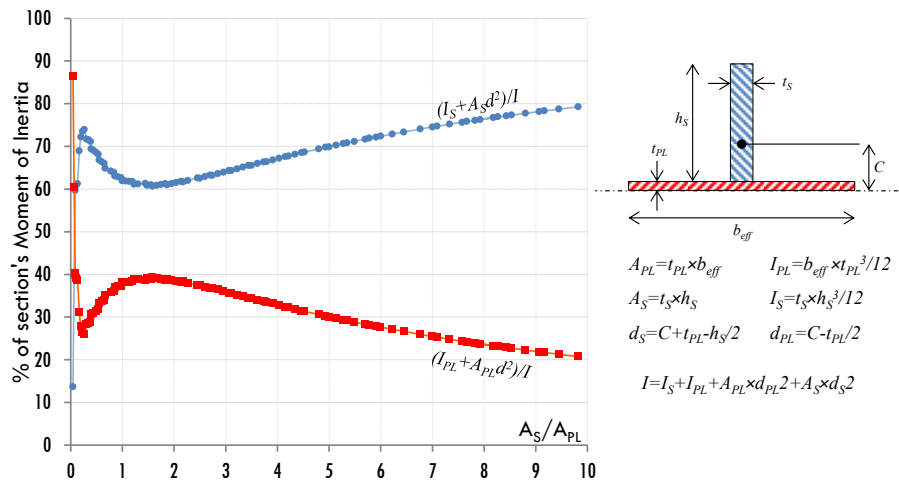


Fig. 4.3: Effect of the ratio of stiffener area over plate area (A_S/A_{PL}) on the EB moment of inertia in stiffened plates with flat-bar ribs

The flexural behaviour of the stiffened plate in the EBA could be greatly influenced by the ratio of the stiffener cross-sectional area over that of the panel plate (A_S/A_{PL}). As an example, the contribution of the plate and stiffener in the overall moment of inertia of the EB are calculated and presented in Fig. 4.3 for stiffened plates with Flat-bar ribs. It should be noted that the Flat-bar stiffener geometry in Fig. 4.3 satisfies the maximum height-to-thickness ratio set by CSA S16

(2014) for Class-1 conditions in flexural compression (i.e., $h_s/t_s \leq 145/F_y^{1/2}$) which terminates the local buckling failure mode.

As seen in the chart, although the stiffener at very low ratios of A_S/A_{PL} (i.e., less than 0.05) barely contributes to the flexural capacity of the EB, it has the dominant effect at higher ratios. It is also noted from the chart that an optimized situation exists at ratios close to 1.5 (i.e., $A_S \approx 1.5A_{PL}$), where the stiffener and the plate contribute to 60% and 40% of the built-up section's overall moment of inertia. After that, as the A_S/A_{PL} ratio increases, the plate's contribution in the overall built-up section's flexural capacity decreases, and the built-up section becomes stiffener-dominant again. Similar charts could be developed for other types of rib profiles as shown in Fig. 4.4. The plate and stiffener contributions in the overall flexural behaviour of the EB depends highly on A_S/A_{PL} ratio as shown in these charts.

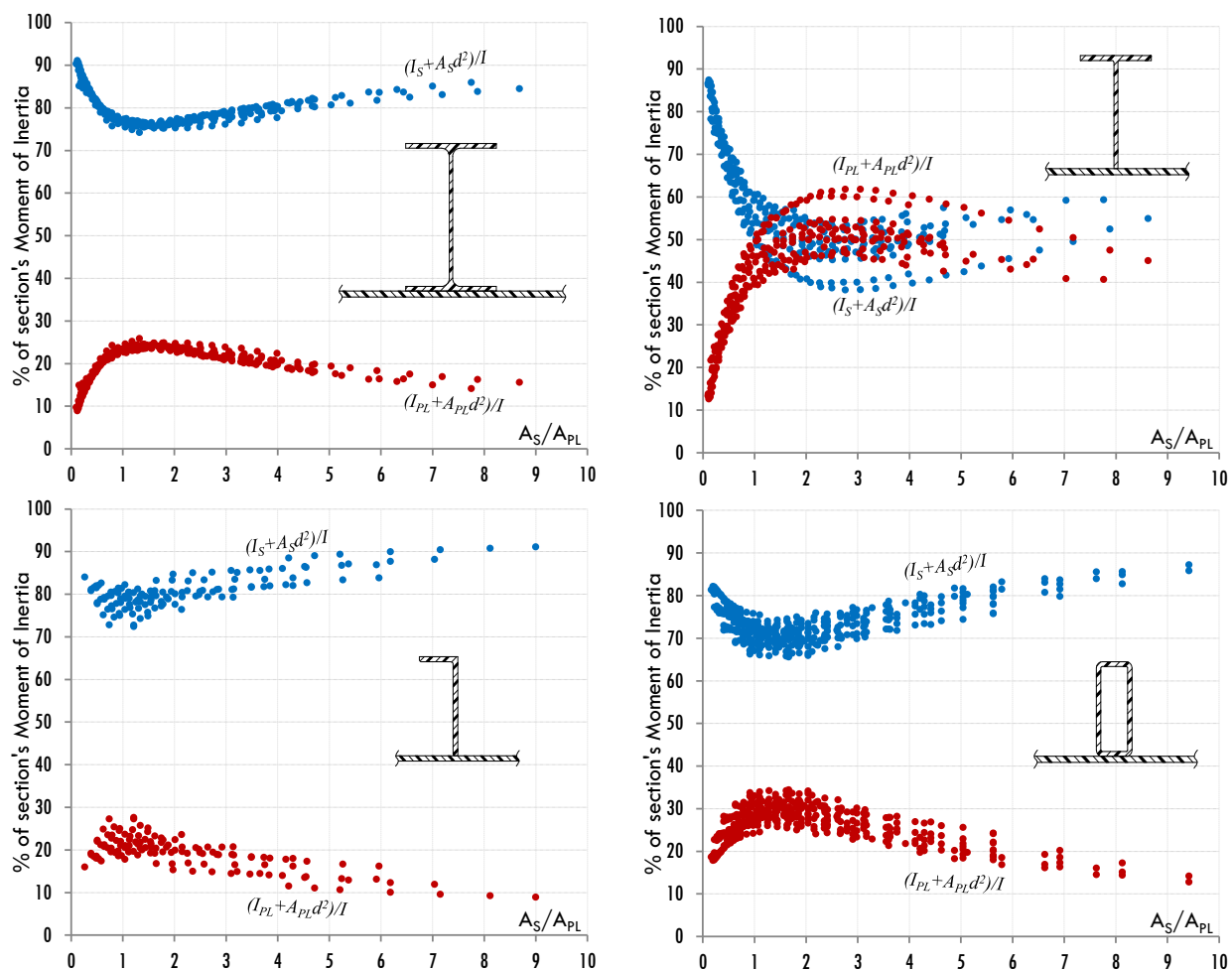


Fig. 4.4: Effect of the ratio of stiffener area over plate area (A_S/A_{PL}) on the EB flexural strength in stiffened plates with various ribs profiles

Although the EBA offers a simple way of estimating the flexural capacity of the stiffened plates and could be applied to any design philosophy, there is a need for assessing its relevance in comparison with more developed analysis methods such as the FE analysis. Thus, a numerical model will be developed in this study to simulate the stiffened plates under lateral uniform pressure. The FE analysis results will be verified against the existing experimental results from the literature and used in comparison with the conventional EBA results.

4.5 Finite Element Modelling and Verification

The FE Modelling in this study uses the standard 4-node “SHELL181” element from the element library of the general-purpose commercial software package, ANSYS (2020-a). This element supports six degrees of freedom (three rotational and three translational DOFs) at each node with the ability to turn the rotational DOFs off to have a “pure membrane” behaviour or turning the translational DOFs off to have “pure bending” conditions. This element has been rigorously tested by ANSYS through benchmark verification examples (ANSYS, 2020-b). Moreover, this software has been previously utilized for similar research by Paik and Seo (2009-a, and 2009-b), where various failure criteria for stiffened plates were investigated.

4.5.1 Geometry, loading, and boundary conditions of the FE models

The numerical analysis in this study consists of two phases of FE Modelling. The first phase aims at the stress distribution in the panel plate of a stiffened plate assembly in order to compare the SDA, LDA, and EBA methods while identifying its load-stress behaviour at key points. The second phase focuses on the effects of panel plate width on the overall behaviour of the stiffened plate from the limit states design perspective. The geometry of the stiffened plate models is shown in Fig. 4.5.

The rib stiffener in all models has a Flat-bar cross-section and designed as a Class-1 section per CSA-S16 (2019) in order to prevent the local buckling. The only load in the FE models is a uniform lateral pressure applied to the panel plate. The pressure is positive when it is applied in the Y direction and vice-versa.

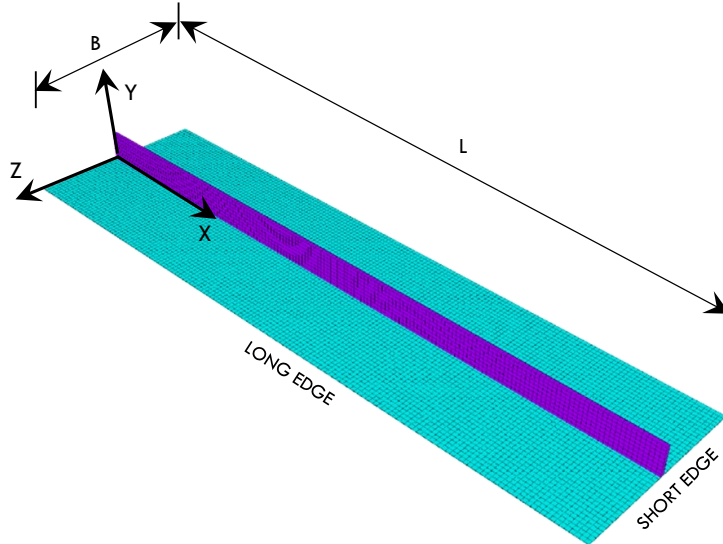


Fig. 4.5: Geometry of the FE models

The plate continuity at the long edges is represented by restraining the $R(X)$ and $U(Z)$ assuming the continuity of the panel plate in Z direction while the short edges could be clamped or simply-supported. Thus, there are two cases of boundary conditions combinations for the FE models in this study, namely simply-supported (S) and clamped (C). Moreover, each of these cases is solved for the negative and positive pressures separately in order to verify the effect of loading nature on the behaviour of the stiffened plates in the large-displacement analysis. Thus, a total of 8 models are generated for the first phase of FE studies, as described in Table 4.2.

Table 4.2. First set of FE models

MODEL	Analysis type	Short edges rotational BC	Short edges in-plane BC	Lateral pressure
SD-S-P	SDA	Simply-supported	N/A	Positive
SD-S-N	SDA	Simply-supported	N/A	Negative
SD-C-P	SDA	Clamped	N/A	Positive
SD-C-N	SDA	Clamped	N/A	Negative
LD-SF-P	LDA	Simply-supported	Fixed	Positive
LD-SF-N	LDA	Simply-supported	Fixed	Negative
LD-CF-P	LDA	Clamped	Fixed	Positive
LD-CF-N	LDA	Clamped	Fixed	Negative

In the second phase, a total of 6 stiffened plate geometries are modeled wherein the only variable is the panel plate width over thickness ratio (λ), and all models are analyzed using the LDA. The details of these models are shown in Table 4.3.

Table 4.3. Second set of FE models

Loading	Simply-supported (S)		Clamped (C)		$\lambda=B/t_{PL}$	A_S/A_{PL}
	Model	Short Edges BC	Model	Short Edges BC		
Positive Pressure	S1-P		C1-P		140	1.32
	S2-P		C2-P		180	1.03
	S3-P		C3-P		220	0.84
	S4-P		C4-P		260	0.71
	S5-P		C5-P		300	0.62
	S6-P	U(X), U(Y)	C6-P	U(X), U(Y), R(Z)	340	0.54
Negative Pressure	S1-N		C1-N		140	1.32
	S2-N		C2-N		180	1.03
	S3-N		C3-N		220	0.84
	S4-N		C4-N		260	0.71
	S5-N		C5-N		300	0.62
	S6-N		C6-N		340	0.54

The steel material model for the plate and stiffener in the FE models is based on the bilinear isotropic behaviour with strain hardening (EN 1993-1-5), which sets the plastic strain limit at 5% for the failure criterion.

4.5.2 Verification of FE Modelling

The FE Modelling approach and the selected element are verified against the results of three experimental tests by Shanmugam et al. (2014). The distributed lateral pressure in the experimental work of Shanmugam et al. (2014) was applied to the specimen using an airbag, and the in-plane axial loads were applied by hydraulic jacks, as shown in Fig. 4.6. The three specimens were identical except for the in-plane loads as 0.0, 170.0 and 300.0 kN for A1, A2, and A3 specimens, respectively. While the in-plane axial load was kept constant throughout the test, the lateral pressure was increased, and the displacement at the center of the plate was monitored (Shanmugam, 2014). The experimental test results for those three specimens and their respective FE analysis

results from the current study are plotted in the charts of Fig. 4.7, in which a good correlation between the FE analysis and experimental results is demonstrated.

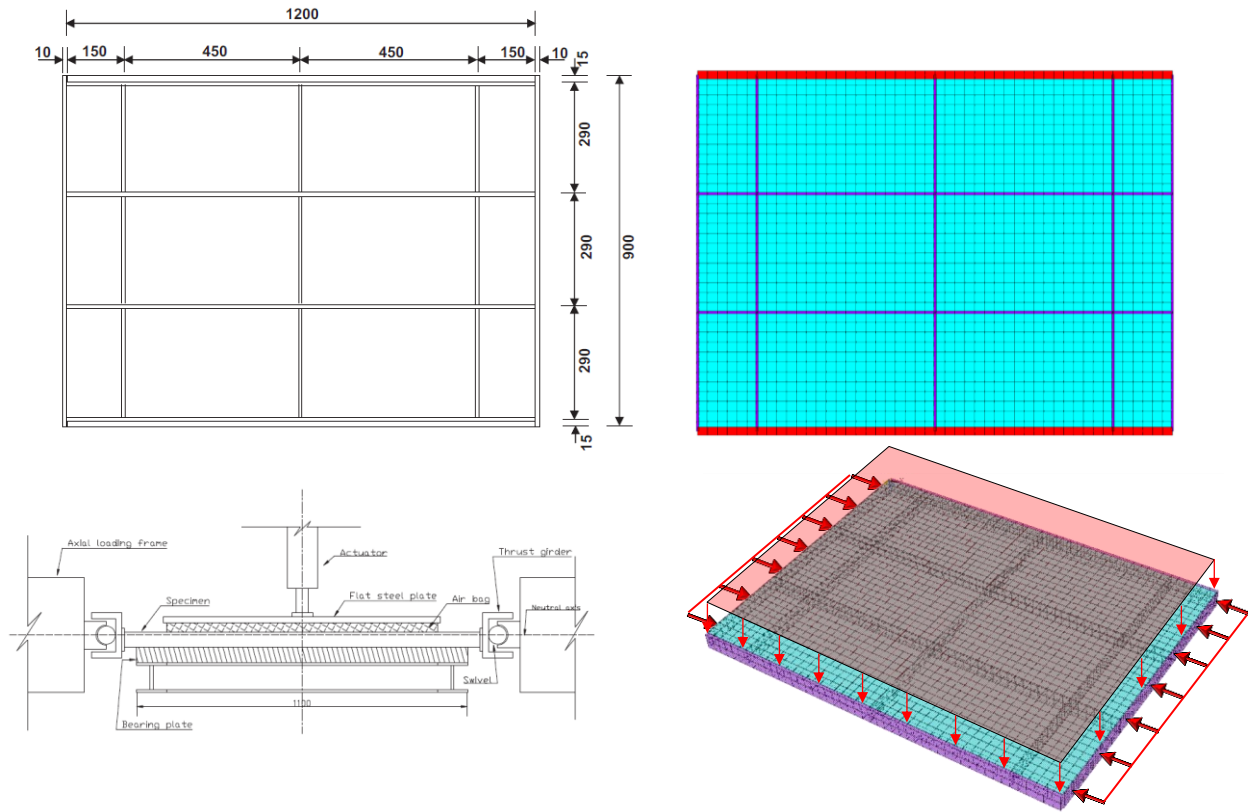


Fig. 4.6: Geometry and load setup for verification model; Left: Experimental specimen of Shanmugan et al. (2014); Right: FE mesh and loading in the current study

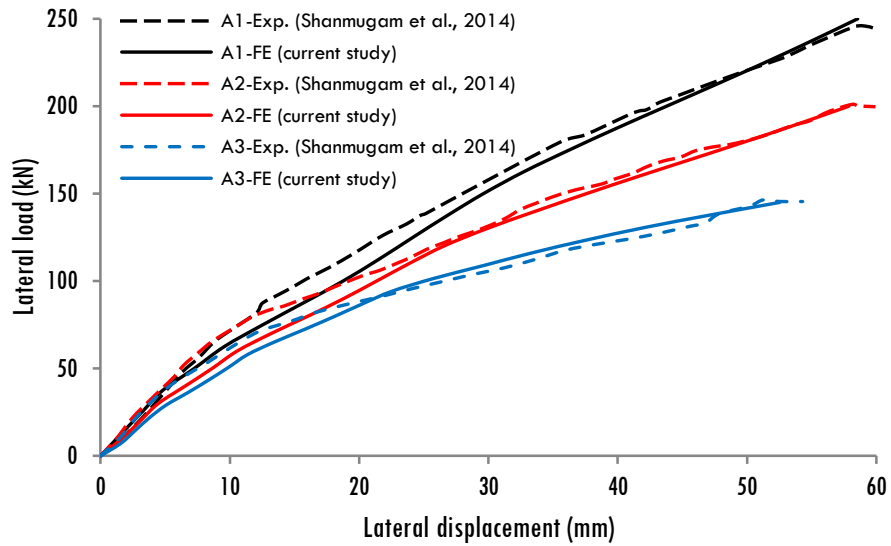


Fig. 4.7: Lateral load-displacement charts for three experimental tests of Shanmugan et al. (2014) and results from the FE analysis

4.5.3 FE analysis output

The FE outputs are the midspan displacements, overall internal forces and stresses at key points. The displacement profile of the stiffened plate under positive pressure is shown in Fig. 4.8. As shown in the figure, the midspan displacement at the stiffener location is significantly smaller than at the mid-panel of the plate. On the other hand, the midspan displacement calculated in the EBA does not correspond to what is shown in Fig. 4.8 as it is unique for the whole cross-section of the EB. In this regard, when the FE analysis results are compared to the EBA, it is beneficial to draw the load-displacement charts for the average of the midspan cross-section (Av.) as well as at the stiffener location (St.).

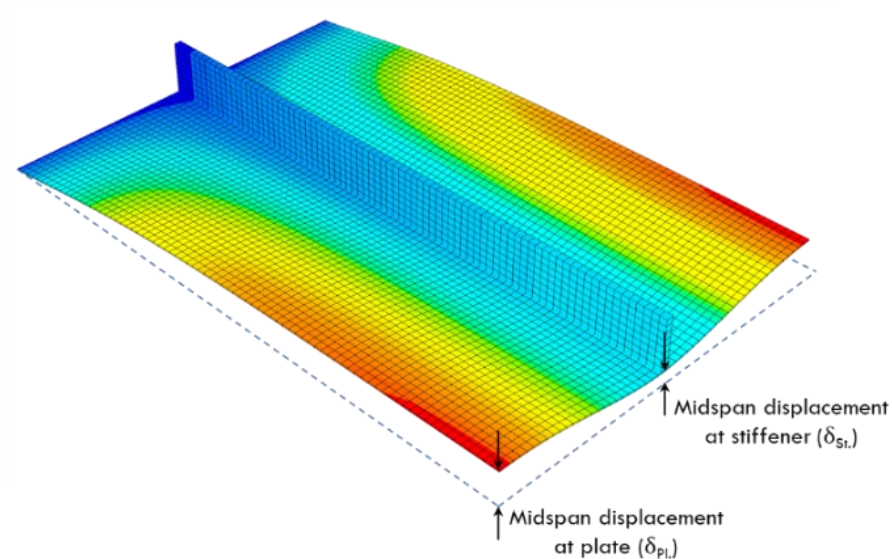


Fig. 4.8: Displacement profile of stiffened plate at midspan (only half of the stiffened plate is shown for better display)

The schematic internal forces and main stresses in a typical element of the panel plate are shown in Fig. 4.9. The membrane forces (N_x and N_z) are only calculated in the LDA, while the bending moments (M_x and M_z) are calculated in both SDA and LDA. Since the plate material is homogeneous and isotropic, the linear distribution of the S_x and S_z stresses through the thickness of the plate is applicable.

The most relevant failure criterion for steel and other ductile materials is the Maximum-Distortion-Energy, or the equivalent (von Mises) stress (Gere and Timoshenko, 2012).

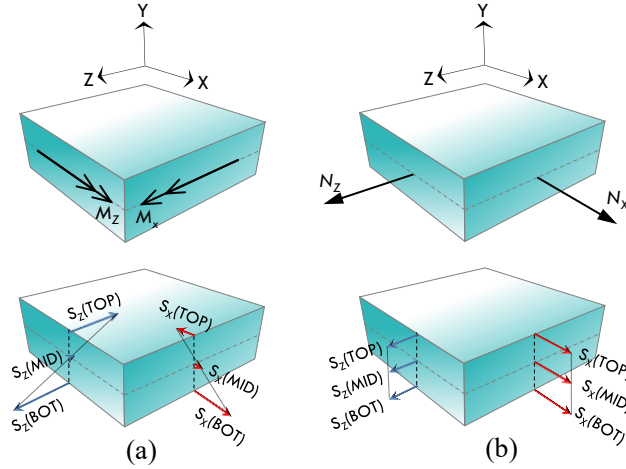


Fig. 4.9: (a) Bending moments and resulting stresses; (b) Membrane forces and resulting stresses

The equivalent stress is defined based on the 9 global structural stress components as follows:

$$S_{EQ.} = \sqrt{\frac{1}{2} \left[(S_x - S_y)^2 + (S_y - S_z)^2 + (S_z - S_x)^2 + 6(S_{xy}^2 + S_{yz}^2 + S_{zx}^2) \right]} \quad (\text{Eq. 4.1})$$

As discussed previously, the governing stresses in the panel plate are the S_x and S_z , while as the plate element is relatively thin, the S_y , S_{xy} , S_{xz} , S_{zx} , and S_{zy} deem negligible (except at the corners of the plate). Thus, Eq. 4.1 simplifies for the panel plate as:

$$S_{EQ.} = \sqrt{S_x^2 + S_z^2 - S_x S_z} \quad (\text{Eq. 4.2})$$

The forces and stresses in Fig. 4.9 and the equivalent stress could be obtained from the FE models in the form of contour displays over the geometry at any load step, or in the time-history format against the applied load. These results will be presented and discussed in the following sections.

4.6 Load-Displacement Analysis

The midspan displacement of the stiffened plates is discussed in this section. In the load-displacement charts presented in this section, $q^* = q\lambda(L/t)^2/E$ and $\delta^* = \delta/t$ are the unitless representers of the pressure and the midspan displacement respectively where q is the uniformly-distributed pressure, λ is the plate width over thickness ratio (B/t), E is the Young's modulus of the plate material, δ is the midspan displacement, and t is the plate thickness.

The midspan load-displacement charts resulted from the clamped, and simply-supported models are presented in Fig. 4.10.

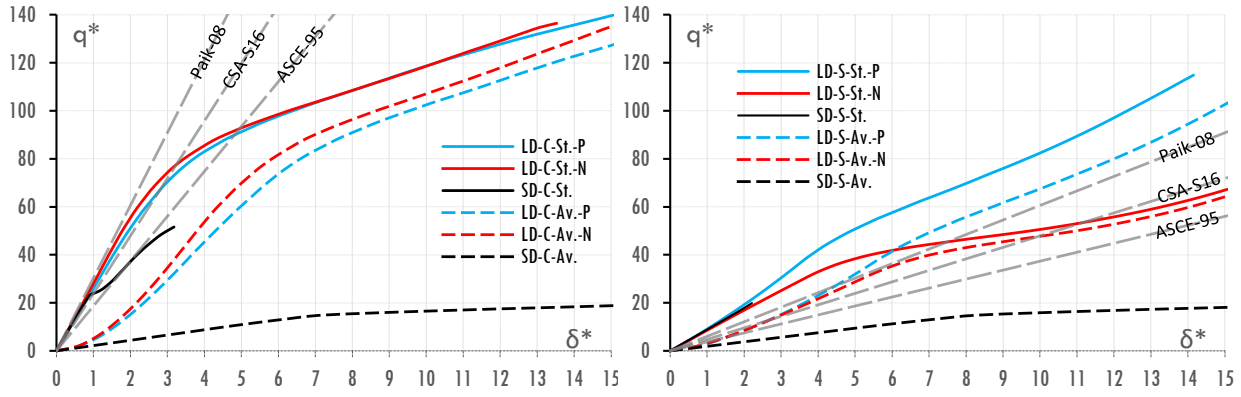


Fig. 4.10: Mid-span load-displacement charts for the clamped (left) and simply-supported (right) models

The charts in Fig. 4.10 result from the same stiffened plate geometry under positive and negative uniform pressures using the LDA and SDA. The linear trends from the EBA based on the panel plate effective widths from the values in Table 4.1 are also plotted in the charts for comparison. As seen in the charts of Fig. 4.10, the average displacements (Av.) from the SDA are unrealistically higher than all others. This is because the displacements of the panel plate are calculated without the consideration of the membrane forces. Another general observation from these charts is that the load-displacement of the stiffened plate follows different trends under positive and negative pressures when the LDA is used.

4.7 Stress Analysis

When a uniform lateral pressure is applied to the stiffened plate, the stiffener mainly exhibits flexural behaviour as a beam element in combination with the panel plate along the longitudinal axis (X-direction). On the other hand, the internal bending and membrane forces are exhibited in the panel plate as discussed previously. The following section provides the distribution of the membrane forces and bending moments in the panel plate through comparisons between the SDA and LDA in order to discuss the effectiveness of each analysis method in capturing the true behaviour of the stiffened plate.

4.7.1 Membrane forces and bending moments in the panel plate

Distinguishing between the flexural and membrane actions in the panel plate is the key to further discussions on the stress analysis of stiffened plates. However, it should be noted that the membrane action is only captured when the LDA is implemented. The membrane forces in the panel plate at $q^*=0.5$ are shown in figures 4.11 and 4.12. These forces are normalized by dividing them by the equivalent yielding force ($N_{Yield}=F_y \times t_{PL}$).

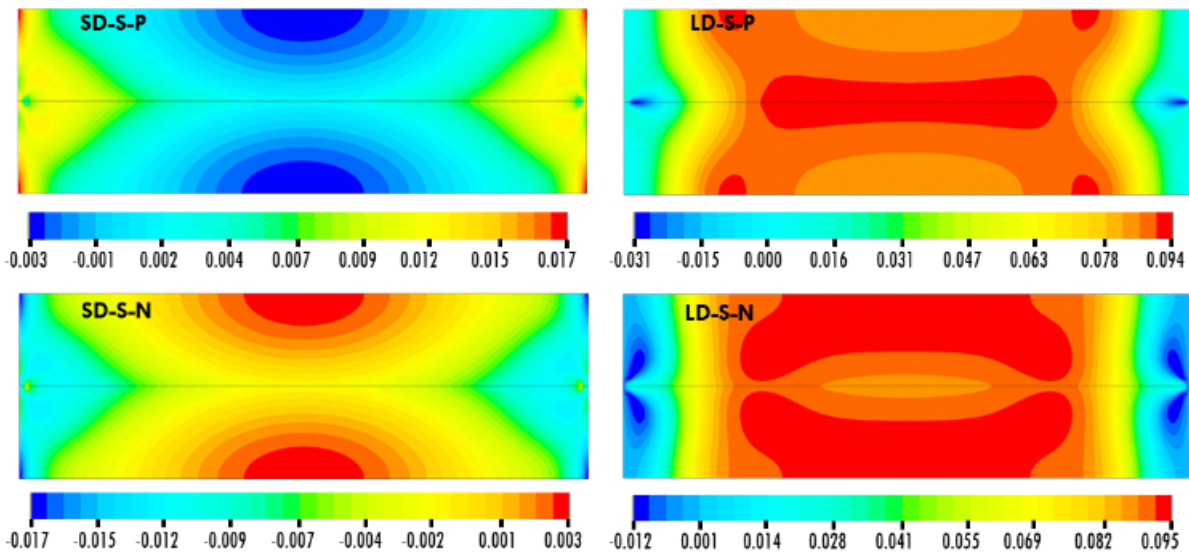


Fig. 4.11: Membrane force ratio N_z/N_{Yield} in the panel plate at $q^*=0.5$ for simply-supported models (stiffener is not shown)

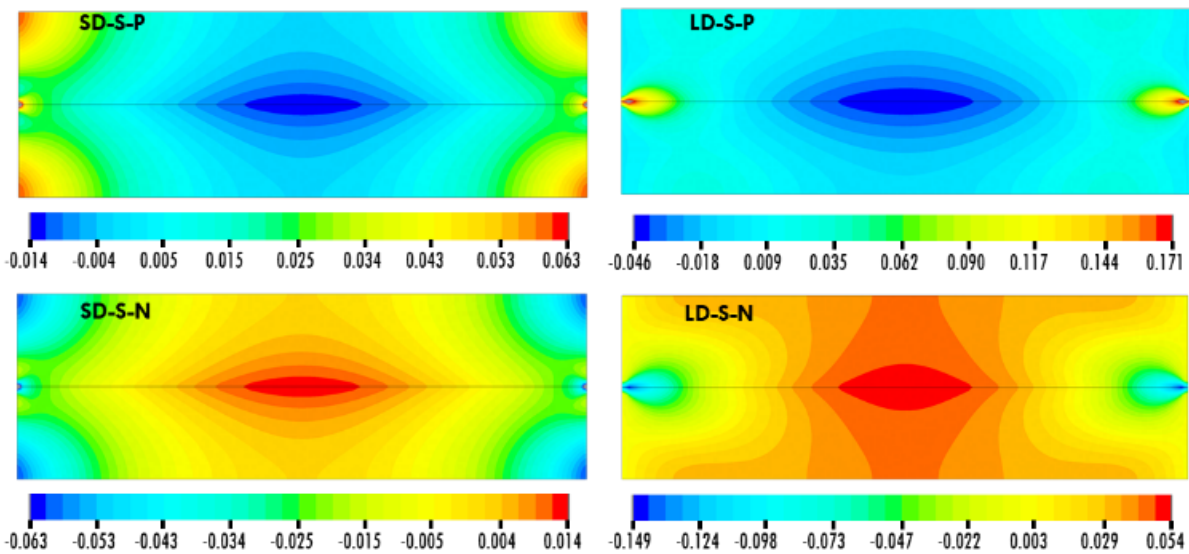


Fig. 4.12: Membrane force N_x/N_{Yield} in the panel plate at $q^*=0.5$ for simply-supported models (stiffener is not shown)

As seen in the figures, there is a fundamental difference between the membrane forces in the global X and Z directions. The panel plate is not stiffened along the Z-axis; thus, it merely has a plate behaviour in that direction while it is *part* of a built-up cross-section along the X-axis. As a result, the N_X forces *exist* in both SDA and LDA since the plate undergoes flexural tension and compression under negative and positive pressures respectively. However, the LDA results in significantly greater N_X under negative pressure while exhibiting significantly smaller N_X values under positive pressure.

This phenomenon is because the membrane forces calculated in the LDA are always tensile, regardless of the direction of the applied pressure. Thus, they are added to the flexural tension but are deducted from the flexural compression in the plate. This phenomenon also explains the different load-displacement charts under positive and negative pressures which was demonstrated in the previous section. Similar results for the membrane forces are expected for the clamped models.

The other aspect of the panel plate behaviour is described in the bending moment contours in figures 4.13 and 4.14. These bending moments are normalized by dividing them by the equivalent yielding moment ($M_{Yield}=F_y \times S_{PL}$).

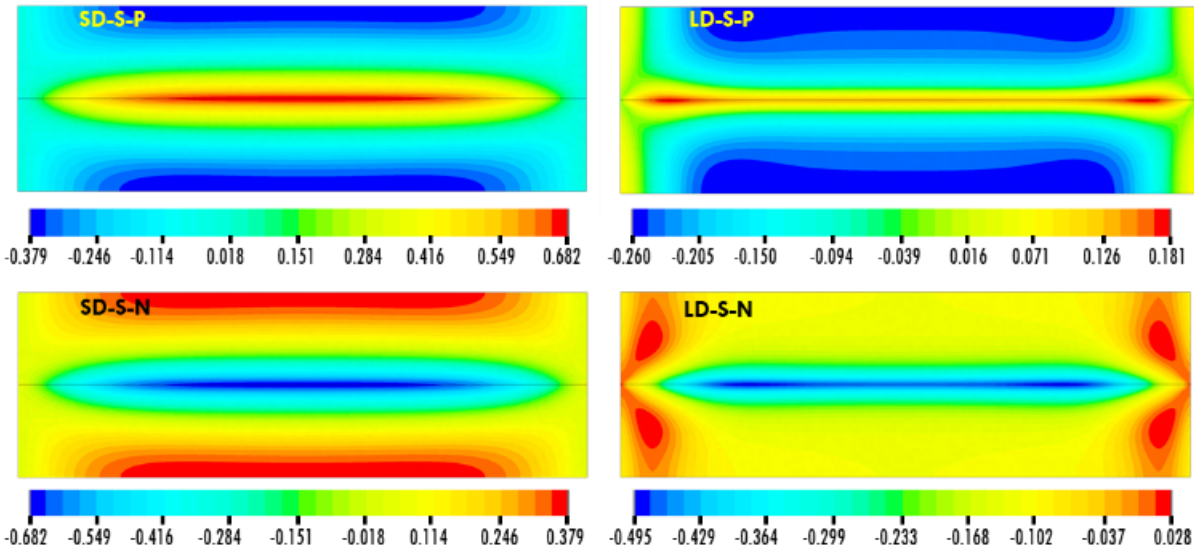


Fig. 4.13: Bending moment M_Z/M_{Yield} in the panel plate at $q^*=0.5$ for simply-supported models (stiffener is not shown)

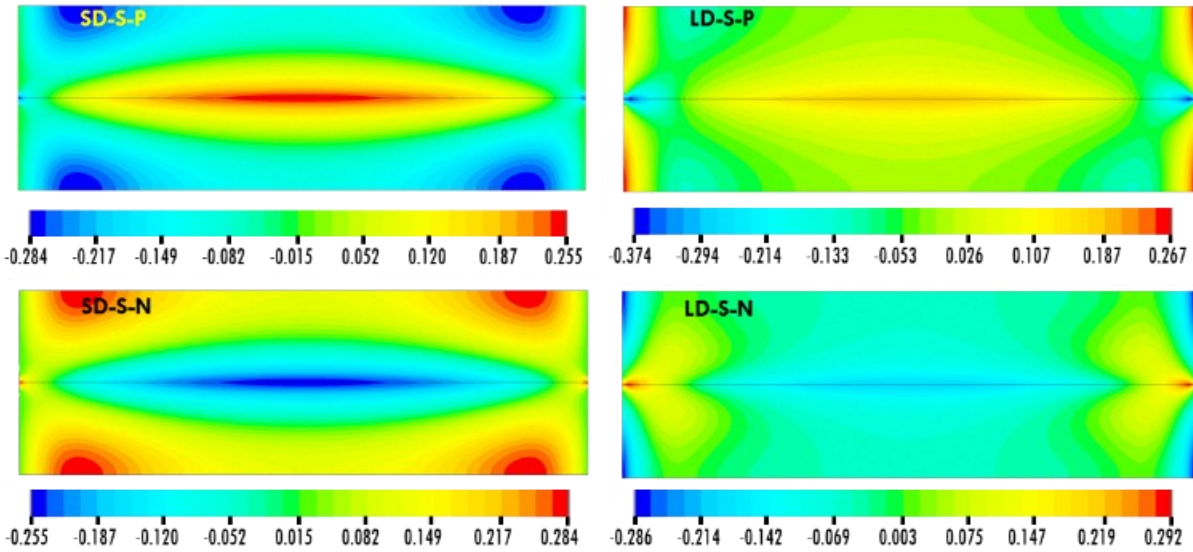


Fig. 4.14: Bending moment M_X/M_{Yield} in the panel plate at $q^*=0.5$ for simply-supported models (stiffener is not shown)

In the SDA, the plate behaviour is dominated by the M_Z bending as it is significantly higher than M_X in both clamped and simply-supported SDA models. On the other hand, the M_Z values decrease substantially when the LDA is implemented. This phenomenon is explained by looking at the N_Z contours of the previous figures for the LD-C and LD-S models. Simultaneously, the M_X values across the panel plate are increased in the LDA compared to the SDA. This phenomenon could be explained through a more in-depth analysis of the stresses across the cross-section of the panel plate.

4.7.2 Global stresses in the panel plate

Following the assessment of the internal forces of the panel plate in the previous section, the plate stresses (S_X and S_Z) are foreseeable per the schematic element in Fig. 4.9. Given that these stresses are combined in the actual analysis, a perfect flexural behaviour suggests that the MID stresses are negligible while the TOP and BOT stresses have the same magnitudes in the opposite directions. On the other hand, a perfect membrane behaviour suggests that the TOP, MID, and BOT stresses be of the same magnitudes in the same directions. The load-stress plots could be extracted for TOP, MID, and BOT stresses at any point in the panel plate in the FE analysis. However, there are *key points* at which the stresses are expected to be significant, thus worth studying from a design perspective. These key points are:

- Point 1: Mid-span under the stiffener,
- Point 2: Mid-span at middle of the panel plate,
- Point 3: End-span under the stiffener, and,
- Point 4: End-span at middle of the panel plate.

The charts in figures 4.15 to 4.18 demonstrate the stress behaviour at these key points.

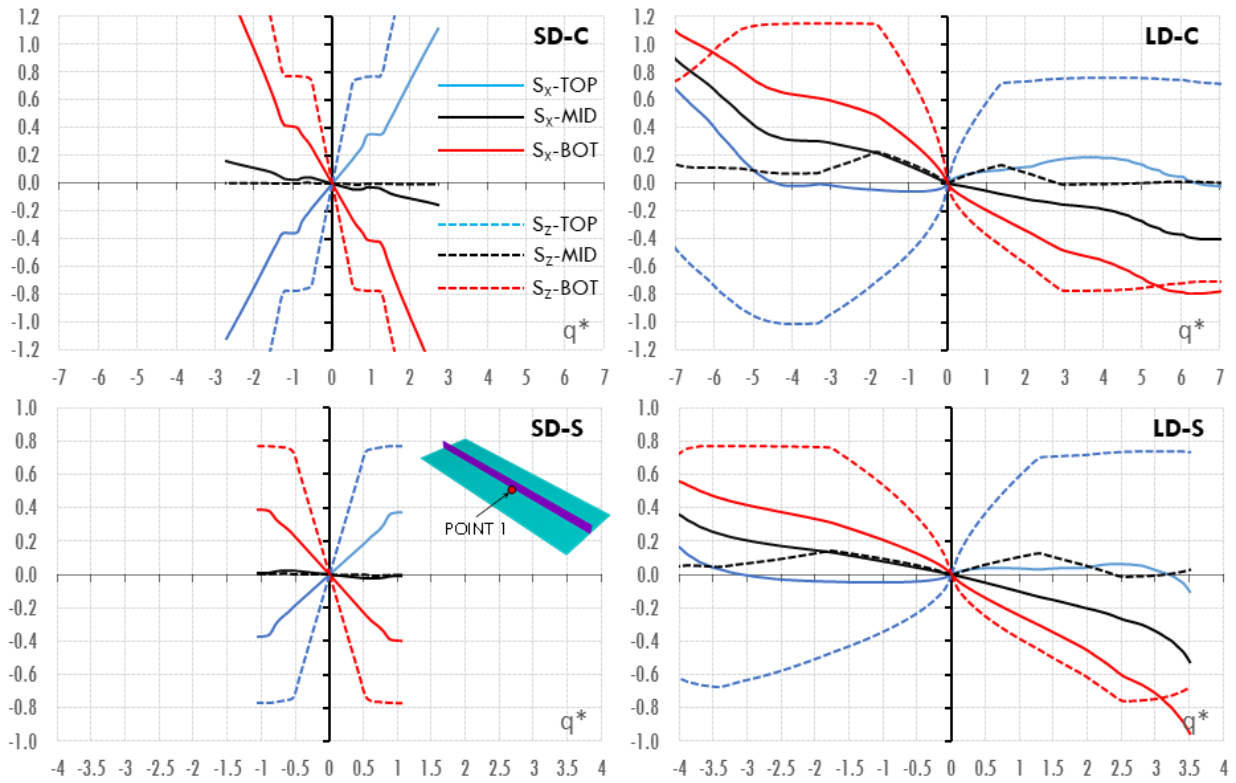


Fig. 4.15: Panel plate load-stress charts at Point 1 for SD-C, LD-C, SD-S, and LD-S

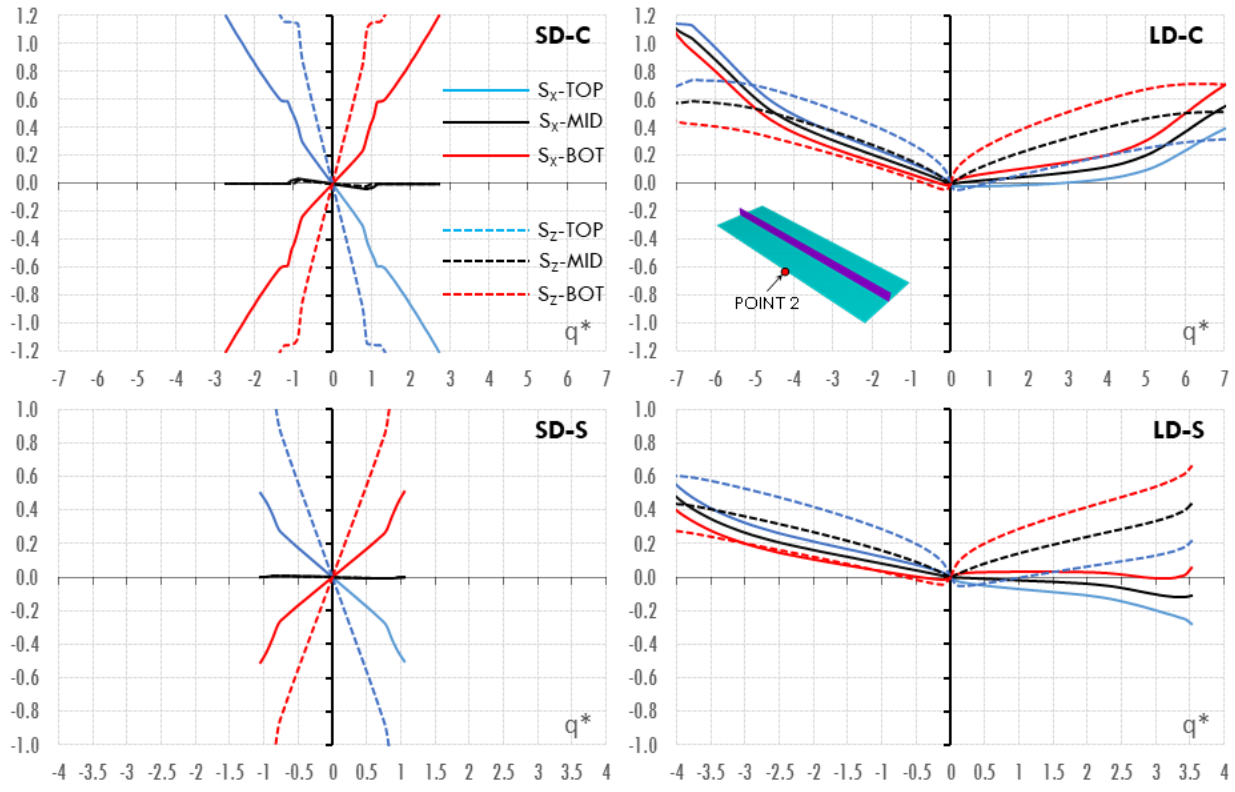


Fig. 4.16: Panel plate load-stress charts at Point 2 for SD-C, LD-C, SD-S, and LD-S

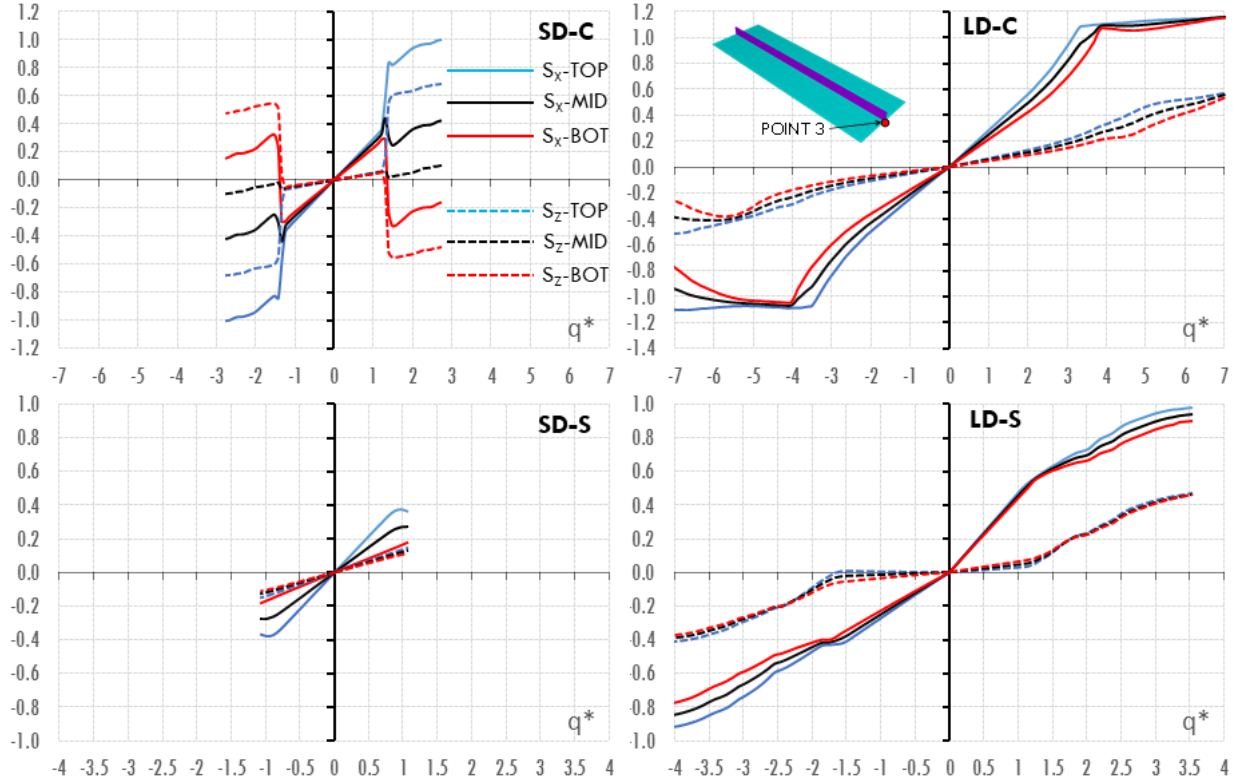


Fig. 4.17: Panel plate load-stress charts at Point 3 for SD-C, LD-C, SD-S, and LD-S

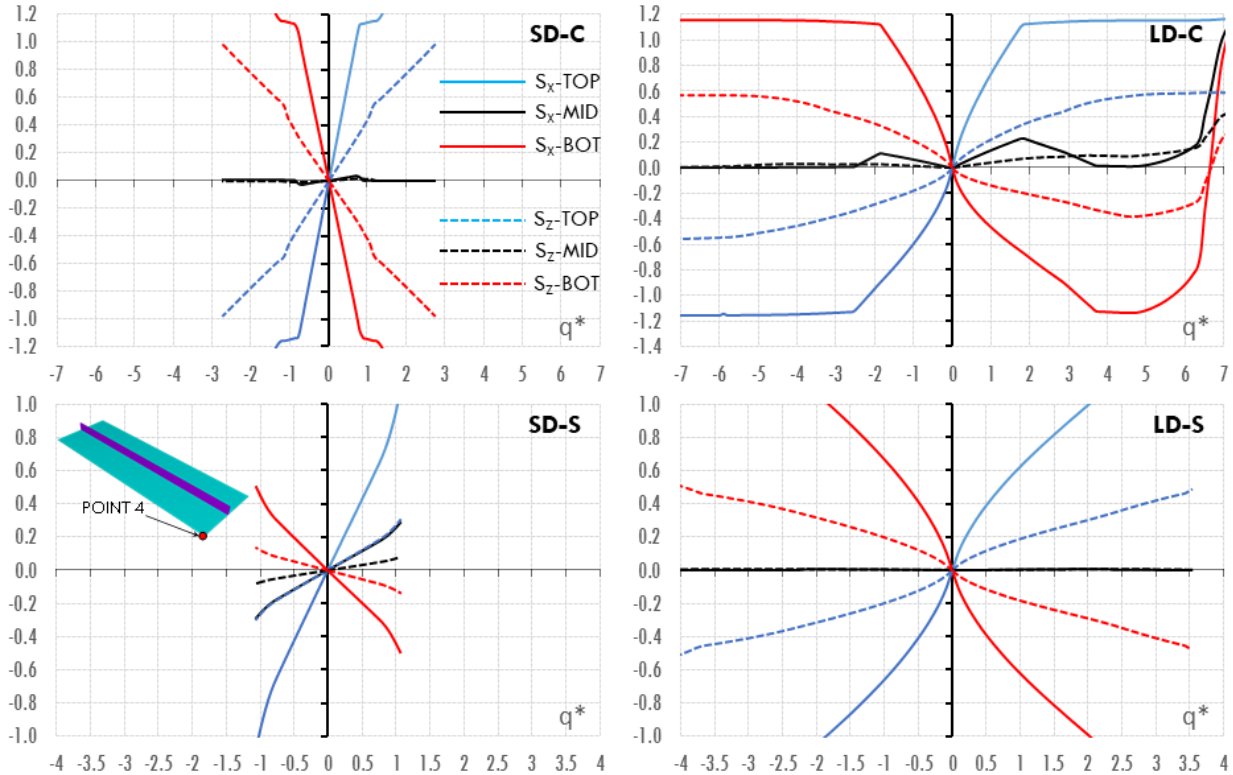


Fig. 4.18: Panel plate load-stress charts at Point 4 for SD-C, LD-C, SD-S, and LD-S

As seen in the load-stress charts in these figures, the SDA merely reflects the bending stresses in all four key points. On the other hand, the load-stress charts resulted from the LDA include the effects of both bending and membrane forces in the panel plate. The von Mises stress distribution in the clamped stiffened plate is shown at four levels of loading in Fig. 4.19.

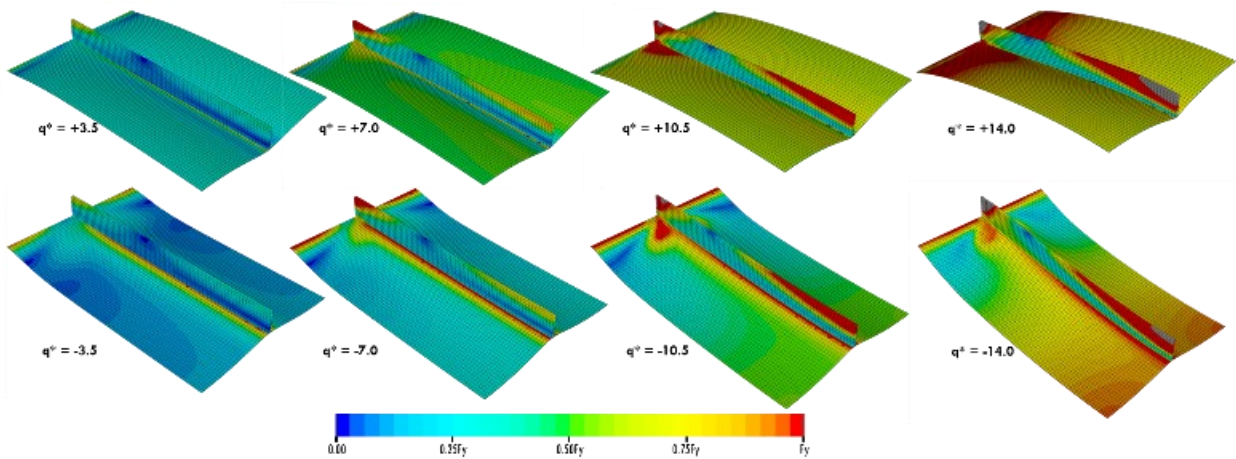


Fig. 4.19: Contour plots of the deformed shape and the von Mises stress distribution in the clamped model at four stages of loading (only half of the plate length is shown for better clarity) upper: positive pressure, lower: negative pressure

4.8 Limit States Design of Stiffened Plates with Parallel Ribs

Depending on their application, various loads are applied to the stiffened plates in industrial structures. The structural engineer decides on the main loading components while coordinating the design based on the applicable failure modes accordingly. The following failure modes are expected for stiffened plates with parallel ribs in industrial applications:

- Global (lateral) buckling of the stiffened plate in axial compression,
- Local buckling of the rib stiffener in flexural compression,
- Plate buckling in flexural compression,
- Yielding of the plate,
- Yielding of the stiffener, and/or,
- Welds fracture under the shear lag effects.

The global buckling of the stiffened plate under direct axial compression has been extensively investigated in the literature, including Paik (2008). The local buckling of the stiffener is generally prevented by implementing the requirements of the design codes for compact sections. The plate buckling in flexural compression is related to the concepts of effective width and effective breadth (Paik 2008), on which basis the equivalent beam analogy (EBA) is used as a conventional design method. The fracture of welds under shear lag effects is out of the scope of the current study as it requires its dedicated investigations. Lastly, the yielding of the panel plate and stiffener under the combined stresses from the internal flexural and membrane actions are the expected failure modes in the FE models of this study.

4.8.1 Ultimate Limit State (ULS)

The ULS involves calculating the stresses in the structural components and verifying them against certain limit states, which are set mainly based on their nature in the design standards. The ULS sets forth the limitations to be satisfied in the design on a case-by-case basis. In this regard, the distribution of the stresses in the stiffened plate must be compared to the principles of the conventional design, which is based on the EBA. The stresses in the EBA are straightforward, i.e., the maximum flexural stresses are at the two ends of the clamped beam and the midspan of the simply-supported beam. Once the portion of the plate width (effective breadth) is determined, the

effective moment of inertia and the section modulus of the EB are calculated, and the flexural resistance of the EB is determined.

4.8.2 Serviceability (displacement) Limit State (SLS)

One key parameter in the structural design of stiffened plates in industrial applications is the maximum displacements of the panel plates and the rib stiffeners. Conventionally, the displacement limits are defined based on the serviceability limit states. In other words, a certain limit is set for the deformation of the structural members such that the functionality of the structure stays intact. Those limits are mainly available for buildings and other types of structures in building codes and other standards. However, industrial structures require the serviceability limit states to be defined on a case-by-case basis regarding the requirements of the equipment assemblies supported or provided by the structural system.

4.8.3 Limit states design based on LDA

As mentioned previously, the structural design of the stiffener follows the panel plate design. Regardless of the analysis method, the stiffener in the stiffened plates of this study is regarded as a beam element with flexural behaviour. In the EBA, the elastic section modulus of the stiffened plate cross-section is calculated, and the elastic bending moment capacity is achieved accordingly.

On the other hand, the ULS design involves the plastic behaviour of the beam element, which collapses when abundant plastic hinges develop. The regions at which the plastic hinges are to be expected are those regions with the highest von Mises stress (see Fig. 4.19) at various stages of loading. It is established that ductile beams are expected to deform in three distinguished regimes (Paik and Thayambali, 2003). The *linear elastic regime* is where there are no plastic hinges formed in the beam. The linear elastic regime ends at a “threshold load” at which the plastic deformations start. Then the beam undergoes a *transition regime* in which the plastic hinges spread until the beam reaches the *large deflection regime* where the plastic hinges are well developed, and the slope of the load-displacement curve decreases significantly (Paik and Thayambali, 2003). The maximum displacement of the beam at the end of the transition and large deflections regimes are estimated by Belenkiy and Raskin (2001) at $0.005L$ and $0.01L$, respectively, while the deflection corresponding to the ultimate load on the linear elastic regime is between $0.001L$ and $0.004L$. The ultimate design load for the beam is obtained by finding *Point A* on the bilinear estimation of the

load-displacement chart, as shown in Fig. 4.20. In the absence of strain measurements at the highest stress points of the beam, the above-mentioned estimated point determines the ultimate load for the beam.

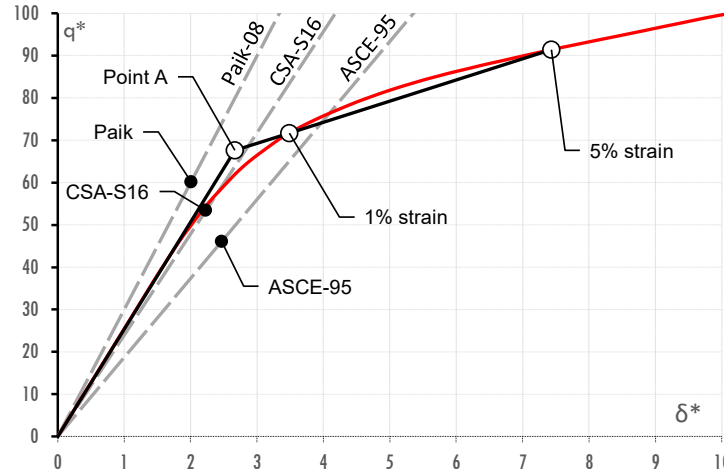


Fig. 4.20: Mid-span load-displacement chart for the C1-N model and the bilinear design points

A more realistic approach is to use the plastic strains as a guide for the design. In this approach, the linear elastic behaviour continues until the first plastic strains appear in the beam. The actual transition regime then starts as the plastic strains grow in different regions of the beam and continue until failure. The von Mises strain at failure for flexural members is recommended by most design codes, including EN 1993-1-5 (2006) at 5%. The authors estimate a maximum von Mises strain of 1% at which the plastic strains start to develop at more than one point in the stiffened plate after reviewing such strains throughout the loading history of all FE models in this study. This point could be used as the indicator of the end of the transition regime. If a straight line is drawn from the point of 5% strain to the point of 1% strain and continued to intercept the linear elastic trend at Point A, the corresponding load is the ultimate load in the ULS design accordingly. This approach is applied to the load-displacement charts of all the models in this study, and the results are presented in Fig. 4.21 in comparison with the design loads from the linear EBA.

As seen in the charts of Fig. 4.21, the ultimate loads obtained from the LDA are significantly greater than those of the linear EBA design for the clamped stiffened plates under both positive and negative pressures, while the corresponding displacements are also larger than those of the linear EBA. On the other hand, the LDA results for the simply-supported models show smaller ultimate displacements under both positive and negative pressures than the linear EBA, while the

ultimate load is only greater for the positive pressure. The ultimate loads obtained from the models under negative pressure are within the same range as those of the linear EBA.

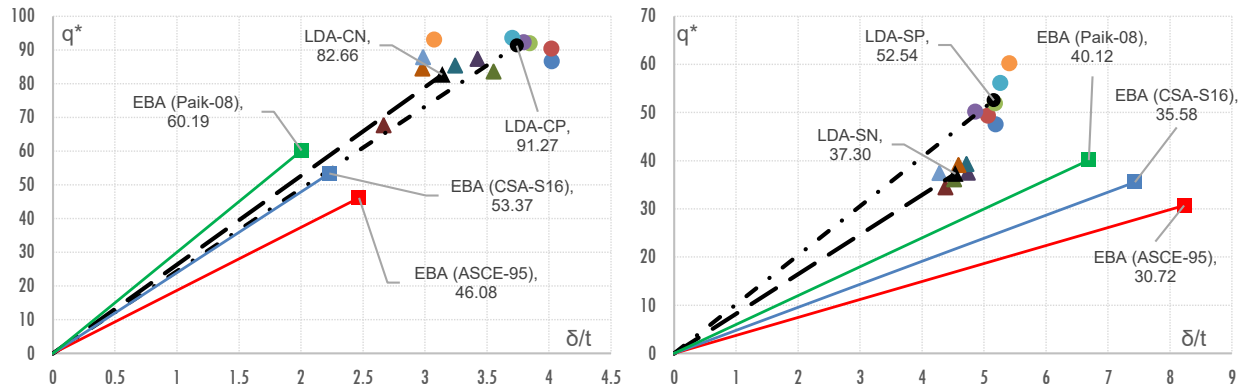


Fig. 4.21: Ultimate load and displacement at Point-A obtained from the LDA in comparison with the conventional EBA methods for the clamped (left) and the simply-supported (right) models

4.9 Conclusions

The case of stiffened plates with parallel ribs under lateral uniform pressure was discussed in this paper from the analysis and design points of view. The main purpose of this study was to compare the linear beam equations which are adopted for the stiffened plate conventionally by the engineers in the form of an Equivalent Beam Analogy (EBA) and the advanced FE analysis using shell elements for the plate and stiffener. The FE analysis was divided into two main categories of Small Displacement Analysis (SDA) and Large Displacement Analysis (LDA). The stress distribution in the panel plate was reviewed in both SDA and LDA in order to verify the potential failure modes and the points at which plastic behaviour could be expected. This study contained a total of 16 FE models, all of which had the same stiffener geometry and panel plate thickness and subjected to either positive or negative uniform pressure over the panel plate. The main geometrical variable was the panel plate width, for which a total of 6 different B/t ratios were studied. Two main cases of clamped and simply-supported end boundary conditions were considered in the FE models and analysis. The following conclusions are obtained from this study;

- The linear beam theory does not correctly represent the actual behaviour of the stiffened plate for the internal stresses in the panel plate. Moreover, the load-displacement estimation provided based on the EBA does not correspond with the actual behaviour of the stiffened plate.

- The internal forces and stresses in the panel plate are not correctly calculated in the SDA as the membrane forces are neglected. Thus, the load-displacement behaviour is not correctly estimated by the FE analysis if the SDA is applied.
- The most accurate method for the FE analysis of stiffened plate is the LDA, in which the contributions of the panel plate and the rib stiffener are calculated based on the combination of internal flexural and membrane stresses.
- The load-displacement behaviour of the stiffened plate is not independent of the nature of the applied uniform pressure. Different load-displacement charts are obtained for the same stiffened plate model under positive and negative uniform pressures.
- The end boundary conditions have a significant effect on the load-displacement of the stiffened plates. However, the stiffened plate does not follow the classical beam theory in which the simply-supported beam has a five times greater displacement under the same uniform load than the clamped beam.
- The ultimate design loads and displacements achieved from the LDA are mainly different from those obtained from the linear beam theory with the EBA.
- In the case of clamped ends, the LDA results in greater ultimate loads and displacements under both negative and positive pressures compared to the linear beam theory using the EBA.
- In the case of simply-supported ends, the LDA results in smaller maximum displacements than the linear beam theory using the EBA, while the ultimate loads resulting from the LDA under positive pressure are greater than the EBA within the same range as the EBA under negative pressure.

CHAPTER 5

Free Vibration of Thin Rectangular Steel Plates with Geometrically-Nonlinear Load-Displacement Behaviour

5.1 Abstract

This paper provides means for obtaining the first three *significant* vibration modes for rectangular plates based on mass participation ratios. A non-dimensional frequency parameter is presented which results into the vibration frequency of rectangular plates at each of these three significant modes. Various aspect ratios and four combinations of boundary conditions at the plate edges are studied. A correlation between the nonlinear load-deformation behaviour of the plate and its vibrational behaviour is also presented accordingly. It is demonstrated that the vibration frequency of the studied rectangular plates increases significantly upon increasing the applied lateral pressure if the large deformation effects are considered in the analysis. The easy-to-follow method of frequency calculation presented in this paper is useful for assessing the dynamic characteristics of rectangular plates with or without lateral pressure that are subject to vibration.

5.2 Introduction

Stiffened plates with rectangular panels are one of the most common forms of thin-walled structures in industrial, naval and aerospace structures. The walls of industrial ducts, ship hauls, rectangular bins and aircraft wings are examples of such plates. The vibration of rectangular plates has gained the attention of many researchers in the past decades. Structural vibration analysis involves studying the vibration properties of any structure that is subjected to any form of vibrating force. Resonance conditions where the forcing frequency and the natural frequency of the structure are the same (or very close) are to be avoided. Although there are no code regulations about the resonance checking, structural engineers tend to set the limits of $\pm 20\%$ as the resonance domain, i.e., if the forcing frequency is within the range of 0.8 to 1.2 times the natural frequency, the structure is considered as "*prone to resonance*". However, there are still questions to be answered e.g.: "How many modes should be considered?" and "Which modes are important?" that are involved with the vibration analysis of structures. The answer to these questions for the cases of

single-degree-of-freedom (SDOF) and multi-degrees-of-freedom (MDOF) structures involve the measurement of the participation of the structural mass in the desired DOFs. For the case of SDOF systems, there is only one mode of vibration and the mass participation for that mode is 100%. The vibration frequency at this mode is often called the “*fundamental frequency*”. The fundamental frequency in MDOF systems corresponds to the first mode in each DOF i.e., the mode with the highest mass participation in each DOF.

While the main aspects of the structural design of rectangular plates are the load-deformation and load-stress behaviour, vibration-induced limit states such as fatigue and loosening of connections might cause unforeseen deficiencies during the service life of the structure if the structure is prone to resonance.

Several studies in terms of closed-form solutions and numerical methodologies to calculate the frequencies of vibration of rectangular plates are available in the literature including Gorman (1982), Soedel (1993), Amabili (2008) and Chakraverty (2009). Effects of several parameters on the natural frequency of rectangular plates are the topic of further research including the studies by Liew et al. (1993) wherein the effects of in-plane isotropic pressure on the vibration response of thick rectangular plates were discussed. More recently, Xiang et al. (2002) presented one of the first known exact solution for the vibration of rectangular multi-span plates with two opposite edges simply supported using the Levy type solution method and the state-space technique. Phillips and Jubb (1974) presented a series of tests to verify the natural frequency of variation of an approximately clamped rectangular plate due to increasing lateral distortion against the existing theory initially presented by Reissner (1955). The initial distortion of the plate in their experimental tests was applied by deflecting the plate using a rigid block at the center of the plate and a hydraulic jack prior to the vibration test. Manzanares-Martinez et al. (2010) presented the lower normal modes of vibration of rectangular plates through experimental and theoretical analysis. Their experimental tests involved employing electromagnetic-acoustic transducers on a thin rectangular plate in order to measure the frequencies of vibration mainly in the acoustic modes with high frequencies.

Cho et al. (2015) studied the vibration of rectangular plates for the case of bottom plate of fluid containers where the plate is in direct contact with fluid. The fluid-structure interaction was the focus of that study using the Lagrange’s equation of motion to relate the potential and kinetic

energies of the plate structure and surrounding fluid kinetic energy. The study of the effects of imperfections on the vibration of rectangular plates was further extended by Zeng et al. (2016) where a loaded side-cracked plate was studied using the Moving-Least-Square (MLS-Ritz) method. Huang and Lin (2016) also studied the vibration of rectangular plates with a straight-through crack using Fourier cosine series with domain decomposition. Lately, Wang et al. (2017) studied the effects of rectangular openings on the vibration characteristics of rectangular plates in order to establish a methodology for noise reduction and vibration control in thin-walled structures with openings using Fourier series.

It has to be mentioned that the concept of *nonlinear vibration of plates* that includes the response of plates to periodic loading with large amplitudes is out of the scope of this paper. This paper mainly focuses on the free vibration and fundamental frequencies of rectangular steel plates with various aspect ratios and the effects of large deformations caused by static lateral pressure on those frequencies.

5.3 Theoretical Background, FE Modelling, and Verification

The earliest attempts on the vibration analysis of rectangular plates in presence of in-plane (membrane and shear) forces were made by Dawe (1969) and followed by alternative solutions including numerical methods by Mei and Yang (1972), Dickinson (1973) and Bassily and Dickinson, (1973). Chan and Foo (1979) were amongst the first to apply the *Finite Strip method* to solve the case of rectangular plate vibration with membrane forces.

The general equation of motion for a rectangular plate under lateral and in-plane loading is presented in Eq. 5.1.

$$D \left[\frac{\partial^2 w}{\partial x^2} + \frac{\partial^2 w}{\partial y^2} \right]^2 + ch\dot{w} + \rho h\ddot{w} = f + q + N_x \frac{\partial^2 w}{\partial x^2} + N_y \frac{\partial^2 w}{\partial y^2} + 2N_{xy} \frac{\partial^2 w}{\partial x \partial y} \text{ (Eq. 5.1)}$$

In which D is the flexural rigidity of the plate calculated as $D=Eh^3/12(1-\nu^2)$, c is the viscous damping, ρ is the mass density per unit volume of plate material, h is the plate thickness and $w(x, y, t)$ is the dynamic displacement at any given point of plate surface at specific time (t). The first and second derivatives of w with respect to t (i.e., \dot{w} and \ddot{w}) represent the velocity and acceleration at a specific time. On the right side of Eq. 5.1, f is the external excitation as a function of time, q

is the lateral pressure applied at the plate surface while N_x , N_y are the membrane forces distributed along the edges of plate and N_{xy} is the in-plane shear force, respectively.

The simplest form of plate vibration analysis represents the free vibration of unloaded rectangular plates with negligible damping. In this case, the forcing terms at the right side and the viscous damping term at the left side of Eq. 5.1 are set to zero and Eq. 5.1 reduces into Eq. 5.2.

$$D \left[\frac{\partial^2 w}{\partial x^2} + \frac{\partial^2 w}{\partial y^2} \right]^2 + \rho h \ddot{w} = 0 \quad (\text{Eq. 5.2})$$

There is an infinite number of natural frequencies (and mode shapes) available from the closed form or numerical solutions to Eq. 5.2 for various boundary conditions of rectangular plates (Amabili, 2008). As an example, the closed form solution to Eq. 5.2 for rectangular plates with all edges simply supported could be presented as Eq. 5.3.

$$\omega_{m,n} = \pi^2 \left[\left(\frac{m}{L} \right)^2 + \left(\frac{n}{B} \right)^2 \right] \sqrt{D/\rho h} \quad (\text{Eq. 5.3})$$

In which m and n indicate the number of wave fronts along the length (L) and breadth (B) of the rectangular plate for any particular mode shape with natural frequency $\omega_{m,n}$. Amabili (2008) verified the natural frequencies of 15 modes of vibration resulted from Eq. 5.3 experimentally for the case of a rectangular aluminium plate.

In another case, the free vibration of rectangular plates with negligible damping in presence of membrane forces was studied by Singh and Dey (1990) using the energy method. They discretized the total energy of free vibration of the system by replacing the derivative terms with their Finite Difference equivalents and used a specific energy minimization technique to solve the resulting eigenvalue problem. One step further into the case of rectangular plate vibration with membrane forces, Leissa and Kang (2002) presented one of the first exact solutions for the case of vibration and buckling of rectangular plates with a particular set of boundary conditions in which two opposite edges of the plate were clamped and the two other edges were simply supported. A linearly variable in-plane load was considered to act at the simply supported edges (Leissa and Kang, 2002). A similar case was presented by Wang et al. (2006) that simplified Eq. 4.1 into the form presented in Eq. 5.4 for the case of free vibration of rectangular plates with membrane forces acting at opposite edges along x axis (Wang et al., 2006).

$$D \left[\frac{\partial^2 w}{\partial x^2} + \frac{\partial^2 w}{\partial y^2} \right]^2 + \rho h \ddot{w} = N_x \frac{\partial^2 w}{\partial x^2} \quad (\text{Eq. 5.4})$$

Wang et al. (2006) used the differential quadrature method to solve this equation and calculated the vibration frequency for six mode shapes of the rectangular plate ($m=1$ to 3 , $n=1$ and 2). They estimated the $w(x,y,t)$ function by $w(x,y)\sin(\omega t)$ and presented the in-plane force N_x with a linear function. More recently, Akhavan et al. (2009) studied a similar case where closed-form solutions for the free vibration analysis of Mindlin plates with uniform and linearly distributed in-plane loading at two opposite edges with simply supported boundary conditions were given for different configurations of boundary conditions at the opposite edges while the plate is resting on elastic foundation. As seen in the previous section, closed-form solutions are mainly available in the literature for simple structural assemblies with basic boundary conditions and loading schemes. On the other hand, numerical approaches give acceptable approximations of the vibrational behaviour of more complex systems. The Finite Element method approximates the flexural vibration of plates by dividing the plate into a mesh of two-dimensional finite elements (i.e. plate elements) in rectangular, triangular or quadrilateral shapes (Petyt, 2010).

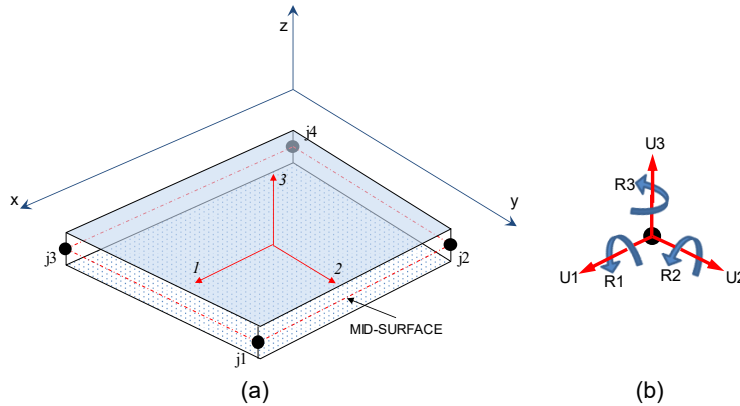


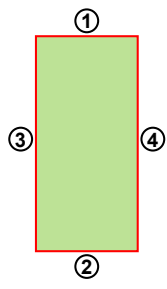
Fig. 5.1: (a) General view of the nodes, surfaces, global and local coordinates of the shell element (b) Local degrees of freedom at a given joint

The element used for the FE Modelling in this paper is the *generalized shell* (Wilson, 2016) with four joints as shown in Fig. 5.1. The shell stiffness formulation is based on a four-point numerical integration where stiffness components are calculated for six degrees of freedom (DOFs) namely U1, U2, U3, R1, R2 and R3 at each node (Powell, 2010). The internal forces of the element are evaluated at the 2-by-2 Gauss integration points and extrapolated to the element joints (Wilson, 2016). The term “generalized shell” is used for this element because it could be

reduced into *plate* (i.e. pure bending) behaviour with only the U3, R1 and R2 DOFs at each node, or *membrane* (i.e. no bending) behaviour with stiffness components only at U1, U2 and R3 accordingly (Wilson, 2016). Regarding the transverse shearing deformations, there are two available options for the generalized shell element namely the *thick-shell* and the *thin-shell* where the element formulations include those deformations in the analysis in the former case based on Reissner-Mindlin plate theory (Reissner, 1945) (Mindlin, 1951) and neglecting them in the latter case based on Kirchhoff-Love plate theory (Love, 1888). Although shearing deformations tend not to affect the overall plate deflections considerably when the plate thickness is less than a decimal fraction of its dimensions, the developer of the generalized shell element (Wilson, 2016) recommends using the thick-plate option for the FE analysis even for the case of thin-plate bending problems. The main issue involved with the Modelling of relatively thin plates in FE analysis is the shear locking. There are several techniques in the literature to reduce or remove this phenomenon including the Reduced Integration method (Hughes et al., 1978), the Discrete Shear Gap (DSG) method (Bletzinger et al., 2000), the Isogeometric analysis (Hughes et al., 2005), the hierarchic family of isogeometric shells (Echter et al., 2013) and the Modified Mindlin plate theory (Senjanovic et al., 2014). The generalized shell element in this paper is a locking-free element, which has been verified for the more complex case of orthotropic thin-walled beams by Minghini et al. (2007).

The geometric nonlinearities (i.e., large displacement effects) are included in the analysis for the static step-by-step procedure in which the equilibrium equations are updated in the deformed configuration of the structure at the end of each step. Large displacements and rotations are accounted for but strains are assumed to be small. The position of each element is tracked during the analysis using an updated Lagrangian formulation (Wilson, 2016).

Table 5.1. Various boundary conditions combinations for a panel of industrial duct walls



Boundary Condition Combination	Edge Number			
	1	2	3	4
CC	Clamped	Clamped	Clamped	Clamped
CS	Clamped	Clamped	Simple	Simple
SS	Simple	Simple	Simple	Simple
SC	Simple	Simple	Clamped	Clamped

This paper considers four combinations of boundary conditions for the case of rectangular plates. These combinations are addressed as *SS*, *SC*, *CS* and *CC* as shown in Table 5.1.

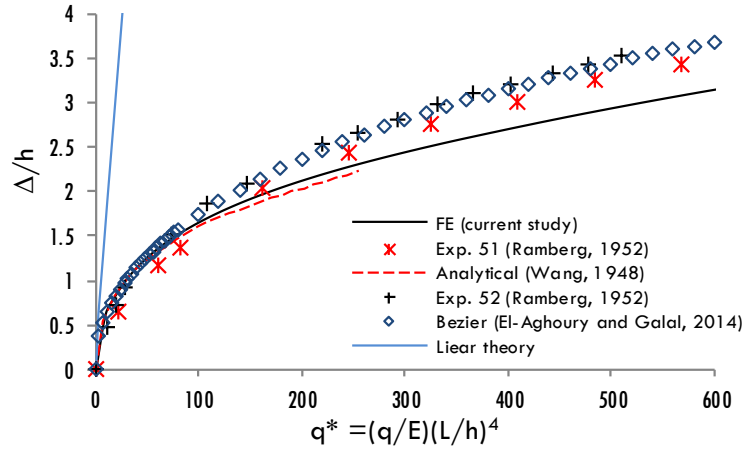


Fig. 5.2: First stage of the validation study: Comparison of the results of FE analysis (current work) with available literature for the nonlinear load-deformation of rectangular plates under lateral uniform pressure

There are three stages of verification of the FE analysis in this paper. In the first stage, as shown in Fig. 5.2, the load-displacement curves resulted from FE static analysis are compared to the results of two experimental tests by Ramberg (1952), one analytical solution by Wang (1948) and one numerical solution by El-Aghoury and Galal (2014). It is seen in the chart (Fig. 5.2) that the FE analysis is in a very good correlation with the experimental and analytical data in the literature.

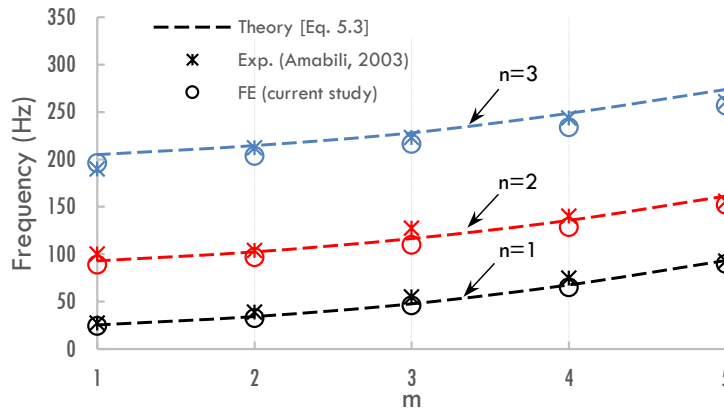


Fig. 5.3: Second stage of the validation study: Comparison of the FE results (current work) with the natural frequencies of 15 modes of vibration of the plate tested by Amabili (2008) and their reported analytical results

In the second stage, as shown in Fig. 5.3, the natural frequencies calculated by the FE modal analysis for the case of a rectangular plate are verified against the experimental data and the closed-

form solution to Eq. 5.3 by Amabili (2008). The results of FE analysis show an excellent correlation with the experimental and analytical results in the literature.

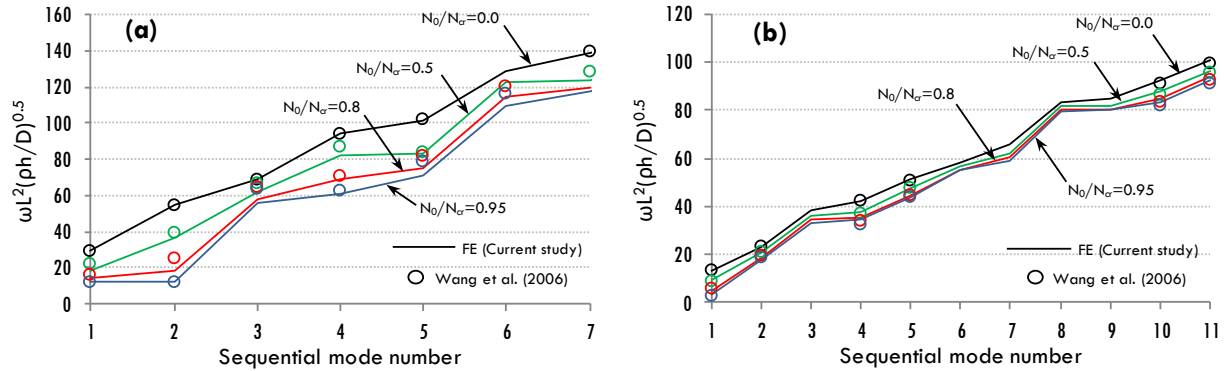


Fig. 5.4: Third stage of the validation study: Non-dimensional frequency $[\omega L^2(\rho h/D)^{0.5}]$ of rectangular SC plates with uniaxial membrane force resulted from FE analysis (current work) against the analytical results of Wang et al. (2006) (a) Plate aspect ratio: 1.0 (b) Plate aspect ratio: 0.5

In the third stage, as shown in Fig. 5.4, the vibration frequencies of two rectangular plates with different aspect ratios at four different levels of membrane forces are verified against the analytical results of Wang et al. (2006). Those four membrane force levels represent 0%, 50%, 80% and 95% of the plate critical buckling load. For the first plate with aspect ratio 1.0 (Fig. 5.4-a), the vibration frequencies of seven modes are reported by Wang et al. (2006) and for the second plate with aspect ratio 0.5 (Fig. 5.4-b), there are six modes reported by Wang et al. (2006). The FE analysis was able to capture all of the reported modes with very good correlation. As seen in the charts, an excellent correlation between the results of FE analysis and the existing experimental, analytical and numerical results from the literature has been achieved for all the three stages of verification.

5.4 Free vibration of Rectangular Plates at Rest

This section presents the modal analysis of rectangular plates at rest i.e., no loads are applied to the plate. To uncouple the analysis results from the plate dimensions, the *non-dimensional frequency parameter* (ω^*) which is used frequently in the literature is adopted here as shown in Eq. 5.5.

$$\omega^* = \omega(L/\pi)^2 \sqrt{\rho h/D} \quad (\text{Eq. 5.5})$$

As mentioned before, several works in the literature address the calculation of vibration frequencies of rectangular plates in various pre-defined mode shapes. Although the pre-defined mode shapes are limited by nature, some of the available closed-form solutions tend to calculate the vibration frequency for any given mode (see Eq. 5.3). On the other hand, numerical techniques such as Finite Element method, allow for the calculation of vibration frequencies for unlimited sequential modes by implementing verified methods such as Eigen and Ritz analysis (Wilson, 2016). As an example, the non-dimensional frequency parameter (ω^*) that is associated with the first 20 modes of free vibration of rectangular plates with 2 different boundary conditions (CC and SS) and 3 different aspect ratios (S=1, S=2 and S=4) are shown in Fig. 5.5.

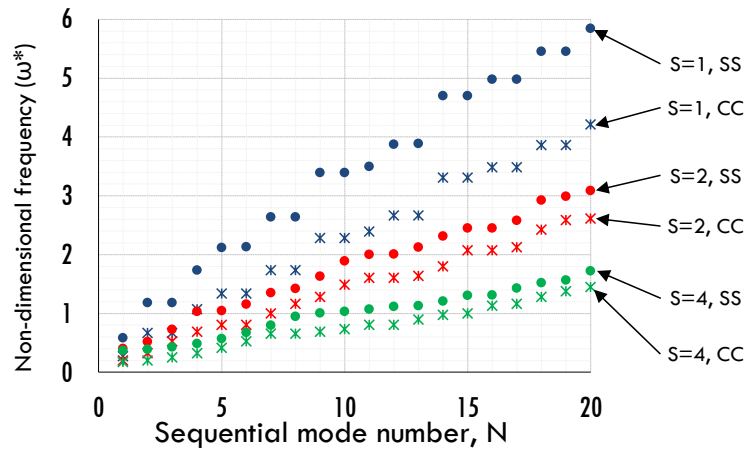


Fig. 5.5: Non-dimensional frequencies associated with the first 20 modes of vibration for simply-supported (SS) and clamped (CC) rectangular plates with aspect ratios S=1.0, S=2.0 and S=4.0

5.4.1 Structurally significant modes

Each of the four nodes of the rectangular plate element in the FE models of this paper involves six DOFs (i.e., translation in and rotation about the global Cartesian axes X, Y and Z). Assuming the uniform distribution of the plate mass over these nodes, the nodal mass participation at each node for every individual vibration mode is determined as a result of the modal analysis. The overall mass participation of the plate at each DOF is then calculated as the summation of all individual nodal mass participations. As an example, the mass participation ratios of the first 20 modes of vibration of the rectangular plate with aspect ratio S=2.0 and SS boundary conditions (see Fig. 5.5 for the frequencies) are shown in Table 5.2.

As seen in the table, the overall mass participation is zero for the three in-plane DOFs i.e., U(X), U(Y) and R(Z). This phenomenon is easily understandable considering the plate geometry and boundary conditions. As for the main DOFs i.e., U(Z), R(X) and R(Y), it is seen in Table 5.2 that the cumulative mass participation ratio reaches 0.884, 0.761 and 0.784 respectively with the consideration of 20 modes.

Table 5.2. Modal mass participation ratios at the six DOFs for the rectangular plate with aspect ratio $S=2.0$ and SS boundary conditions

MODE	ω^*	MODAL MASS PARTICIPATION RATIO					
		UX	UY	UZ	RX	RY	RZ
1	0.20	0	0	0.682	0	0	0
2	0.32	0	0	0	0	0.524	0
3	0.52	0	0	0.076	0	0	0
4	0.68	0	0	0	0.537	0	0
5	0.80	0	0	0	0	0	0
6	0.80	0	0	0	0	0.131	0
7	1.00	0	0	0	0.059	0	0
8	1.16	0	0	0.027	0	0	0
9	1.27	0	0	0	0	0	0
10	1.48	0	0	0.075	0	0	0
11	1.59	0	0	0	0	0.115	0
12	1.59	0	0	0	0	0.004	0
13	1.63	0	0	0	0.021	0	0
14	1.79	0	0	0.008	0	0	0
15	2.07	0	0	0	0	0.014	0
16	2.07	0	0	0	0	0	0
17	2.11	0	0	0.014	0	0	0
18	2.42	0	0	0.003	0	0	0
19	2.58	0	0	0	0.011	0	0
20	2.59	0	0	0	0	0	0
TOTAL:		0	0	0.884	0.761	0.784	0

In order to better visualize these mode shapes and their mass participations, they are displayed schematically in Fig. 5.6. It is obvious that higher cumulative mass participations are achievable by considering greater number of modes but it should also be noted that individual modes with great mass participations are already achieved in the three *significant* DOFs. In this case, they are mode 1 for U(Z), mode 2 for R(Y) and mode 4 for R(X) with mass participation ratios of 0.682,

0.524 and 0.537, respectively. Similar outcomes for the mass participation ratios are obtained for the other boundary conditions combinations and aspect ratios. In all cases, the first two sequential modes correspond to the highest mass participation for U(Z) and R(Y) respectively. On the other hand, the third significant mode i.e., the mode with the highest mass participation along R(X) does not necessarily correspond to the third sequential mode. These three mode shapes are considered as the “*significant modes*” and will be the topic of the upcoming parametric studies in this paper.

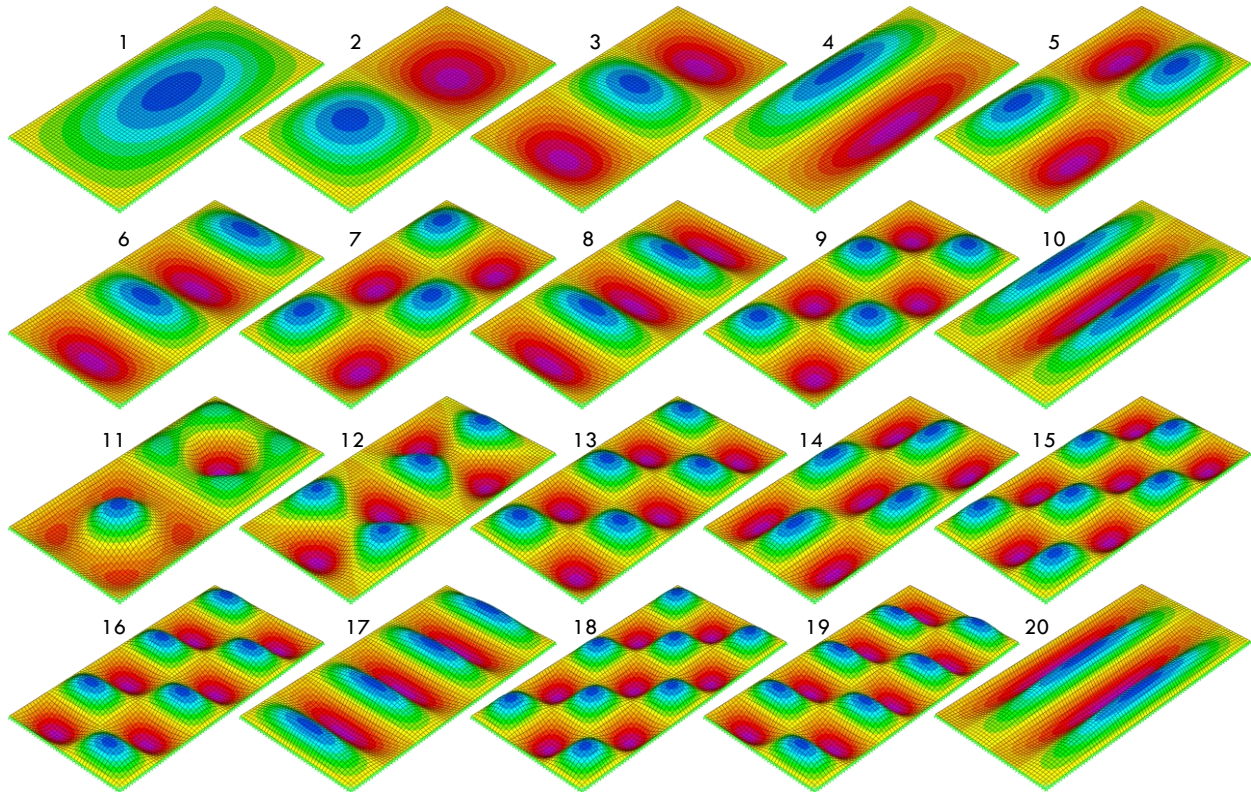


Fig. 5.6: Visual display of the first 20 modes of vibration for a rectangular plate with aspect ratio $S=2.0$ and SS boundary conditions

5.4.2 Vibration frequencies of significant modes for rectangular plates at rest

The frequency parameters of rectangular plates with various aspect ratios between 1.0 and 4.0 are shown in Fig. 5.7 and Table 5.3 for the three significant modes of vibration. Based on these charts, it is observed that although an increase in the plate aspect ratio tends to lower the fundamental frequencies, this effect diminishes as the aspect ratio reaches higher values. It is also seen in the charts of Fig. 5.7 that the plate aspect ratio has a greater effect on the 2nd significant frequency than those of the other two modes.

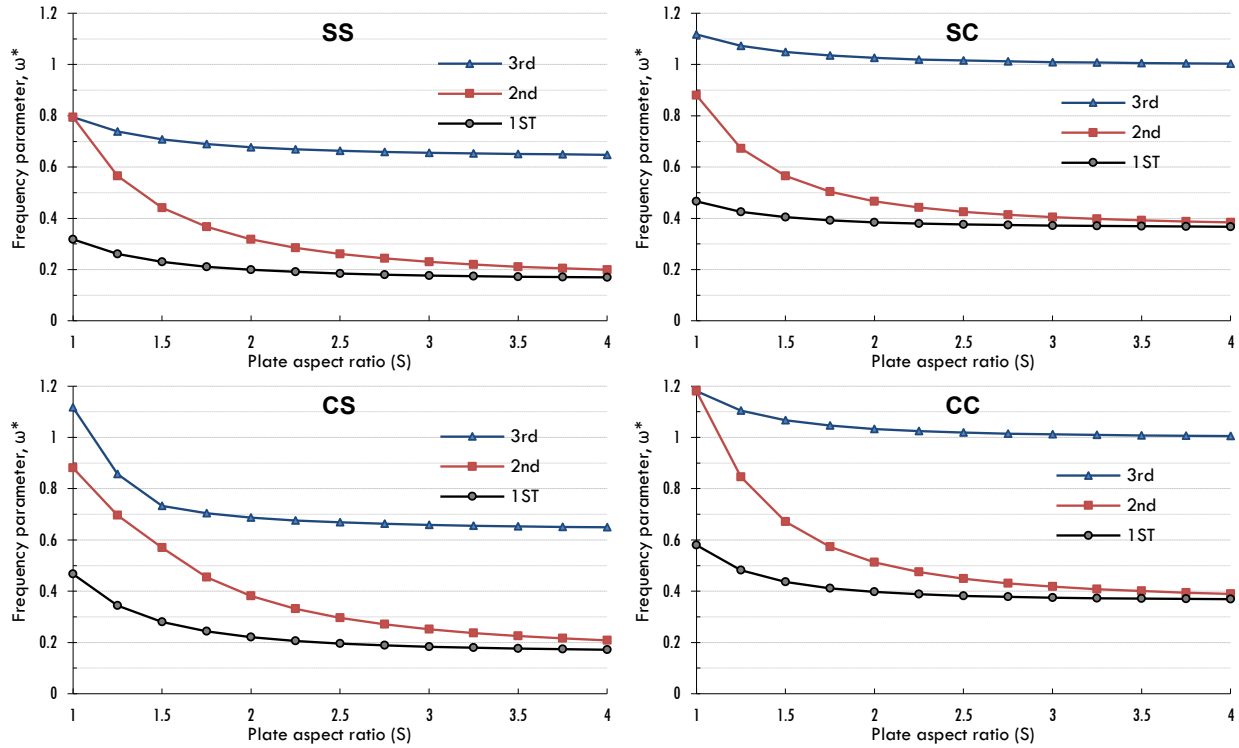


Fig. 5.7: Frequency parameter associated with the three significant modes for rectangular plates with various boundary conditions and aspect ratios

Table 5.3. Values of ω^* associated with the three significant modes for rectangular plates with various boundary conditions and aspect ratios

ASPECT RATIO (S)	SS			SC			CS			CC		
	1 ST	2 nd	3 rd	1 ST	2 nd	3 rd	1 ST	2 nd	3 rd	1 ST	2 nd	3 rd
1	0.3181	0.7946	0.7946	0.4668	0.8805	1.1172	0.4667	0.8805	1.1171	0.5797	1.1814	1.1814
1.25	0.2610	0.5659	0.7383	0.4253	0.6724	1.0729	0.3441	0.6958	0.8564	0.4819	0.8452	1.1044
1.5	0.2300	0.4417	0.7077	0.4043	0.5654	1.0492	0.2803	0.5696	0.7326	0.4357	0.6715	1.0669
1.75	0.2113	0.3668	0.6893	0.3922	0.5044	1.0351	0.2436	0.4549	0.7047	0.4112	0.5729	1.0459
2	0.1992	0.3182	0.6773	0.3847	0.4668	1.0260	0.2209	0.3813	0.6875	0.3969	0.5129	1.0331
2.25	0.1909	0.2849	0.6691	0.3796	0.4422	1.0198	0.2061	0.3314	0.6762	0.3879	0.4744	1.0247
2.5	0.1849	0.2611	0.6632	0.3761	0.4253	1.0154	0.1960	0.2962	0.6683	0.3820	0.4486	1.0189
2.75	0.1805	0.2435	0.6589	0.3735	0.4133	1.0121	0.1888	0.2706	0.6627	0.3778	0.4305	1.0147
3	0.1772	0.2301	0.6556	0.3716	0.4043	1.0096	0.1835	0.2514	0.6585	0.3748	0.4174	1.0116
3.25	0.1746	0.2196	0.6530	0.3701	0.3975	1.0077	0.1795	0.2367	0.6553	0.3726	0.4077	1.0093
3.5	0.1725	0.2114	0.6510	0.3689	0.3923	1.0062	0.1764	0.2252	0.6528	0.3709	0.4003	1.0074
3.75	0.1708	0.2047	0.6493	0.3679	0.3881	1.0049	0.1740	0.2160	0.6508	0.3695	0.3945	1.0059
4	0.1695	0.1992	0.6480	0.3672	0.3847	1.0039	0.1721	0.2086	0.6492	0.3685	0.3899	1.0047

It should be noted that the values presented in Table 5.3 as the non-dimensional frequency parameters could be used for interpreting a reasonable approximation of ω^* for any plate aspect ratios by using a linear interpolation.

5.5 Free vibration of rectangular plates with uniform lateral pressure and large deformation effects

As discussed earlier in section 5.2, the lateral load and in-plane forces affect the natural frequency of rectangular plates (See Eq. 5.1). Although the effect of directly-applied in-plane forces on the vibration of plates is not studied in this paper, a correlation between the lateral pressure and in-plane forces will be the main parameter in this section.

The classical plate theory establishes the lateral load-displacement behaviour of thin rectangular plates mainly based on the assumption of pure flexural behaviour that follows a linear trend. This assumption along with other less significant assumptions involved with Kirchhoff's plate theory are used widely by the design engineers as the accepted design basis for thin-walled structures. On the other hand, regardless of the boundary conditions, if the maximum deflection of the plate exceeds a certain limit, the linear load-displacement assumption does not reflect the true behaviour (see Fig. 5.2). This deflection limit is defined as a portion of the plate thickness e.g. $\Delta > 0.5t$ (Levy, 1941a), $\Delta > 1.0t$ (Timoshenko and Woinowsky-Kreiger, 1959) (Ugural, 1981) and $\Delta > 0.2t$ (Bakker et al., 2008) where Δ is the maximum deflection at the center of plate as shown in Fig. 5.8.

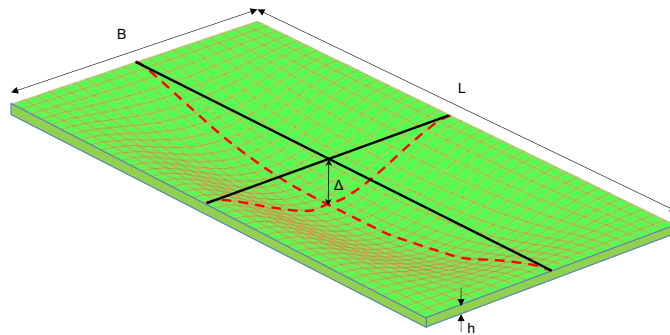


Fig. 5.8: Deformation of a CC rectangular plate under uniform lateral pressure

The nonlinear load-displacement behaviour of thin plates with large deformations is governed by von-Kármán equations (von-Kármán, 1910). One of the main assumptions in von-Kármán equations is that all strain components are small and linear elasticity is applicable to the plate

material. Kirchhoff's plate hypothesis is also applicable to von-Kármán equations indicating that the stresses normal to the middle surface of the plate are negligible and the strains are linearly distributed through the thickness of the plate. The main advantage of von-Kármán equations over the classical plate theory is the consideration of membrane stresses that generate in the plate as a result of large deformations. There are a number of experimental, analytical and numerical works on rectangular plates with geometrical nonlinearities based on von-Kármán equations including Ramberg et al. (1942), Wang (1948), Little (1999), Young and Budynas (2002), El-Aghoury and Galal (2014) and Rezaiefar and Galal (2016) where the load-displacement and load-stress curves for various geometries and boundary conditions were presented.

A sequential analysis method is adopted in this section in order to study the effects of nonlinear load-deformation behaviour on the free vibration properties of rectangular plates. The analysis consists of two stages for a series of uniform lateral pressure values. At the first stage, the uniform lateral pressure is applied to the plate and a nonlinear static large deformation analysis is performed. At the end of this stage, a modal analysis is performed on the plate and the frequencies of the three significant modes are recorded. This procedure is repeated for various lateral pressure values. The results of this analysis are presented in the charts of Fig. 5.9 as the non-dimensional frequency parameter against the unitless pressure $(P/E)(L/h)^4$ for various aspect ratios and boundary conditions combinations.

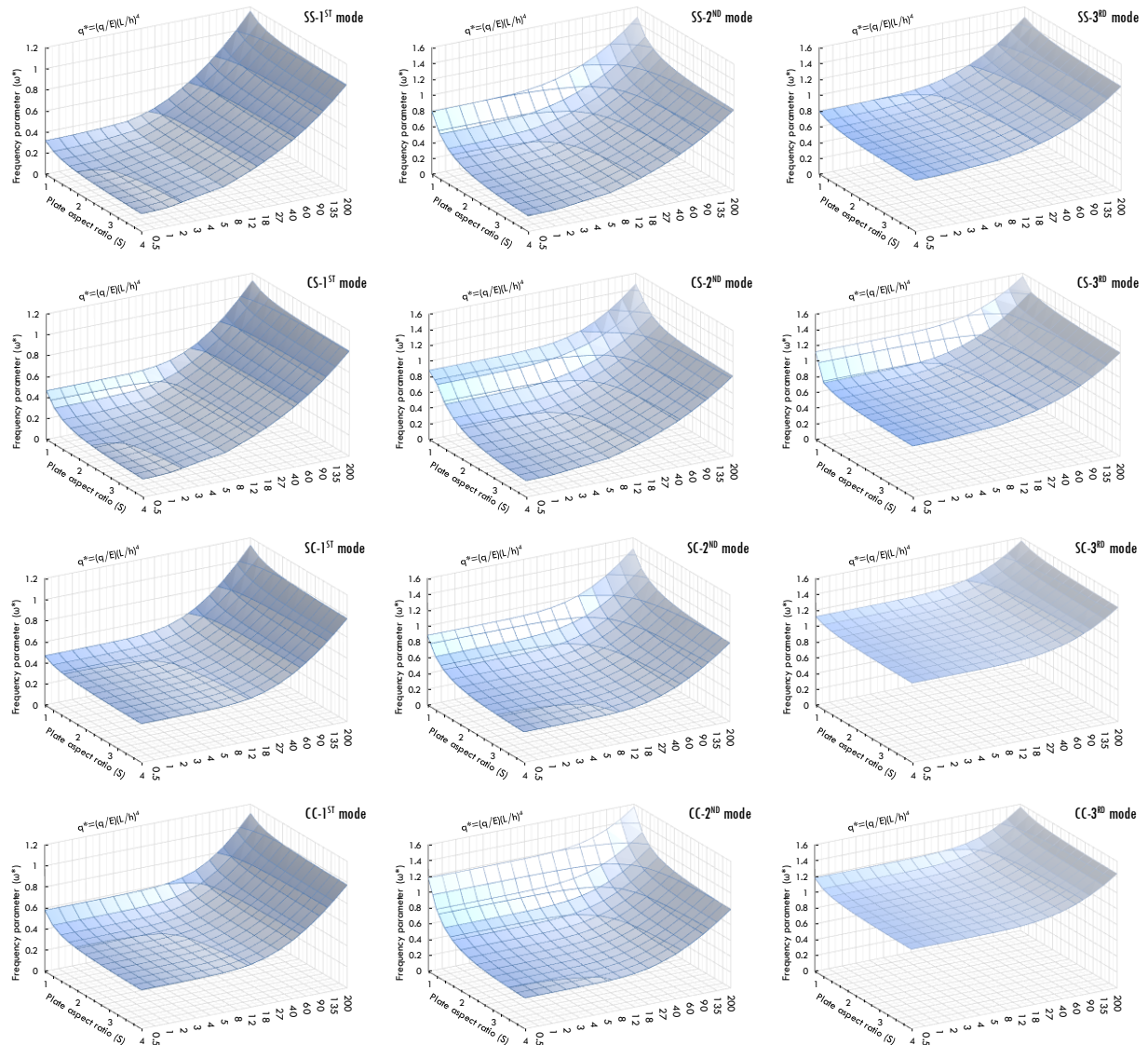


Fig. 5.9: Non-dimensional frequency parameter charts for plates with different boundary conditions and aspect ratios under various non-dimensional pressure (q^*) values

It is seen in the charts of Fig. 5.9 that the vibration frequencies of the three significant modes increase with the applied uniform pressure for all the studied cases. Although the charts presented in Fig. 5.9 could be used directly for specific cases, these charts are converted into more meaningful data by dividing the frequency parameter at each pressure by the value of the frequency parameter at rest (values presented in Table 5.3) and presented in the charts shown in Fig. 5.10.

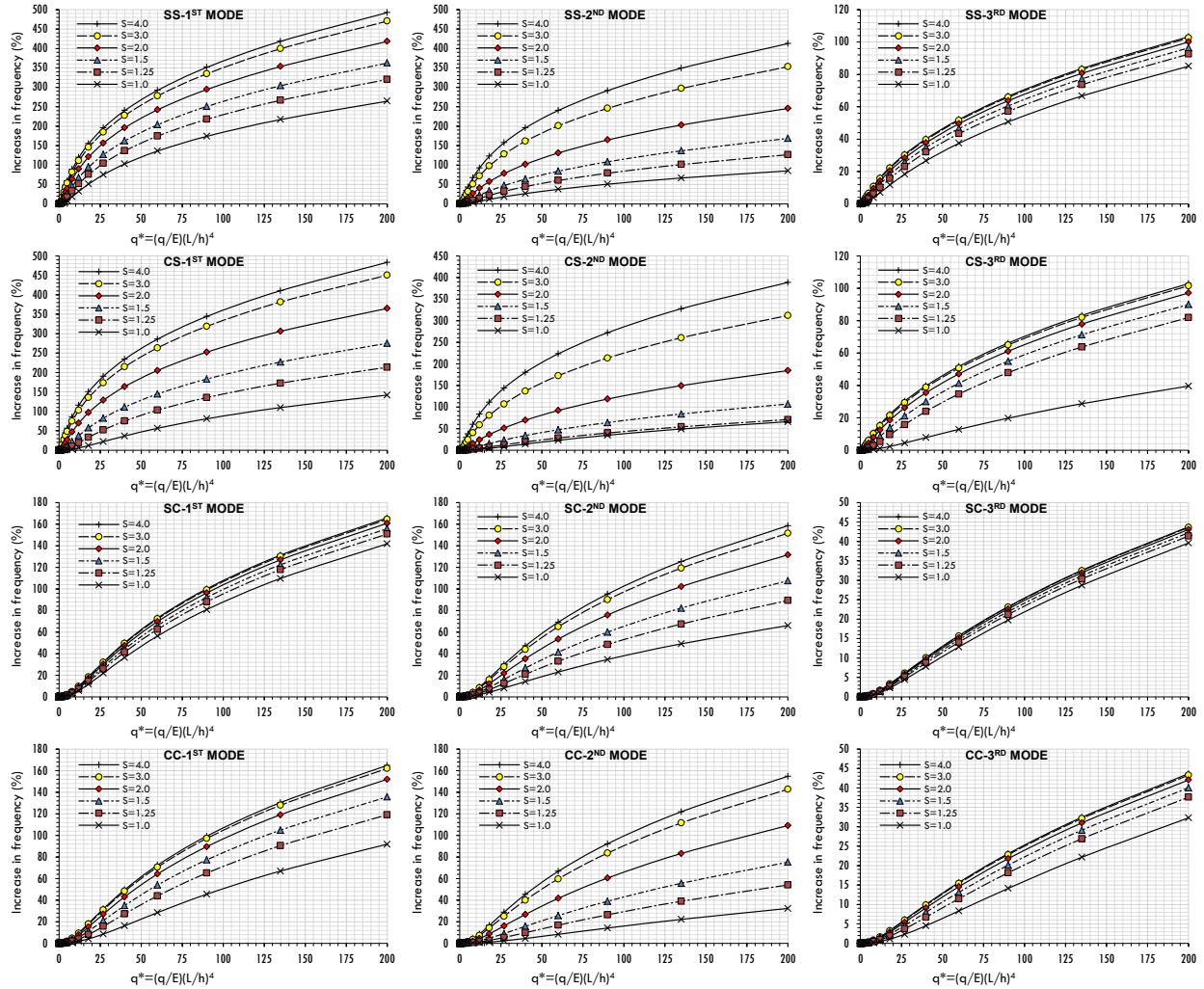


Fig. 5.10: Non-dimensional frequency parameter charts for plates with different boundary conditions and aspect ratios under various uniform lateral loads

5.6 Analysis example

The walls of an industrial duct segment consist of 8 mm steel plates ($F_y=300$ MPa, $E=200000$ MPa, $\nu=0.3$ and $\rho=7850$ kg/m³) with relatively rigid stiffener ribs placed at 1.2 m intervals per the static analysis and design. The duct cross-section is a 3.0×3.0 square with fully welded corners. The internal negative pressure acting on the duct walls is 31.6 kPa. The working and cut-off frequencies of the fan are 90 Hz and 35 Hz, respectively. It is required to verify if the designed duct wall plates will cause resonance with the fan. A resonance margin of $\pm 20\%$ is to be considered for the study.

Solution:

Based on the problem definitions, each individual wall panel is a 3000×1200×8 mm rectangular plate. The stiffened plate with fully welded duct corners suggests the CCSS boundary conditions.

$$\begin{aligned} \text{Plate aspect ratio:} \quad S &= 3000/1200 = 2.5 \\ \text{Plate flexural rigidity:} \quad D &= Eh^3/12(1-\nu^2) = 9.377 \quad \text{kN.m} \\ & \quad (L/\pi)^2 \times (\rho h/D)^{0.5} = 0.0121 \end{aligned}$$

The cut-off frequency of the fan corresponds to zero pressure on the walls thus, it is compared to the significant natural frequencies at rest based on the values from Table 5.3 as following:

$$\begin{aligned} \omega^*(1^{\text{st}} \text{ mode}) &= 0.196 \quad \text{Thus: } \omega_1 = 0.196/0.0121 = 16.2 \text{ Hz} \\ \omega^*(2^{\text{nd}} \text{ mode}) &= 0.2962 \quad \text{Thus: } \omega_2 = 0.2962/0.0121 = 24.5 \text{ Hz} \\ \omega^*(3^{\text{rd}} \text{ mode}) &= 0.6683 \quad \text{Thus: } \omega_3 = 0.6683/0.0121 = 55.3 \text{ Hz} \end{aligned}$$

The problem requires the verification of fan frequencies with ±20% margins:

$$\begin{aligned} \text{Working frequency:} \quad \text{Lower limit: } 90-20\% &= 72.0 \text{ Hz} \\ & \quad \text{Upper limit: } 90+20\% = 108.0 \text{ Hz} \\ \text{Cut-off frequency:} \quad \text{Lower limit: } 35-20\% &= 28.0 \text{ Hz} \\ & \quad \text{Upper limit: } 35+20\% = 42.0 \text{ Hz} \end{aligned}$$

It is seen that none of the three significant natural frequencies of the plate at rest falls within the 20% margins of the cut-off frequency of the fan.

At working conditions, the fan produces a uniform pressure of 31.6 kPa (0.0316 MPa) on the wall, thus:

$$\text{Unitless pressure:} \quad (P/E)(L/h)^4 = (0.0316/2e5)(1200/8)^4 = 79.99 \approx 80.0$$

Using the charts from Fig. 5.10 to obtain the increase in frequencies as shown in Fig. 5.11, the frequencies at the 1st, 2nd and 3rd significant modes should be increased by 270%, 155% and 59% respectively to account for the working condition of the duct walls:

$$\begin{aligned} \omega_{1(\text{work})} &= 16.2+270\% = 59.9 \text{ Hz} \\ \omega_{2(\text{work})} &= 24.5+155\% = 62.5 \text{ Hz} \\ \omega_{3(\text{work})} &= 55.3+59\% = 87.9 \text{ Hz} \end{aligned}$$

It is seen that the 3rd significant natural frequency of the plate falls within the 20% margins of the working frequency of the fan (i.e. 72.0 < 87.9 < 108.0). This indicates that the plate is prone to resonance with the fan at working conditions.

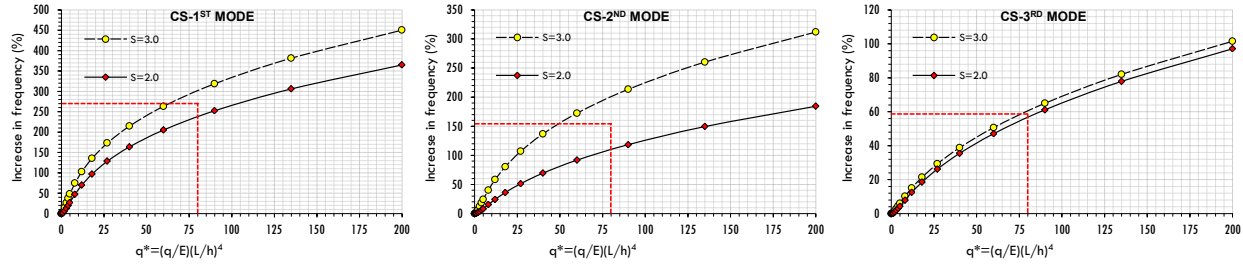


Fig. 5.11: Application of the pressure-frequency charts in an example

In order to verify these results, the plate in the example is also modeled using FE analysis. The frequencies at rest and at the given pressure (31.6 kPa) are listed in Table 5.4 along with their difference in percentage. It is seen that the results obtained from the proposed method in this paper are in excellent correlation with the results obtained from the FE analysis.

Table 5.4. Frequencies resulted from the method in this paper and case-specific FE analysis

	P= 0.0 (rest)			P= 31.6 kPa		
	1 ST	2 ND	3 RD	1 ST	2 ND	3 RD
Proposed method in this paper	16.2	24.5	55.3	59.9	62.5	87.9
FE analysis	16.37	24.76	55.83	61.88	64.33	88.97
Discrepancy (%) [†]	1.05	1.06	0.96	3.3	2.93	1.22

$$†: \text{Discrepancy} = 100 \times (\omega_{FE} - \omega) / \omega$$

5.7 Concluding remarks

This paper presented the case of free vibration of rectangular plates with and without lateral pressure. It was shown that although an unlimited number of mode shapes could be considered for the vibration analysis of rectangular plates, there are only three modes with structural significance that need to be considered in the structural design. These three modes are:

- 1- The mode shapes with one curvature along the breadth and length of the plate.
- 2- The mode shape with one curvature along the breadth and two curvatures along the length of the plate.
- 3- The mode shape with two curvatures along the breadth and one curvature along the length of the plate.

Non-dimensional vibration frequencies for these three significant modes were provided for four boundary conditions combinations and varying aspect ratios from 1.0 to 4.0. The frequency of

vibration for any rectangular plate could be easily calculated by using these non-dimensional frequencies.

The effects of lateral pressure on the vibration frequencies of rectangular plates were studied in the last section of this paper based on the concept of large displacement analysis. It was demonstrated that for rectangular plates with various aspect ratios and boundary conditions combinations, the vibration frequencies increase significantly (up to 450%) with the lateral pressure. The charts and tables given in this paper for the vibration frequencies are all non-dimensional. Thus, they could be used for specific cases of rectangular panel plate design regardless of plate material, thickness and aspect ratios.

This work could be continued into the nonlinear vibration domain by studying the vibration interactions and the influence of loading frequencies on the dynamic response of the plate.

CHAPTER 6

SUMMARY, CONCLUSIONS, LIMITATIONS AND RECOMMENDATIONS FOR FUTURE WORKS

6.1 Summary

The purpose of this study was to evaluate the current methods for the structural design of the stiffened plates of the walls of industrial ducts and similar structures and seek potential improvement to them by taking into consideration the effects of large displacements in the analysis.

In Chapter 3, two sets of empirical design equations were provided using verified numerical analysis of multi-span plates with internal line supports under uniform lateral pressure that take into account the effects of large deformations nonlinearities. These equations stand for the design of plate length and thickness by applying stress and displacement criteria to the plate structure.

In Chapter 4, the case of stiffened plates with parallel ribs under lateral uniform pressure was discussed. The main purpose of this chapter was to compare the linear beam equations which are adopted for the stiffened plate conventionally by the engineers in the form of an Equivalent Beam Analogy (EBA) and the advanced FE analysis using shell elements for the plate and stiffener. The FE analysis was divided into two main categories of Small Displacement Analysis (SDA), and Large Displacement Analysis (LDA). The stress distribution in the panel plate was reviewed in both SDA and LDA in order to verify the potential failure modes and the points at which plastic behaviour could be expected. This chapter contained a total of 16 FE models, all of which had the same stiffener geometry and panel plate thickness, and subjected to either positive, or negative uniform pressure over the panel plate. The main geometrical variable was the panel plate width, for which a total of 6 different B/t ratios were studied. Two main cases of clamped, and simply-supported end boundary conditions were considered in the FE models and analysis.

In Chapter 5, the case of free vibration of rectangular plates with and without lateral pressure was discussed. It was shown that although an unlimited number of mode shapes could be considered for the vibration analysis of rectangular plates, there are only three modes with

structural significance that need to be considered in the structural design. Non-dimensional vibration frequencies for those three significant modes were provided for four boundary conditions combinations and varying aspect ratios from 1.0 to 4.0. The effects of lateral pressure on the vibration frequencies of rectangular plates were studied in the last section of Chapter 5 based on the concept of large displacement analysis.

6.2 Concluding Remarks

The following conclusions are derived from the studies conducted in this study:

- The assumptions involved in the design of panel plates of the walls of rectangular ducts are often not correct. The edge panels and the typical panels in such assemblies have different boundary conditions.
- A duct wall plate designed by the LDA, if used appropriately in conjunction with well-defined limit states, will be up to 40% more economical compared to the conventionally designed plates that use the linear beam theory.
- The linear beam theory does not correctly represent the actual behaviour of the stiffened plate for the internal stresses in the panel plate. Moreover, the load-displacement estimation provided based on the EBA does not correspond with the actual behaviour of the stiffened plate.
- The internal forces and stresses in the panel plate are not correctly calculated in the SDA as the membrane forces are neglected. Thus, the load-displacement behaviour is not correctly estimated by the FE analysis if the SDA is applied.
- The most accurate method for the FE analysis of stiffened plate is the LDA, in which the contributions of the panel plate and the rib stiffener are calculated based on the combination of internal flexural and membrane stresses.
- The load-displacement behaviour of the stiffened plate is not independent of the nature of the applied uniform pressure. Different load-displacement charts are obtained for the same stiffened plate model under positive and negative uniform pressures.
- The end boundary conditions have a significant effect on the load-displacement of the stiffened plates. However, the stiffened plate does not follow the classical beam theory

in which the simply-supported beam has a five times greater displacement under the same uniform load than the clamped beam.

- The ultimate design loads and displacements achieved from the LDA are mainly different from those obtained from the linear beam theory with the EBA.
- In the case of clamped ends, the LDA results in greater ultimate loads and displacements under both negative and positive pressures compared to the linear beam theory using the EBA.
- In the case of simply-supported ends, the LDA results in smaller maximum displacements than the linear beam theory using the EBA, while the ultimate loads resulting from the LDA under positive pressure are greater than the EBA within the same range as the EBA under negative pressure.
- The frequency of vibration for any rectangular plate could be easily calculated by using empirical non-dimensional frequencies provided in Chapter 5.
- For rectangular plates with various aspect ratios and boundary conditions combinations, the vibration frequencies increase significantly (up to 450%) with the lateral pressure if the LDA is applied.
- The calculation of the modal frequencies of rectangular duct walls without the consideration of the LDA effects is irrelevant and misleading.

6.3 Limitations

The studies in this thesis were entirely on the basis of numerical analysis and FE modelling. Although some experimental results from the literature were utilized in order to evaluate the modelling procedure, meshing, elements, boundary conditions, and analysis settings, the need for case-specific experimental tests on the studied topics was undeniable during the work. The numerical work was focusing on the Ultimate Limit States concept for the structural design of the stiffened plates. Thus, the thermal behaviour was not within the scope of the studies.

In Chapter 3, the goal was to involve the effects of geometrical nonlinearities in the overall behaviour of the duct wall panel plates in order to establish grounds for a more economical design procedure based on the LDA. The experimental research that was used as the reference for the

validation of the FE analysis in that chapter were from six decades ago while the boundary conditions in those tests were different from what was then associated with the case of the walls of rectangular ducts. Despite the fact that those differences in the boundary conditions became the main distinguishing factor at the end, the authors could have achieved more realistic results if an experimental program was designed and performed accordingly in parallel. Moreover, the thermal behaviour of the plates should be studied in a different work in which the temperature gradients as well as thermal expansion of the panels are the main topics.

In Chapter 4, the shortcomings of the existing design analogy that is based upon the linear beam theory for the stiffened plates were demonstrated and explained. Similar to Chapter 3, an experimental testing program would have been greatly beneficial. Moreover, it was not feasible to produce sufficient FE models in order to achieve the required statistical data to establish an empirical design method for the stiffened plate on the basis of LDA without exceeding the space limitations for one journal article in this chapter. The authors believe that such work must be presented in a separate article which is beyond the scope of this thesis.

In Chapter 5, there was a need to extend the numerical analysis for the case of stiffened plates with flexible stiffeners. However, such an extension requires a basis with more simplified boundary conditions which was the topic of the chapter. Moreover, a more realistic loading frequency such as flow-induced vibration in the example at the end of the chapter could have been more beneficial. Unfortunately, such data was not found in the literature by the author at the time of the preparation of Chapter 5. As mentioned in the introductions of the chapter, the concept of nonlinear vibration was out of the scope of the studies.

6.4 Recommendation for Future Works

It is essential that further investigations on more combinations of rib stiffeners and panel plate geometries be done in the future in order to establish a robust empirical design method based on the LDA and key parameters. Such investigations must include other types of rib stiffener profiles, more realistic boundary conditions for case-specific applications, nature of applied loads, and the effects of thermal stresses. This work could also be continued into the nonlinear vibration domain by studying the vibration interactions and the influence of loading frequencies on the dynamic response of the stiffened plates. In all stages of the work on the stiffened plates of the walls of

industrial ducts, experimental testing shall provide realistic data on which basis, more advanced FE modelling could be developed. The data presented in chapters 3,4 and 5 of this thesis could be used in order to design an experimental test setup for a realistic investigation of the case of rectangular duct walls. Both load-displacement behaviour and the modal frequencies are achievable from such experiments if designed and executed properly.

References

- Akhavan, H., Hosseini Hashemi, Sh., Rokni Damavandi Taher, H., Alibeigloo, A., Vahabi, Sh. (2009). Exact solutions for rectangular Mindlin plates under in-plane loads resting on Pasternak elastic foundation. Part II: Frequency analysis. *Computational Material Science*, 44, 951-961.
- Amabili, M. (2006). Theory and experiments for large-amplitude vibrations of rectangular plates with geometric imperfections. *Journal of Sound and Vibration*, Volume 291, pp. 539-565.
- Amabili, M. (2008). *Nonlinear vibrations and stability of shells and plates*. Cambridge university press, Cambridge.
- ANSYS, I. (2013-a). *ANSYS mechanical APDL theory reference*. (P. Kohnke, Ed.) Canonsburg, PA: SAS IP, Inc. P. 586-587
- ANSYS, I. (2013-b). *ANSYS mechanical APDL element reference*. Canonsburg, PA: SAS IP, Inc. P. 805-820
- AISC. (2003). *Manual of steel construction, load and resistance factor design*. Third edition, American Institute of Steel Construction, Inc.
- ASCE. (1995). *The structural design of air and gas ducts for power stations and industrial boiler applications*. Air and gas duct structural committee of the energy division of the American Society of Civil Engineers (ASCE) Reston, VI.
- Badran, S. F., Saddek, A. B. & Leheta, H. W., 2013. Ultimate strength of Y and T stiffeners subjected to lateral loads with three different levels of initial imperfection. *Elsevier Ocean Engineering*, Volume 61, pp. 12-25.
- Bakker, M. C., Rosmanit, M., and Hofmeyer, H. (2008). Approximate large-deflection analysis of simply supported rectangular plates under transverse loading using plate post-buckling solutions. *Thin-Walled Structures*, 46, 1224-1235.

- Bassily, S. F. and Dickinson, S. M., (1973). Vibration of plates subject to arbitrary inplane loads. Applied Mechanics, Summer Conference, Georgia Institute of Technology, Atlanta, Georgia.
- Bedair, O., 2009. Analysis and Limit State Design of Stiffened Plates and Shells: A World View. ASME Applied Mechanics Reviews, 62(2), pp. 20801.1-20801.16.
- Bezier, P. (1972). Numerical control: mathematics and applications. New York: Wiley.
- Bletzinger, K., Bischoff, M., Ramm, E. (2000). A unified approach for shear-locking-free triangular and rectangular shell finite elements. Computers and Structures, 75, 321-334
- Blodgett, O. W., 1966. Design of Welded Structures. James F. Lincoln arc welding Foundation.
- Brubak, L., Andersen, H. and Hellesland, J., 2013. Ultimate strength prediction by semi-analytical analysis of stiffened plates with various boundary conditions. Elsevier Thin-Walled Structures, Volume 62, pp. 28-36.
- Brubak L, and Hellesland J., (2007-a). Semi-analytical buckling strength analysis of plates with arbitrary stiffener arrangements. Journal of Constructional Steel Research, Volume 63, pp. 532-543.
- Brubak L, and Hellesland J., (2007-b). Semi-analytical postbuckling and strength analysis of arbitrarily stiffened plates in local and global bending. Thin-Walled Structures, Volume 45, pp.. 6210-633.
- Brubak L, and Hellesland J., (2007-c). Computational postbuckling and strength analysis of arbitrarily stiffened plates in local and global bending. Thin-Walled Structures, Volume 45(6), pp. 620–33.
- Brubak, L. and Hellesland, J., (2008). Strength criteria in semi-analytical, large deflection analysis of stiffened plates in local and global bending. Elsevier Thin-Walled Structures, Volume 46, pp. 1382-1390.
- Canadian Standards Association, (2016). CSA Standard S16-10 Design of Steel Structures. Mississauga, ON: Canadian Standard Association.
- Chakraverty, S. (2009). Vibration of Plates. Boca Raton: CRC Press.
- Chan, H.C., Foo, O., (1979). Vibration of rectangular plates subjected to in-plane forces by the finite strip method, journal of sound and vibration, 64 (4), 583-588.
- Cho, D.S., Kim, B.H., Vladimir, N., Choi, T.M. (2015). Natural vibration analysis of rectangular bottom plate structures in contact with fluid. Ocean Engineering, 103, 171-179.

- Ciarlet, P., G., (1980). A Justification of the von Kármán Equations. *Archive for Rational Mechanics and Analysis*, Volume 73, pp. 349-389.
- David, A., Hugues, F., Dauchez, N., (2018). Vibrational response of a rectangular duct of finite length excited by a turbulent internal flow. *Journal of Sound and Vibration*, 422, pp. 146-160.
- Dawe, D. J. (1969). Discrete analysis of the lateral vibration of rectangular plates in the presence of membrane stresses. *Aeronautical Research Council (London)*, Paper No. 1062.
- Dickinson, S. M., (1973). Lateral vibration of rectangular plates subject to inplane forces. *Journal of sound and Vibration*, 29, 505
- Dvorkin, E. N., and Bathe, K.-J. (1984). A continuum mechanics based four-node shell elements for general non-linear analysis. *Engineering Computations*, Vol. 1, 77-89.
- Echter, R., Oesterle, B., Bischoff, M. (2013). A hierarchic family of isogeometric shell finite elements. *Computational Methods in Applied Mechanical Engineering*. 254, 170-180.
- El Aghoury, I. M., and Galal, K. (2014). Design of rectangular industrial duct plates subjected to out-of-plane pressure considering nonlinear large deformations. *Thin-Walled Structures*, Vol. 77, 1-7.
- Gorman, D. J. (1982). *Free Vibration Analysis of Rectangular Plates*. New York: Elsevier North Holland Inc.
- Huang, C. S., Lin, Y. J. (2016). Fourier series solutions for vibrations of a rectangular plate with a straight through crack. *Applied Mathematical Modelling*, 40(23–24), 10389-10403.
- Hughes, T. J. R., Cohen, M., Haroun, M. (1978). Reduced and selective integration techniques in the finite element analysis of plates. *Nuclear engineering and design*, 46, 203-222.
- Hughes, T. J. R., Cotrell, J. A., Bazilevs, Y., (2005). Isogeometric analysis: CAD, finite elements, NURBS, exact geometry, and mesh refinement. *Comput. Methods Appl. Mech. Engrg.*, 194, 4135-4195.
- Ibearugbulem, O. M., Ettu, L. O., and Ezeh, J. C. (2013). Direct integration and work principle as new approach in bending analyses of isotropic rectangular plates. *The International Journal of Engineering and Science (IJES)*, 2(3), 28-36.
- Imrak, C. E., and Gerdemeli, I. (2007). The problem of isotropic rectangular plate with four clamped edges. *Sadhand*, 32(3), 181-186.
- Kaldas, M., M., and Dickinson, S., M., (1981-a). The flexural vibration of welded rectangular plates. *Journal of Sound and Vibration*, Volume 75(2), pp. 163-178.

- Kaldas, M., M., and Dickinson, S., M., (1981-b). Vibration and buckling calculations for rectangular plates subject to complicated in-plane stress distributions by using numerical integration in a Rayleigh-Ritz analysis. *Journal of Sound and Vibration*, Volume 75(2), pp. 151-162.
- Katsikadelis, J. T., Nerantzaki, M., S., (1994). Non-Linear Analysis of Plates by the Analog Equation Method. *Journal of Computational Mechanics*, 14, pp. 154-164.
- Leheta, H., W., Badran, S., F., Elhanafi, A., S., (2015). Ship structural integrity using new stiffened plates. *Thin-Walled Structures*, Volume 94, pp. 545-561.
- Leissa, A. W., Kang, J. H., (2002). Exact solutions for vibration and buckling of an SS-C-SS-C rectangular plate loaded by linearly varying in-plane stresses. *International Journal of Mechanical Sciences*, 44, 1925-1945.
- Levy, S. (1941a). Bending of rectangular plates with large deformations. Report No. 737-National Advisory Committee for Aeronautics.
- Levy, S. (1941b). Square plate with clamped edges under normal pressure producing large deformations. Report No. 740, National Committee for Aeronautics.
- Levy, S. (1942). Square plates with clamped edges under normal pressure. Report No.847, National Committee for Aeronautics.
- Liew, K. M., Xiang, Y., and Kitipornchai, S. (1993). Transverse vibration of thick rectangular plates - IV: Influence of Isotropic In-plane Pressure. *Computers and Structures*, 49(1), pp. 69-78.
- Little, G. H. (1999). Efficient large deflection analysis of rectangular plates with general transverse form of displacement. *Computers and Structures*, 71, 333-352.
- Liu, Z., J. (2014). Nonlinear analysis of flue gas ductwork for power plant. Structures Congress, Structural Engineering Institute of ASCE, Boston, MA, April 3-5, 2014.
- Love, A. E. H. On the small free vibrations and deformations of elastic shells, *Philosophical trans. of the Royal Society (London)*, 1888, Vol. série A, N° 17 p. 491–549.
- Manzanares-Martínez, B., Flores, J., Gutiérrez, L., Méndez-Sánchez, R.A., Monsivais, G., Morales, A., Ramos-Mendieta, F. (2010). Flexural vibrations of a rectangular plate for the lower normal modes. *Journal of Sound and Vibration*, 329, 5105-5115.
- Mei, C. and Yang, T. Y., (1972). Free vibration of finite element plates subject to complex middle-plate force systems. *Journal of Sound and Vibration*, 23, 145.

- Mindlin, R. D. (1951). Influence of rotatory inertia and shear on flexural motions of isotropic, elastic plates. *ASME Journal of Applied Mechanics*, 18, 31-38.
- Minghini, F., Tullini, N., Laudiero, F. (2007). Locking-free finite elements for shear deformable orthotropic thin-walled beams. *Int. J. Numer. Meth. Engng.* 72, 808-834.
- Ojeda, R. B., Prutsky, G., Lawrence, N. and Thomas, G., 2007. A new approach for the large deflection finite element analysis of isotropic and composite plates with arbitrary orientated stiffeners. *Elsevier Finite Elements in Analysis and Design*, Volume 43, pp. 989-1002.
- Paik, J. K., 2008. Some recent advances in the concepts of plate-effectiveness evaluation. *Elsevier Thin-Walled Structures*, Volume 46, pp. 1035-1046.
- Paik, J. K. and Seo, J. K., (2009-a). Nonlinear finite element method models for ultimate strength analysis of steel stiffened-plate structures under combined biaxial compression and lateral pressure actions-Part I: Plate elements. *Elsevier Thin-Walled Structures*, Volume 47, pp. 1008-1017.
- Paik, J. K. and Seo, J. K., (2009-b). Nonlinear finite element method models for ultimate strength analysis of steel stiffened-plate structures under combined biaxial compression and lateral pressure actions-Part II: Stiffened panels. *Elsevier Thin-Walled Structures*, Volume 47, pp. 998-1007.
- Paik, J. K. & Thayamballi, A. K., 2003. *Ultimate limit states design of steel-plated structures*. Chichester: Wiley.
- Petyt, M. (2010). *Introduction to finite element vibration analysis / Second edition*. Cambridge University Press, ISBN 978-0-521-19160-9.
- Phillips, I. G., and Jubb, J. E. M. (1974). The effect of distortion on the lowest natural frequency of a rectangular steel plate. *Journal of sound and vibration*, 33(1), 41-48.
- Powell, G. H. (2010). *Modelling for Structural Analysis: Behaviour and Basics* (1st ed.). Berkeley, CA: Computers and Structures, Inc.
- Ramberg, W., McPherson, A. E., and Levy, S. (1942). Normal-pressure tests of rectangular plates. Washington: Technical Note No.849, National Advisory Committee for Aeronautics.
- Reissner, E. (1945). The effect of transverse shear deformation on the bending of elastic plates. *ASME Journal of Applied Mechanics*, 12, 68-77.
- Reissner, E. (1955). On transverse vibration of thin, shallow, elastic shells. *Quarterly of applied mathematics*. 13, 169-176.

- Rezaiefar, A., Galal, K., (2016). Structural design of stiffened plates of industrial duct walls with relatively long panels undergoing large deformations. *Thin-Walled Structures*, 108, 406-415.
- Sapountzakis, E., J., and Dikaros, I., C., (2012). Large deflection analysis of plates stiffened by parallel beams. *Engineering Structures*, Elsevier. 35, pp. 1021-1041.
- Senjanović, I., Vladimir, N., Hadžić, N. (2014). Modified Mindlin plate theory and shear locking-free finite element formulation. *Mechanics Research Communications*, 55, 95-104.
- Singh, j. P., Dey, S. S., (1990). Transverse vibration of rectangular plates subjected to inplane forces by a difference based variational approach. *International Journal of Mechanical Science*, 32(7), 591-599.
- Shanmugam, N. E., Dongqi, Z., Choo, Y. S. and Arockiaswamy, M., (2014). Experimental studies on stiffened plates under in-plane load and lateral pressure. *Elsevier Thin-Walled Structures*, Volume 80, pp. 22-31.
- Soedel, W. (1993). *Vibrations of Shells and Plates*. New York: Marcel Dekker Inc.
- Timoshenko, S., and Woinowsky-Kreiger, S. (1959). *Theory of plates and shells* (2nd ed.). New-York: McGraw-Hill.
- Thanga, T., Halabieh, B., and Sivakumaran, K. S. (2011). Strength of plates of rectangular industrial ducts. *Procedia Engineering*, Elsevier, 14, 622-629.
- Timoshenko, S., and Woinowsky-Kreiger, S. (1959). *Theory of plates and shells* (2nd ed.). New-York: McGraw-Hill.
- Triotsky, D., (1976). *Stiffened plates: Bending, stability and vibrations*. Elsevier Scientific Publishing Co. Amsterdam, The Netherlands.
- Ugural, A. C. (1981). *Stresses in plates and shells* (1st Edition ed.). Mc Graw-Hill.
- Von-Kármán, T. (1910). Festigkeitsprobleme im Maschinenbau. *Encyklopadie der Mathematischen Wissenschaften*. 4(4), 311–385.
- Wang, C. T. (1948). Bending of rectangular plates with large deflections. Technical Note No.1462, National Advisory Committee for Aeronotics.
- Wang, D., and El-Sheikh, I. (2005). Large-deflection mathematical analysis of rectangular plates. *Journal of Engineering Mechanics*, ASCE, 131(8), 809-821.
- Wang, X., Gan, L., Wang, Y. (2006). A differential quadrature analysis of vibration and buckling of an SS-C-SS-C rectangular plate loaded by linearly varying in-plane stresses. *Journal of Sound and Vibration*. 298, 420-431.

- Wang, M., Li, K., Qiu, Y., Li, T., Zhu, X. (2017). Free vibration characteristics analysis of rectangular plate with rectangular opening based on Fourier series method. *Chinese Journal of Ship Research*, 12(4) 102-109.
- Wilson, E. L. (2016). *CSI analysis reference manual for SAP2000, ETABS, SAFE and CSIBridge*. Computers and Structures Inc. Berkeley, CA
- Xiang, Y., Zhao, Y. B., Wei, G. H., (2002). Levy solutions for vibration of multi-span rectangular plates. *International journal of Mechanical Sciences*, 44, 1195-1218.
- Xu MC, Guedes Soares C., (2011-a). Experimental study on the collapse strength of narrow stiffened panels. *Proceedings of 30th international conference on offshore mechanics and arctic engineering (OMAE2011)*, ASME paper OMAE 2011-50293.
- Xu MC., Guedes Soares C., (2011-b). Numerical study of the effect of geometry and boundary conditions on the collapse behaviour of short stiffened panels. *Advances in marine structures*. London, UK, Taylor & Francis Group, p. 229–37.
- Xu MC, Guedes Soares C., (2013). Experimental study on the collapse strength of wide stiffened panels. *Marine Structures*, (30), 33-62.
- Yamaki, N., Chiba, M., (1983). Nonlinear vibrations of a clamped rectangular plate with initial deflection and initial edge displacement – Part I: Theory. *Thin-Walled Structures*, Volume 1, pp. 3-29.
- Yamaki, N., Otomo, K., Chiba, M., (1983). Nonlinear vibrations of a clamped rectangular plate with initial deflection and initial edge displacement – Part II: Experiment. *Thin-Walled Structures*, Volume 1, pp. 101-119.
- Young, W. C., and Budynas, R. G. (2002). *Roark's formulas for stress and strain*, vol. 6. New York: McGraw-Hill.
- Zeng, H.C., Huang, C.S., Leissa, A.W., Chang, M.J. (2016). Vibrations and stability of a loaded side-cracked rectangular plate via the MLS-Ritz method. *Thin-Walled Structures*, 106, 459-470.